UNIVERSITY COLLEGE LONDON (UCL)

The effect of temperature uncertainty on Proton Exchange Fuel Cell (PEFC) performance

by

Mozhdeh Noorkami

A thesis submitted in partial fulfillment for the
degree of Master of Philosophy

in the
Faculty of Engineering Sciences
Chemical Engineering Department

July 2016

Declaration of Authorship

I, Mozhdeh Noorkami, declare that this thesis titled, 'The effect of temperature uncertainty on Proton Exchange Fuel Cell (PEFC) performance' and the work presented in it are my own. I confirm that:

- This work was done wholly or mainly while in candidature for a research degree at this University.
- Where any part of this thesis has previously been submitted for a degree or any other qualification at this University or any other institution, this has been clearly stated.
- Where I have consulted the published work of others, this is always clearly attributed.
- Where I have quoted from the work of others, the source is always given. With the exception of such quotations, this thesis is entirely my own work.
- I have acknowledged all main sources of help.
- Where the thesis is based on work done by myself jointly with others, I have made clear exactly what was done by others and what I have contributed myself.

Signed:

Date:

“Before you speak, let your words pass through three gates: at the first gate, ask youreslf, ’is it true?’, at the second gate ask, ’is it necessary?’ at the third gate ask ’is it kind?’ ”

Rumi

UNIVERSITY COLLEGE LONDON (UCL)

Abstract

Faculty of Engineering Sciences
Chemical Engineering Department

Master of Philosophy

by Mozhdeh Noorkami

The temperature of operation is a key parameter in determining the performance and durability of a polymer electrolyte fuel cell (PEFC). Controlling temperature and understanding its distribution and dynamic response is vital for effective operation and design of better systems. The sensitivity to temperature means that uncertainty in this parameter leads to variable response and can mask other factors affecting performance. It is important to be able to determine the impact of temperature uncertainly and quantify how much PEFC operation is influenced under different operating conditions.

Here, a simple lumped mathematical model is used to describe PEFC performance under temperature uncertainty. An analytical approach gives a measure of the sensitivity of performance to temperature at different nominal operating temperatures and electrical loadings. Whereas a statistical approach, using Monte Carlo stochastic sampling, provides a 'probability map' of PEFC polarisation behaviour. As such, a polarisation 'area' or 'band' is considered as opposed to a polarisation 'curve'. Results show that temperature variation has the greatest effect at higher currents and lower nominal operating temperatures. Thermal imaging of a commercial air-cooled stack is included to illustrate the temporal and spatial temperature variation exerienced in real systems.

Acknowledgements

I would like to express my appreciation and thank to my supervisors, Dr. Dan Brett and Prof. Eric Fraga, for their tremendous supports.

I would especially like to thank Dr. Joakim Beck, Vikram Sundara, Krisztian Ronaszegi, Quentin Meyer, James Robinson and Mayowa Obeisun for their assistance to help me to achive my goals.

Also a special thanks to Tobias Neville, Elnaz Alizadeh and Fereshteh Darvishian for their continuous support throughout the ups and downs in the past few years. It would have been very difficult without them.

And finally I would like to thank my parents for being always there for me. Words cannot express how grateful I am for all they have done for me. . . .

Contents

List of Figures

List of Tables

Symbols

Roman symbols

a	Water activity	-
A	Area	cm^2
A_c	Specific area of catalyst layer	cm^{-1}
c	Molar concentration	$mol\,cm^{-3}$
D	Diffusion coefficient	$cm^2\,s^{-1}$
F	Faraday's constant	$C\,mol^{-1}$
H	Height	cm
i_{ref}	Reference exchange current density	$A\,cm^{-2}$
i	Current density	$A\,cm^{-2}$
k	Thermal conductivity	$W\,m^{-1}K^{-1}$
K	Electrode absolute permeability	cm^2
L	Length	cm
M	Molar mass	$kg\,mol^{-1}$
n	Electron number of electrochemical reaction	-
p	Pressure	Pa
R	Universal gas constant	$J\,mol^{-1}K^{-1}$
s	Liquid water saturation	-
S	Source term of governing equations	-
T	Temperature	$^\circ C$
u	Velocity vector	$m\,s^{-1}$
V	Cell potential	V

Greek symbols

ω	Angular frequency	rads^{-1}
α	Transfer coefficient	-
ε	Porosity	-
ζ	Stoichiometric flow ratio	-

η	Overpotential	V
λ	Membrane water content	-
μ	Viscosity	$kg\,cm^{-1}s^{-1}$
ν	Kinetic viscosity	$m^2\,s^{-1}$
ρ	Density	$kg\,cm^{-3}$
σ	Membrane conductivity	$S\,cm^{-1}$
ϕ	Potential	V
ω	Species molar fraction	-
$\psi_i\ \xi$	Parametric coefficients	-

Sub/Superscrips

a	Anode	-
av	Average value	-
c	Cathode	-
ch	Channel	-
ct	Catalyst layer	-
d	Diffusion layer	-
eff	Effective	-
g	Gas	-
H_2	Hydrogen	-
in	Inlet	-
k	Species	-
l	Liquid	-
m	Membrane	-
O_2	Oxygen	-
oc	Open circuit	-
r	Relative values	-
ref	Reference values	-
s	Solid; Specific	-
sat	Saturation	-
tot	Total	-
w	Water	-
N_2	Nitrogen	-

Chapter 1

Introduction

In recent years, climate change and sustainability have risen to be the two of the most concerning issues globally. Sustainability is “to meet the present needs without compromising the demands of future generation ”, which concerns three main areas: society, economy and environment. Climate change is one of the critical factors, which affect environmental sustainability. Scientists have spent decades examining the possible causes leading to climate change. One of the main causes of climate change is the atmospheric temperature rise due to greenhouse gas emissions [1]. Increase in concentration of greenhouse gases is a critical issue, which has been studied for last decades. To reduce the emission of greenhouse gases, alternative sources of energy need to be considered.

The main greenhouse gases emitted by human activities at the global scale are carbon dioxide produced by combustion of fossil fuels; methane that can be liberated from agricultural activities such as fertiliser use; nitrous oxide also from agricultural activities and fluorinated gases (F gases) that are mainly released from industrial processes such as refrigeration [2]. Figure 1.1(a) shows that CO_2 has the largest contribution among the greenhouse gases and also the majority of it comes from combustion of fossil fuels and deforestation and decay of biomass [2]. Figure 1.1(b) shows that the majority of greenhouse gas emissions are produced for energy supply, transport and industry.

Figure 1.1(c) shows that based on the research in 2008, 85% of global energy is provided by fossil fuels and 15% by renewable energies, such as nuclear energy(2%) and bioenergy, direct solar energy, ocean energy, wind energy, hydropower and geothermal energy.

Data collected in 2010 shows that 91% of CO_2 emission comes from fossil fuels and cement and 9% comes from land use change, such as deforestation and decay of biomass. Data shows that there is a 0.28% rise in annual CO_2 emission from 2011 to 2012 [2].

To reduce the impact of CO_2 on the environment and human health, an alternative to fossil fuels is required with lower greenhouse gas emissions. Also, limited amount of fossil

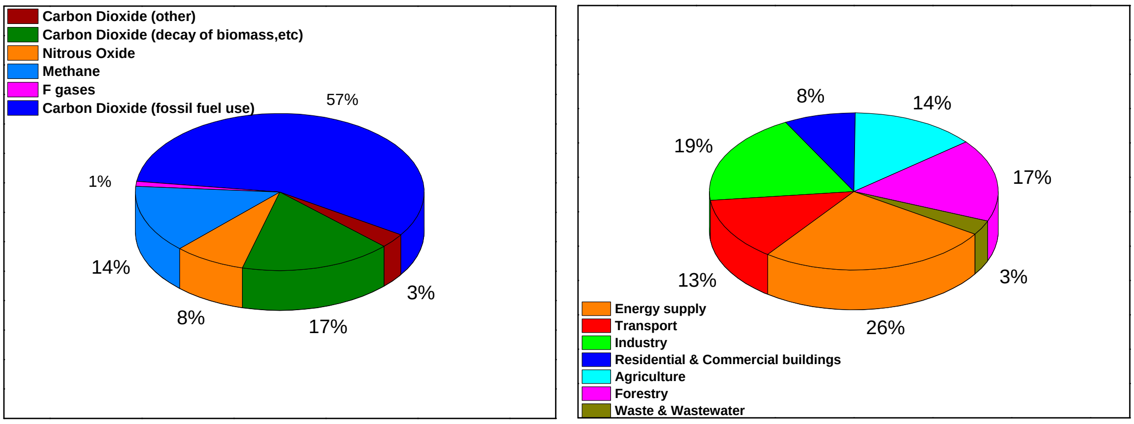

(a) Global shares of greenhouse gases emission in 2004 [2]

(b) Details of the sources of greenhouse gas based on global emissions from 2004 1.1(a)

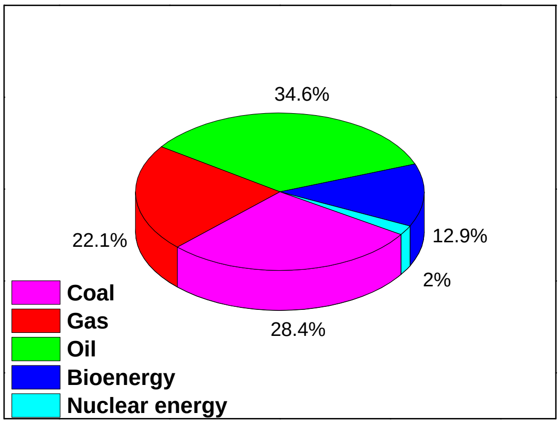

(c) Shares of energy resources in total global energy supply in 2008 [2]

FIGURE 1.1: Global gas emissions and details about the sources of emissions and shares of energy resources are described in this figure

fuels and very long replenishing time is another reason to consider renewable energies as an alternative to produce energy [2].

In the last 150 years, researchers and developers have been looking into hydropower, nuclear energy and renewables as an alternative to fossil fuels to face the environmental concerns, technological demands and economic issues. There are different sources of energy, which converts directly mechanical energy or heat to electricity with zero or very low CO_2 emission (wind, hydropower, nuclear, bio-fuels, biomass and solar).

To achieve an alternative, hydrogen is recognised as a clean, sustainable, potentially low cost energy vector, which can be used for stationary power, transportation, industrial, residential and commercial sectors. Hydrogen can be produced by using clean technologies to be stored and transported by trucks or pipelines in order to be used in fuel cells, turbines and engines.

One of the fastest growing technologies in the renewable energy industry are fuel cells. A fuel cell is a device that converts the chemical energy of fuels directly to electricity. Fuel cells come in a range of sizes and types for various applications. Low temperature fuel cells can be used in laptops, electronic devices and vehicles.

Fuel cells are particularly promising for transportation. Currently there are many taxis and buses running with hydrogen fuel cells for a cleaner environment. For example, Hyundai has plans to manufacture 1,000 vehicles running with fuel cells by 2015 and 10,000 more to be released soon after to fulfil the aim to minimise the CO_2 emission to zero [3]. The UK's first hydrogen powered ferry was released in July 2013 in Bristol harbour to show the technical and commercial benefits of hydrogen fuel cell technology [4].

1.1 Challenges

The key problem with the renewable industry is that it is limited to the availability of resources, geographical and environmental constraints and capital and operational costs of technologies. Renewable energy is still facing two major challenges in order to displace fossil fuels. First the capital and operation costs (i.e. wind turbine, solar panel, electrolysis of hydrogen) needs to become cost competitive with fossil fuels, and the second challenge is to determine an effective way of storing energy.

To realise a hydrogen economy, it is critical to consider how to produce and store hydrogen in a safe and functional way. Steam Methane Reforming (SMR) reacts high temperature steam with fossil fuels to produce hydrogen and carbon monoxide in a strongly endothermic reaction. Currently, 95% of hydrogen for industrial applications is produced by SMR where there are other methods like electrolysis and thermolysis are also known to produce hydrogen by using electricity obtained from wind or solar energy. In the UK, wind energy provides 1.5% of overall electricity, which is provided by 2434 wind turbines and 3391 MW of installed capacity [5].

For wider spread commercialisation, fuel cell technology needs to become cheaper and more efficient in order to allow hydrogen to be a larger scale substitute to fossil fuels. To achieve a more efficient and better performance fuel cell, it is important to learn about uncertainties involved in the physical and operational parameters and measuring conditions. When operating fuel cells, there is always a level of uncertainty in the operating parameters and physical state of the system that leads to variable and unpredictable performance. This uncertainty can be due to fluctuations and distribution of operating parameters, measurement accuracy, random errors, unoptimised / unstable control, etc. [6].

1.2 Research overview and aims and objectives

Temperature is one of the parameters in a fuel cell system with the highest uncertainty as it is a function of operating point, reactant flow rate and ambient conditions; it is also temporally variant under dynamic conditions and spatially heterogeneous. Temperature is an important component in fuel cell operation and plays a key role in cell performance [7–9]. Water transport is directly influenced by temperature, affecting the mobility of species in the electrolyte and access and removal of water at the electrodes and propensity to flooding [10].

The intention of this study is to provide fuel cell developers with an understanding of the sensitivity of polarisation performance to uncertainty in the temperature of the system (spatial and temporal). A key outcome is that conventional polarisation curves should be considered as “polarisation areas” or “bands” with variable uncertainty across their operating range.

In this work, a simple mathematical lumped model is used to examine the effect of temperature on the parameters and fundamental physical and chemical properties that determine PEFC performance. First, an analytical approach is adopted that examines the sensitivity of the models to small changes in temperature by using the differential $\frac{dV}{dT}$ to map the operating range of polarisation and nominal operating temperature. However, this does not capture the stochastic nature of the uncertainty associated with practical operation, so a second analysis is performed that applies a statistical treatment to develop a “probability map” of fuel cell polarisation performance. In order to support the statistical study, an experimental characterisation of a commercial air-cooled stack is performed that uses high-resolution thermal imaging to characterise the kind of spatial and temporal temperature uncertainty that can be expected in a practical operating system.

1.3 Thesis outline

The structure of this report is as follows: Chapter two discusses relevant literature review and identifies possible gaps in prior knowledge. Chapter three presents two mathematical models to consider analytical and statistical behaviour of temperature on overall performance of a fuel cell. In chapter four, experimental methodology with thermal imaging is presented to confirm the presence of temperature distribution temporally and spatially, chapter five shows the application of temperature/ current mapping to find temperature variation in 16 segments of fuel cell stack and chapter six and seven present the results for modelling and experimentation respectively. Finally, in chapter eight, conclusion and future work are shown to complete the report.

Chapter 2

Background and related work

2.1 Introduction to fuel cells

A fuel cell converts chemical energy of fuels to electricity. It has three main parts, the electrodes - cathode and anodes - and electrolyte. The nature of the electrolyte defines the type and name of the fuel cell. There are different types of fuel cells for various applications. Table 2.1 summarises some of the advantages and disadvantages of different types of fuel cells [11, 12]. The focus of this study is on the low temperature Polymer Electrolyte Fuel Cell (PEFC).

Figure 2.1 presents a PEFC, which consists of different parts including gas channels, attached with collectors which are the passage for reacting gases. The Gas Diffusion Layer (GDL) has a porous nature which makes the diffusion of reactants and removal of produced liquid water at the cathode side easier. It is also a good electrical conductor, by producing low electrical resistance between the catalyst layer and the collector. The catalyst layer is where electrochemical reactions occur. In PEFC the most commonly used catalyst is platinum. The catalyst has the role of speeding up the reactions occurring inside the cell. In this case, the reaction at the anode is hydrogen molecules breaking into positive ions (protons) and at the cathode oxygen molecules reacting with the protons, which migrate through the membrane from anode to cathode.

Figure 2.1 illustrates the reaction between hydrogen and oxygen in a fuel cell. Hydrogen enters into the cell from the anode side, react at the electrode and loses electrons. The resultant positive ions travel towards the cathode through the proton exchange membrane and the free electrons travel through the external circuit towards the cathode. On the cathode side, air enters the cathode, where the reaction between the hydrogen ions (electrons) and oxygen molecules takes place.

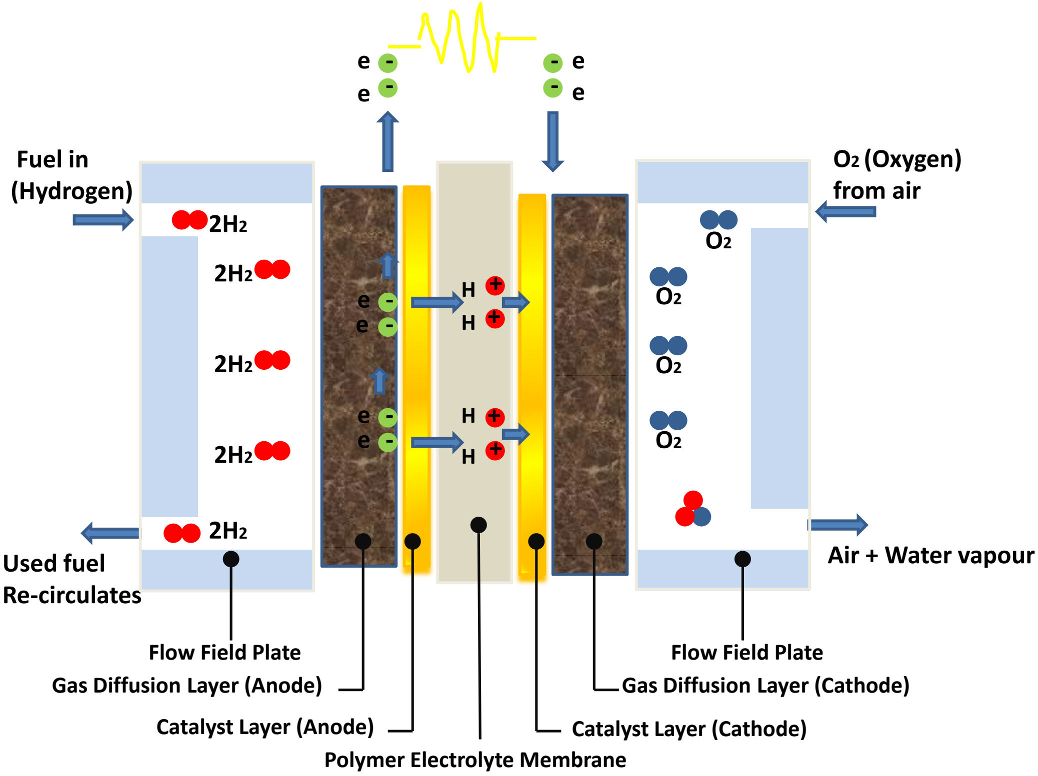

FIGURE 2.1: PEFC diagram to show the different parts of the system and how the species move across the MEA

The reactions that take place inside the PEFC are as follows:

Reaction at anode

$$2H_2 \rightarrow 4H^+ + 4e^- \tag{2.1}$$

Reaction at cathode

$$O_2 + 4H^+ + 4e^- \rightarrow 2H_2O \tag{2.2}$$

Overall cell reaction

$$2H_2 + O_2 \rightarrow 2H_2O \tag{2.3}$$

The operating temperature for the PEFC is mainly lower than $100°C$ to avoid excessive loss of water. Also, the high current density of this type of fuel cells form a lightweight and compact system, which results in more desirable device for portable uses. One of the other advantages is the use of a solid electrolyte, which makes the sealing of the electrodes easier. PEFCs have less problems with corrosion compared to high temperature fuel cells, which makes low temperature fuel cells have a longer stack life. However, one of the main disadvantages of PEFCs is the risk of flooding, which can occur with poor water management.

There are three main challenges for fuel cells:

Types of Fuel Cell	**Advantages**	**Disadvantages**
SOFC	* Fuel flexibility * Non-precious metal catalyst * High quality waste heat for Co-generation	* Limited range of material selection * Sealing issues * High temperatures results in irregular component expansion
MCFC	* Fuel flexibility * Non-precious metal catalyst * Higher efficiency than PEFC and PAFC	* Corrosive and mobile electrolyte * Loss of electrolyte due to high temperature accelerates degradation of the cells
PAFC	* Mature technology * Co generation is available * Excellent reliability and long-term running * Almost inexpensive electrolyte	* Slow reduction in the cathode side * Electrolyte is a corrosive liquid * Complex system configuration similar to PEFC
DMFC	* Simple structure * Good durability for low power and long operating hours	* Poor cell efficiency * Poor durability for short term operating and high power
PEFC	* Quick start up * Highest power density compared to other types	* Complex system configuration * Water and thermal management difficulties

Table 2.1: Characteristics of different types of fuel cells

- Economics - which considers costly aspects of fuel cell such as expensive components.
- Durability - It is crucial to use materials and operation models that prolong the life of the system. This also has an effect on economy of ownership.
- Reliability- A fuel cell has different applications and it is essential to use optimum operating conditions in order to meet the specifications considering the environmental concerns.

2.2 Characteristics of fuel cell performance

There are different mathematical models presented in the literature for different purposes to describe mass , energy balance and electrochemistry of the reactions occurring in fuel cells over single or multiple dimensions. To validate the models with experiments, it is important to explain briefly the various methods to validate the cell performance.

The most commonly used method to validate the theoretical data with experiments is the polarisation *V-I* curve, where voltage is plotted versus current density. Cell voltage is affected by different losses, such as thermodynamics, activation, ohmic and concentration losses, which are demonstrated in Figure 2.2.

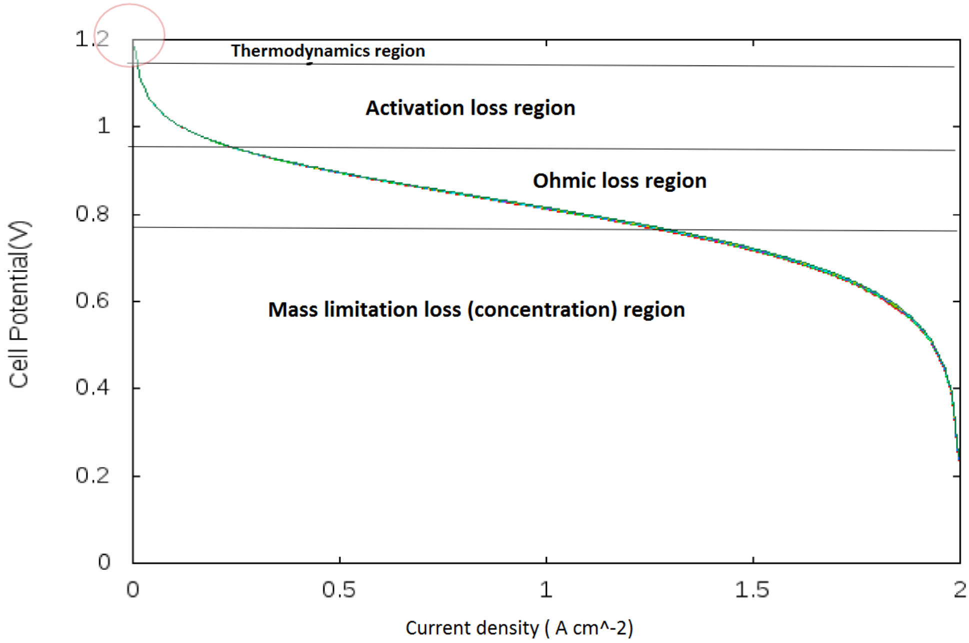

FIGURE 2.2: A polarisation *V-I* curve with voltage losses

Activation is the result of breaking the molecules to ions and trasnfer the positive ions across the membrane [13, 14]. Activation is a function of exchange current density, which is defined as the rate of reduction or oxidation at equilibrium. The value of exchange current density i_0 varies with the type of catalyst used in the reaction, electrode roughness, the metal compositions and soluble species concentrations. Exchange current density is also a function of temperature, which improves exponentially with increasing temperature [14]. To obtain a better performance, larger i_0 is favourable to increase the reaction kinetics.

The ionic and electron transfer produces ohmic resistance inside the cell, this is particularly significant for the membrane electrolyte [13, 15]. Electrical resistance is often assumed to be negligible; where the ionic resistance is a function of membrane conductivity, which depends on the type of the membrane used in the fuel cells. To achieve good conduction, it is essential to keep the membrane humidified. Temperature plays a key role to increase the rate of conductivity in the membrane and also to maximise the rate of reaction; however, the membrane needs to be hydrated to allow the proton conduction with minimal resistance. Therefore, choosing the right value of temperature is a trade off between membrane hydration and conduction at the desirable level to minimise ohmic loss.

The other major loss mechanism is mass transport limitation. When the concentration of reactants drops to zero in the catalyst layer, the current density becomes limiting. Mass transport limitation dominates at higher current densities and is a function of diffusion coefficient and reactant concentrations [10, 13, 16].

The open circuit voltage (OCV) before current is drawn is defined by the thermodynamics of reaction and the Nernst equation, which accounts for the concentration of reactant species [13]. Open circuit voltage E_O occurs, when there is no current density available in the cell.

2.3 Electrochemical description of a fuel cell

The *V*-*I* curves present the total cell voltage of the fuel cell by considering the losses involved in thermodynamics and kinetics of the reaction, mass and charge transfer happening in the cell. The overall polarisation curve is generated by subtracting the relevant over-potentials from the open circuit potential that can be seen in Equation 2.4:

$$V_{cell} = E - \eta_{act} - \eta_{ohmic} - \eta_{conc} \tag{2.4}$$

where E is open circuit voltage at zero current density. The Nernst equation is used to describe the thermodynamics. η_{act} is the activation loss due to kinetics of reaction, which depends on the rate of the reactions at the surface of the electrodes. η_{ohm} is the ohmic loss taken to be exclusively due to the ionic resistance of the electrolyte membrane, which is a function of water content and temperature. η_{con} is concentration loss and is a function of the activity of reactants and products and also rate of diffusion of species through the GDL.

2.3.1 Fuel cell thermodynamics

Thermodynamic analysis describes the magnitude and the direction of the reaction using the Nernst equation. The first law of thermodynamics is used to calculate the maximum useful energy required to do work [13]:

$$\Delta U = Q - W \tag{2.5}$$

where in Equation 2.5, Q and W represent heat supplied to the system and work done by the system and U is internal energy. To calculate the total work done by the system, Equation 2.6 is defined as:

$$W = W_p + W_e \tag{2.6}$$

where W_e is the electrical work needed to transport the electrons and W_p is the mechanical contribution at constant pressure and temperature, which depends on the change of volume only. Equation 2.7 shows the same phenomenon as follows, where P is pressure and ΔV is change of volume.

$$W_p = P\Delta V \tag{2.7}$$

by using the second law of thermodynamics, the next equation is defined to calculate the heat loss from the system. Equation 2.8 explain the entropy change of the fuel cell, ΔS, in terms of the heat transfer, δQ, and temperature T.

$$\Delta S = \frac{\delta Q}{T} \tag{2.8}$$

to calculate the maximum useful work, the change in Gibbs free energy at constant temperature and pressure is described in Equation 2.9 following up the Equation 2.10 to determine enthalpy change, ΔH, assuming constant pressure.

$$\Delta G = \Delta H - T\Delta S \tag{2.9}$$

Enthalpy change is defined by

$$\Delta H = \Delta U - P\Delta V \tag{2.10}$$

By combining Equations 2.6, 2.7 and 2.8 and substituting into Equation 2.5, the internal energy in terms of work done and change of entropy is determined and substituting the obtained expression and Equation 2.10 into Equation 2.9 gives the Gibbs free energy in terms of electrical work, which means the electrical work in a closed system at constant pressure and temperature is caused by the change in Gibbs free energy of the system.

$$\Delta G = -W_e = -nFE \tag{2.11}$$

Equation 2.11 provides a direct relationship between the thermodynamics of the reaction (ΔG) and the electrical potential (E). To calculate the potential change when the system is not operating at standard conditions, the Nernst equation is described as:

$$E = E_0 - \frac{RT}{n_a F} log(\frac{p_{(w)}}{p_{(H_2)} p_{(O_2)}^{0.5}}) \tag{2.12}$$

where E_0 is the maximum voltage achieved depending on fuel cell temperature at standard conditions and the second term accounts for the effect of temperature and reactant/product concentrations.

2.3.2 Reaction kinetics

The rate at which a reaction is attained at the surface of the electrodes is affected by the kinetics of the reactions. The thermodynamics of the reaction was previously described for the equilibrium state, when there is no current flow occurring. A potential change at the electrodes due to the kinetics of reaction is called activation overpotential.

The Tafel equation is used to describe the activation overpotential, which is a function of the exchange current density. Exchange current density, i_0, is the rate of the reaction at the reversible potential. i_0 is often measured experimentally; however, there are some expressions available in literature to calculate it theoretically [13].

Empirical equation 2.13 is used in this work to calculate i_0 as a function of i_0^{ref} [14], which is reference exchange current density to work as a third electrode to measure the rate of current transfer. To overcome the inaccuracy of the potential measurement under load, a commonly used technique is to insert a third electrode as a reference electrode. The overpotential at the third electrode is negligible as it draws no current; therefore, the measured over potential only applies to the working electrodes to determine the net current transferred across the MEA.

$$i_{0,c} = i_0^{ref}\, a_c\, L_c\, (\frac{P_{O_2}}{P^{ref}})^{\gamma}\, exp(\frac{-E_c}{R.T}\, (1 - \frac{T}{T^{ref}})) \tag{2.13}$$

In Equation 2.13, i_0^{ref} is a reference exchange current density [13], a_c is catalyst specific area cm^2 mg^{-1}, l_c is catalyst loading $mg(pt)\, cm^{-2}$, P_{O_2} is oxygen partial pressure, P_{ref} is reference operating pressure, E_c is reaction activation energy $J\, mol^{-1}$ and R is universal ideal gas constant. To determine the thermal sensitivity of the reaction kinetics, the effect of temperature on i_0 is essential where exchange current density can be described by the Tafel equation as a function of the ratio of oxidised and reduced concentration. The magnitude of this ratio (C_O/C_R) depends on the rate and kinetics of electrons, which temperature plays a key role in this case. Therefore, it is crucial to capture the effect of temperature on the rate of electron transfer across the electrodes to learn about the sensitivity of reaction kinetics in MEA.

Figure 5.4 shows that i_0 behaves exponentially with temperature from 30 to 90°C, where at lower temperature there is a larger slope of i_0 than higher temperature. The graph shows that kinetics of reaction improves with temperature due to higher rate of current transfer as a result of significant mobility of species at higher temperature resulting in more collision between the species and higher rate of reaction.

Partial pressure of oxygen, Pr_{O_2} at the cathode can be found by Equation 2.14, where P_{air} is the total pressure of air going into the cell, i is current density and P_w is the total pressure of water produced at the cathode [14].

$$Pr_{O_2} = \frac{P_{air}}{exp(\frac{4.192\,i}{T^{1.344}})} - P_w \tag{2.14}$$

Current experimental studies show that the anodic kinetics are negligible compared to cathodic one due to significant exchange current density. The value of exchange current density is dependent on reactant concentration c_R^*, activation barrier ΔG, temperature and the number of possible reaction sites (i.e. the reaction interface roughness) [13].

Therefore, the anodic kinetics is not considered in the calculation due to its negligible effect. The typical $i_{0,c}$ value is $3 \times 10^{-9} A\,cm^{-2}$ [13]. Equation 2.15 defines the activation loss at the electrode, where n_c is the number of free electrons, α_c is transfer coefficient at the cathode, i is current density and i_0 is exchange current density.

$$\eta_{act} = \frac{RT}{\alpha_c n_c F} \times log(\frac{i}{i_0}) \tag{2.15}$$

2.3.3 Fuel cell charge transport

Ohmic losses are another type of over-potential occurring in the fuel cell, which affects the cell voltage. Ohmic losses occur as a result of ionic resistance in the electrolyte and electronic resistance in the bipolar plates, electrodes and gas diffusion layers.

Ohmic loss is a function of current density and internal resistance, which is the sum of the electrical and ionic resistances. Electrical resistance is assumed negligible in this work because of its relatively small effect on the cell potential compares to the electrolyte [17]. Equation 2.16 is used to describe the ohmic losses, where l is membrane thickness and σ_m is membrane conductivity ($S \quad cm^{-1}$).

$$\eta_{ohmic} = (\frac{l}{\sigma_m})i \tag{2.16}$$

Ionic resistance is a function of membrane thickness and conductivity, and it is typically assumed to be in the range of 0.1-0.2 $\Omega.cm^2$ [14]. To capture the effect of temperature on membrane conductivity and resistance, an empirical Equation 2.17 is used to calculate the membrane conductivity, where c_m is defined as water content [16],

$$\sigma_m = (0.00514 \times c_m - 0.000326) \times exp(1268(\frac{1}{303} - \frac{1}{T})) \tag{2.17}$$

Conductivity is a function of the water activity and water content of the membrane. Equation 2.18 is used to calculate the membrane water content [18], Where a_m is an empirical term, which depends on water activity of the electrodes. To estimate conductivity, anodic water activity or average of the two electrodes are usually used with respect to β, which is a design parameter depending on operating conditions [10] and defines the contribution of water activity at each electrodes.

$$c_m = 0.043 + 17.18 \times a_m - 39.85 \times a_m^2 + 36 \times a_m^3 \tag{2.18}$$

In Equation 2.19, a_a and a_c are water activities at anode and cathode respectively.

$$a_m = \beta \times a_a + (1 - \beta) \times a_c \tag{2.19}$$

To calculate water activity at the electrodes, partial pressure of reactants must be divided to water saturation pressure. In Equation 2.20, $M_{w,a/c}$ is mass flux of vapour water at the electrodes, $M_{H2/O2}$ is mass flux of hydrogen and oxygen and P is the total pressure and P_w^{sat} is water saturation pressure.

$$a_{a/c} = \frac{M^v_{w,a/c}}{(M^v_{w,a/c} + M_{H_2/O_2})} \times \frac{P}{P_w^{sat}} \tag{2.20}$$

Relative water content is a function of pressure and it is normally determined experimentally. Experimental data show that increased water content at high pressure improves membrane conduction, which makes ohmic losses smaller.

To calculate water activity, Equations 2.21 to 2.26 are used to describe the mass flux for hydrogen, oxygen and water respectively at the anode and cathode, where λ is stoichiometric ratio of species, A active area, n is the number of electrons at the electrodes, M is mass flux, y_w is mole fraction of water, RH is relative humidity and P_w^{sat} is saturation pressure of water.

$$M_{H_2} = \lambda_{H_2} \frac{iA}{n_a F} \tag{2.21}$$

$$M_{O_2} = \lambda_{O_2} \frac{iA}{n_c F} \tag{2.22}$$

$$M^v_{w,a} = \frac{y_{w,a,in}}{1 - y_{w,a,in}} M_{H_2} \tag{2.23}$$

$$M^v_{w,c} = \frac{y_{w,c,in}}{1 - y_{w,c,in}} M_{O_2} \tag{2.24}$$

$$y_{w,a,in} = RH_{fuel}[\frac{P^{sat}_w}{P}] \tag{2.25}$$

$$y_{w,c,in} = RH_{air}[\frac{P^{sat}_w}{P}] \tag{2.26}$$

2.3.4 Fuel cell mass transport

Insufficient reactant at the surface of the electrodes cause a mass transport limitation, which reduces the total cell voltage. Increase in concentration of reactants, temperature or agitation of fluid can improve mass transport and reduce the limitation providing on the cell voltage.

Overpotentials with respect to mass transport limitations are called concentration losses, which results in a limiting current density i_L. Limiting current density would be achieved, when the reactant concentration in the catalyst layer drops to zero, which in this study is hydrogen as this work looks at PEFC with hydrogen as a fuel. The resulting current density would be termed the limiting current density. The diffusion coefficient has a linear relationship with i_L as larger diffusion can lead to more reaction and larger i_L.

To determine the concentration loss, overpotential at the anode is considered negligible due to insignificant concentration difference between the hydrogen ions concentration and initial hydrogen molecules concentration. Equation 2.27 is used to describe the concentration loss due to diffusion on cathode side [13],

$$\eta_{conc} = \frac{RT}{n_c F} log(\frac{i_{L,c}}{i_{L,c} - i}) \tag{2.27}$$

where n_c is the number of free electrons at cathode and $i_{L,c}$ is the cathodic limiting current density. Cathodic $i_{L,c}$ is defined by the Equation 2.28, where δ is the GDL thickness.

$$i_{L,c} = n_c \, F \, D^{eff} \, \frac{c_{(O_2)}}{\delta} \tag{2.28}$$

where $C_{(O_2)}$ is oxygen concentration and can be found by using the ideal gas law equation and x_{O2} is the molar fraction of oxygen.

$$c_{(O_2)} = x_{(O_2)} \frac{P}{RT} \tag{2.29}$$

The next term is the effective diffusion coefficient D^{eff}, which depends on the binary diffusion coefficient of oxygen and nitrogen in the air and also the porosity of the electrodes. The porosity proposed is the ratio of pore volume to total volume. The typical porosity of electrodes in fuel cells is 0.4, which means 40% of the total volume consists of pores [13]. It is important to emphasise that the empirical Bruggemann correlation used in this work to calculate the effective diffusion coefficient is achieved fully experimentally and it is applicable for dry GDL; however, there are some theoretical models available in the literature, which include the effect of liquid water on effective diffusion coefficient [19] that can only be used for modelling purposes as they have not been validated by experiments. As previously mentioned, this work's focus is to show the effect of temperature on PEFC model by keeping the model simple; therefore, it is assumed a single vapour phase water only to avoid any complexity. Equation 2.30 describes how diffusion coefficient is calculated empirically using binary diffusion coefficient, $D_{(O_2,N_2)}$, and porosity, ϵ.

$$D_{eff} = D_{(O_2,N_2)} \, \epsilon^{1.5} \tag{2.30}$$

The binary diffusion coefficient is calculated by the equation 2.31, which is a function of temperature and pressure and $D^{ref}_{O2,N}$ that is looked up from the literature [14].

$$D_{(O_2,N_2)} = D^{ref}_{(O_2,N_2)} \, (\frac{T}{T^{ref}})^{3/2} \, (\frac{P^{ref}}{P}) \tag{2.31}$$

2.4 Uncertainty associated with fuel cells performance

One of the most important issues that adds complexities in design is the level of uncertainty in operating and design characteristics. Uncertainty can affect the system performance due to addressing inaccuracy in experiments that results in heat/power losses and side reactions.

Researchers have been working on different approaches to learn more about different types of uncertainty and their impact on system performance [6]. There are different types of uncertainty that need to be considered:

1. Uncertainty in physical expressions in modelling (Model Uncertainty) such as rate of reaction, heat transfer, conductivity and relative humidity models.
2. Uncertainty in chemical/physical properties (Parametric Uncertainty) such as conductivity, diffusivity, porosity.
3. Uncertainty in environmental conditions, power demands and prices (External Uncertainty).
4. Uncertainty in measurement (sensors, control systems, human error, etc.)

There is an increasingly amount of work that is dedicated to examine uncertainty in modelling. Giannakoudis et al. consider uncertainty in environmental conditions such as weather fluctuation and operating efficiency of sub-systems [20]. Giannakoudis et al. aim to achieve an optimal design system by considering the economic, environmental and operating perspective, while considering design uncertainties as fluctuations in the realistic operating conditions.

They present two main possible approaches dealing with uncertainty in modelling, including deterministic and probabilistic (stochastic) form. In a deterministic method, uncertainty can be described in either specific bound or finite number of fixed parameter values. In this case the set of discrete points for the fixed parameter values in each iteration can be used. In a stochastic method, uncertainty can be expressed through probability distribution which lies within a region where there is a probability that the parameter resides within that region. Sampling is an appropriate way of finding a set of discrete points randomly without any particular trend. There are different methods to do the computational sampling such as Monte Carlo, Latin Hypercube Sampling and etc., which can be used for different applications.

Santarelli et al. look at the impact of temperature change between 50-80$^{\circ}C$ on cathode exchange current density, internal current density and internal resistance. In this work an electrochemical model is used to determine how the V-I curve is affected at different temperatures, and also to compare the analytical results with the experimental data as it can be seen in Figure 2.3 [9]. Results presented in Figure 2.4 show that the exchange current density increases by $10^{-4} A\,cm^{-2}$ from 50 to 80°C, which means higher temperature has a significant effect on rate of reaction [9].

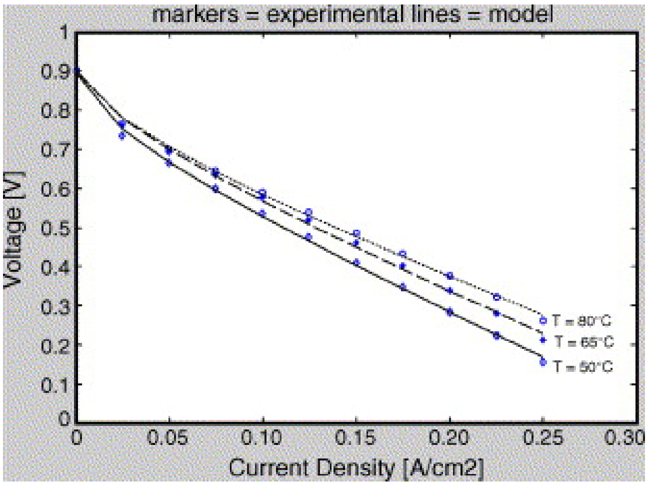

FIGURE 2.3: Polarisation curve for temperature 50°C, 65°C and 80°C are presented and compared with experimental data. markers show the experimental data and lines show modelling data

In Figure 2.5, cell resistance is plotted versus temperature as the error bars [9]. The graph shows that the cell resistance decreases with temperature by 0.3 $\Omega\, cm^2$ within the defined range of temperature. The estimated uncertainty is noted as about 1% in this work. As temperature increases, conductivity gets improved and results in lower resistance. All the above results are verified with experimental data obtained by [21] and [22], which shows a good agreements with regression and experimental results. Santarelli et al. apply an analytical approach to introduce the temperature values into the model, which can be improved by using randomisation to generate the spatial arrangement of temperature samples to avoid any association between temperatures and the outputs. It would be useful to consider a larger range of temperature in order to capture more details about the parametric variation at different temperature values.

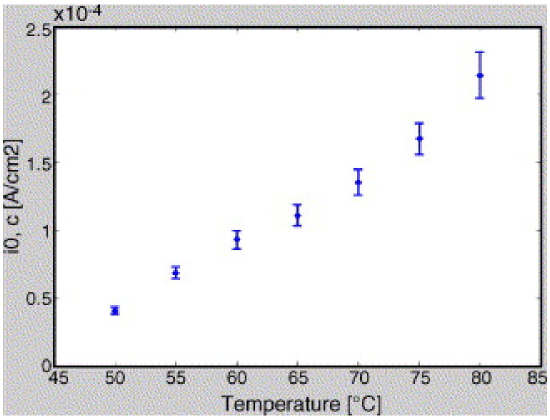

FIGURE 2.4: Values of exchange current density vs. operating temperature

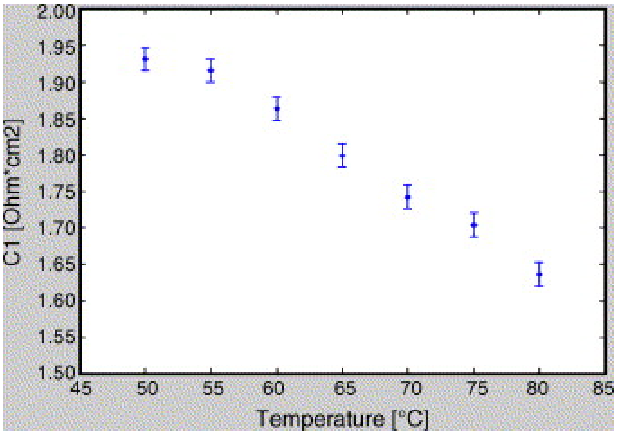

FIGURE 2.5: Values of internal current density vs. operating temperature

Mawardi and Pitchumani focus on uncertainty of materials and operating parameters, which impacts on the performance of fuel cells by applying a one dimensional, non isothermal model [6] to present the fuel cell material and operating parameters with uncertainty, which are shown in terms of continuous probability distribution with mean of μ and standard deviation of σ. The mathematical model used by Mawardi and Pitchumani looks at the molar flux of species in the x-direction across the electrodes and the membrane, which is described in Equation 2.32. Also they look at the water transfer across the membrane, which is a good conductor when fully hydrated. To determine the flux of water, Equation 2.33 is proposed to look at the net effect of electro-osmotic drag, diffusion and convection of water due to pressure and concentration gradients, where N_i is molar flux of species, ω_i is mass source for species and W_i is molar mass of species.

$$\frac{dN_i}{dx} = \frac{\omega_i}{W_i} \tag{2.32}$$

To calculate molar flux of liquid water, Equation 2.33 is used, where l subscript denoted for liquid water, D_l the diffusion coefficient for liquid water in the membrane, k_p the hydraulic permeability of the membrane, μ_v the viscosity of liquid water and η_d is the electro-osmotic drag coefficient.

$$N_l = D_l\frac{dc_l}{dx} - \epsilon_w^{mem} c_l \frac{k_p}{\mu_v}(\frac{dP}{dx}) + \frac{\eta_d I}{F} \tag{2.33}$$

Parametric analysis is performed to determine the effects of uncertainty in the operating parameters on the power density for several values of fuel cell temperatures and pressures on the anode and cathode. This paper contains a deterministic PEFC model, which presents a basic stochastic model to generate the input samples as a probability distribution [6].

This model includes model uncertainty by looking at the transfer coefficient α_a and α_c as well as operating uncertainty in cell temperature T, pressure at the electrodes P_a ,P_c, relative humidity RH_a, RH_c, stoichiometry and dry gas mole fraction at the cathode and the anode.

As it can be seen in Figure 2.6, the uncertainty in each of the above parameters are expressed as a probability distribution function and quantified by the distribution's mean value [6]. The degree of uncertainty is described by using the coefficient of variation (CV) which is computed by standard deviation over mean value ($CV = \sigma/\mu$).

The sampling method called Latin Hypercube Sampling (LHS) is the technique used in Mawardi's paper to select the combination of input uncertain parameters. This method generates N samples for M uncertain parameters. To achieve this, one dimensional distribution should be divided to N intervals and one sample is picked randomly from each interval. This method is a technique to reduce the number of runs with more effective sampling process and the main advantage of this method, compared to other methods such as Monte Carlo, is that the random variables are considered only once as each interval is sampled one time only.

The output obtained is validate with experimental values obtained by Springer et al. [15] and also numerical prediction by Rowe and Li [23]. Figure 2.7 shows that voltage loss decreases monotonically with current density due to increase in ohmic loss in the membrane [15, 23]. The obtained results show a good agreement with the numerical predictions over the entire range of current density. On the other hand, the experimental data has a sharp drop of voltage over current density due to presence of CO in the inlet hydrogen, which develops CO poisoning on the catalyst surface that results in slower electrochemical reaction. The graph shows that the sharp drop exists between current density of 0.2 and 0.4 $A\,cm^{-2}$ due to dominant limitation of mass transport rate so as current density increases the partial pressure of oxygen at the catalyst surface /cathode interface rapidly decreases; therefore, less oxygen reaching the reaction site so the sharp voltage drop appears.

Mawardi and Pitchumani also study the relationship between the number of samples and convergence of standard deviation and mean value. The goal is to determine the impact of number of samples on the mean and standard deviation power density. The results obtained show that higher number of samples achieve mean and standard deviation

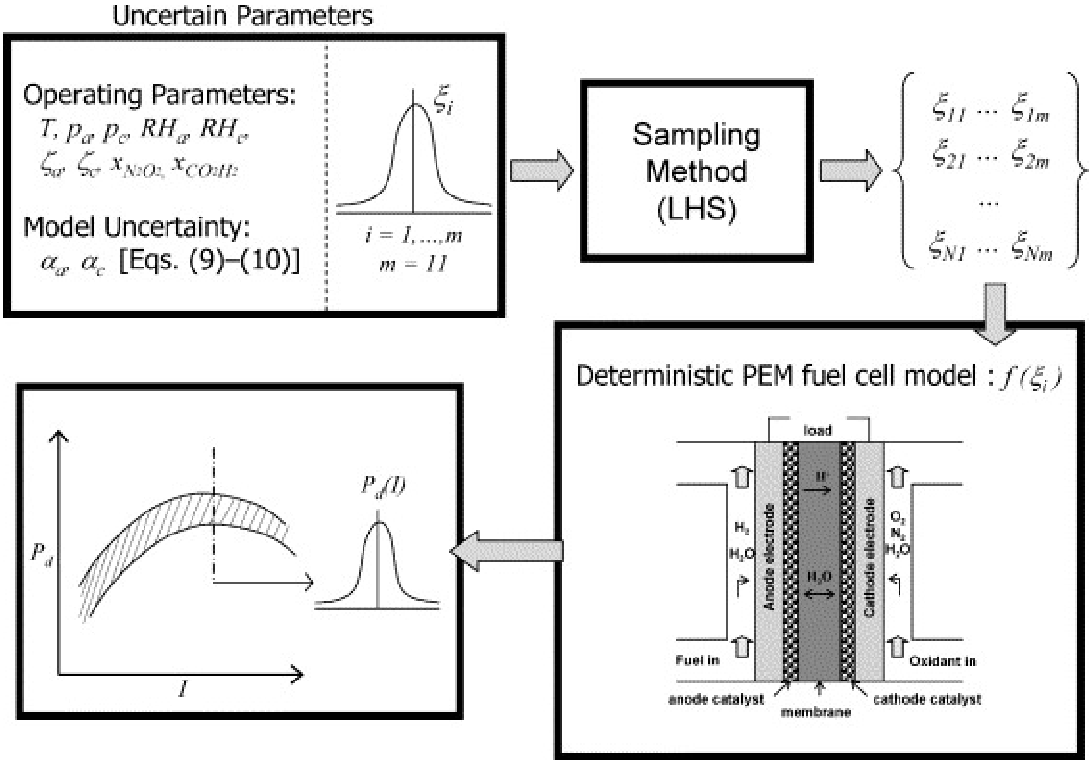

FIGURE 2.6: Methodology presented by Mawardi and Pitchuman to calculate the effect of parametric uncertainty on cell performance

convergence within 0.1% and 3.0%, while the samples are generated by Gaussian distribution [6]. The output distribution shows the skewness, which suggests nonlinearity between the power density and input uncertainty.

To characterise the distributions, Mawardi and Pitchumani calculated the CV to compare the distributions for different operating conditions. The results show that CV of the power density increases with input uncertainty for various operating parameters within the given standard deviation; however, higher temperatures lead to lower CVs of power density for all input CVs. Therefore, power density increases with temperature as does the standard deviation and mean values; moreover, the increase in standard deviation is not as significant as increase in mean values, which results in lower CV of power density with temperature.

The above statement indicates that fuel cells should be operating at high temperature to increase the mean power density; however, higher temperature would leads to larger water transport that causes the risk of flooding. Also it is important to consider minimising variance power density for low temperatures. Balancing these two considerations is one of the important concerns about robust operating regimes.

Figure 2.8 shows the mean power density versus standard deviation of power density for different temperatures at three input CVs, which shows the ratio of standard deviation of m number of parameters for N number of samples to their mean values [6]. Each sample represents a combination of uncertain parameter values, $\xi : 1, ..., m$ and the mathematical model used to simulate the performance for each sample $1, .., N$.

The graphs show that optimal mean power density increases with temperature and decreases with input CV. This result shows that the fuel cell cannot be operated at

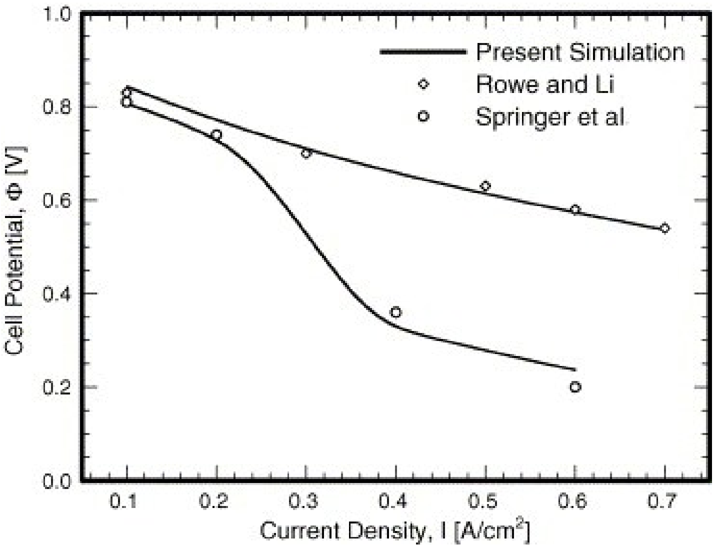

Figure 2.7: The simulation obtained by Mawardi and Pitchumani shows the relationship between the results from stochastic modelling and experimental data collected by Springer et al. and numerical data gained by Rowe and Li

the maximum power density without corresponding increase in the variability. As can be seen in Figure 2.8, for a given temperature, standard deviation increases as input uncertainty increases; therefore, in order to reach the maximum power density, it is inevitable to avoid variability [6].

The major aim is to maximise mean power density by choosing the optimal cell temperature for a given input CV and desired standard deviation power density. Results are based on parametric studies over a selected range of three principal operating parameters in order to illustrate the methodology of fuel cell design under uncertainty using stochastic simulations.

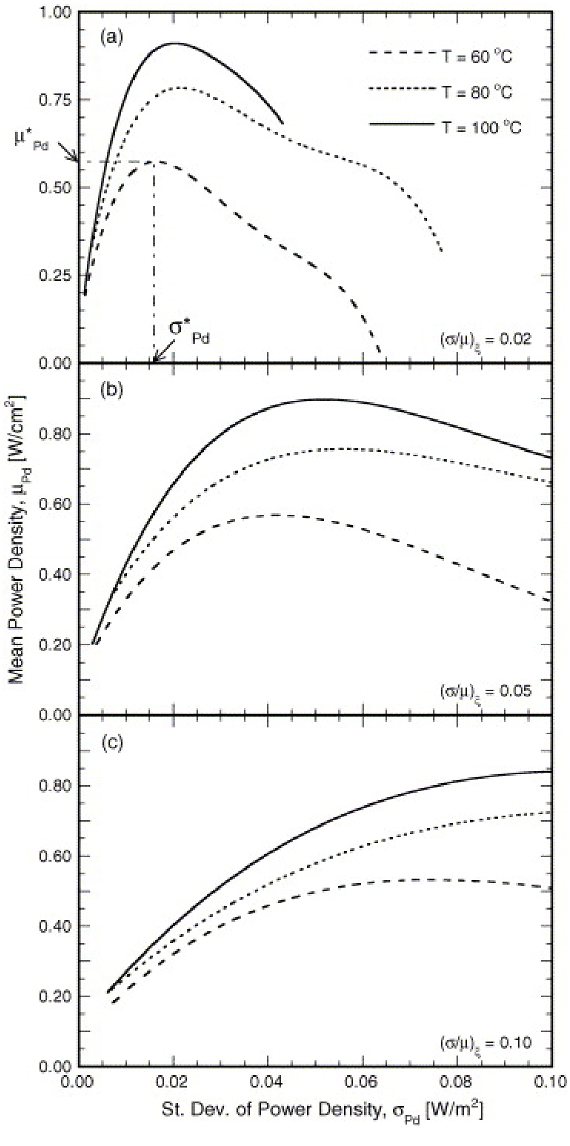

FIGURE 2.8: Presents the data for the mean power density (σp_d) in the range of 00.10 $W\,cm^2$ and for the three input uncertainty levels $[\frac{\sigma}{\mu}]_{xi}$ and the three temperatures. (a) shows power density at various temperatures at CV = 0.02, (b) shows at CV = 0.05 and (c) shows at CV = 0.1

As future work, this model can be extended to include multi-dimensional and multi-phase aspects. Also, a stochastic modelling framework may be combined with a numerical optimisation scheme to provide a robust design tool for stochastic optimisation under uncertainty.

One of the most commonly used ways of approaching uncertainty is to determine the impact of the parameter uncertainties on other variables; for example, the effect of temperature on degradation rates. Placca et al. study the effect of temperature uncertainty on the performance of PEFCs by considering the effect of degradation [24]. First, a non degrading semi-empirical model is used that is validated against experiments. The main assumption is that the concentration loss is taken as negligible; therefore, the current density is kept up to 1 $A\,cm^{-2}$ in order to prevent concentration loss [24]. Also, the electrical resistance is assumed to be negligible due to low electrical-to-ionic resistance ratio.

The simple mathematical model is used by Placca et al. as follows [24]:

$$V_{cell} = E_{Nernst} + \eta_{activation} + \eta_{ohmic} \tag{2.34}$$

Where $\eta_{activation}$ and η_{ohmic} are both negative values and also an empirical correlation is used to show the relationship between the effect of degradation rate on active area with time in Equation 2.35 [24].

$$A = 2.5 + 50exp(-K2 \times t) \tag{2.35}$$

where A is active area, $K2$ is degradation rate (hr^{-1}) and t is time (hr).

To present the results in uniform and Gaussian distributions, sampling is used to achieve the acceptable mean and standard deviation. Results show that there is a constant 1% CV of input voltage with current density are distributed for both Gaussian and uniform distributions. The non degrading model results show that voltage increases with temperature where the main assumption in this model is that all other components such as degradation rate are constant. Placca et al. also describe a similar model, which describes the impact of variation in temperature and degradation rate on cell performance [24].

In the model presented by Placca et.al, two sets are studied. In the first set temperature is assumed constant and degradation rate K_2 of the membrane is randomly chosen and in the second set K_2 is kept constant while temperature is randomly chosen. For each set, the data are presented in both uniform and Gaussian distributions. The results in Figure 2.9 is presented to show the variation of cell voltage in both cases of stochastical temperature distributions [24]. It can be seen that cell voltage are more spread for the

Gaussian distribution than the uniform one with the same probability for each interval. To show the effect of degradation rate, Figure 2.10 is presented to show the effect of degradation rate over time for Gaussian and uniform distributions [24]. It can be seen that cell voltage are more spread for Gaussian distribution, which is an expected results to get higher cell active area degradation with time.

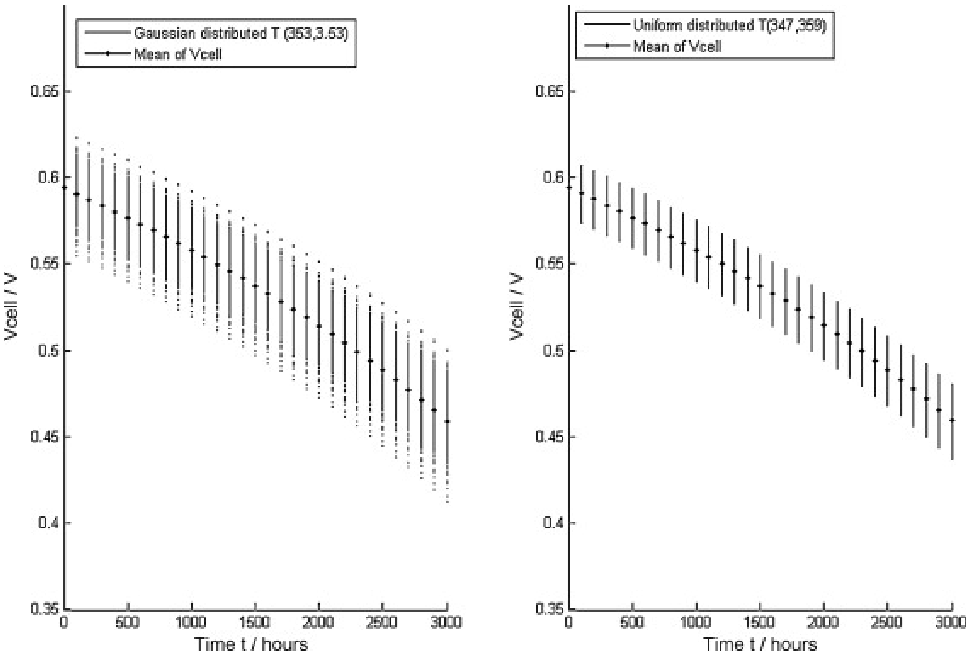

FIGURE 2.9: shows the V_{cell} for 1000 samples generated by Gaussion distribution on the left with mean temperature of $80°C$ at $30\,A$ current and $3.53°C$ standard deviation. On the right, the spread of V_{cell} is presented by uniform distribution within the range of $74 - 86\,°C$ with constant degradation rate of 0.0002

In order to analyse the effect of major parameters of this model, the Response Surface Method (RSM) is applied. RSM is a statistical method to distinguish the relationship between the variables and the response variables [24]. To determine the interaction between these two parameters an optimisation approach needs to be considered for further calculation.

In summary, this section has covered some of previous research on uncertainty applied to fuel cells performance and degradation. The next section presents some of the work related to the effect of temperature on fuel cells performed previously in literature.

2.5 Review of effect of temperature on fuel cell performance

There are many factors that lead to temperature variation in fuel cells, including pressure drop, concentration loss, humidification variation, thermal conductivity of materials and

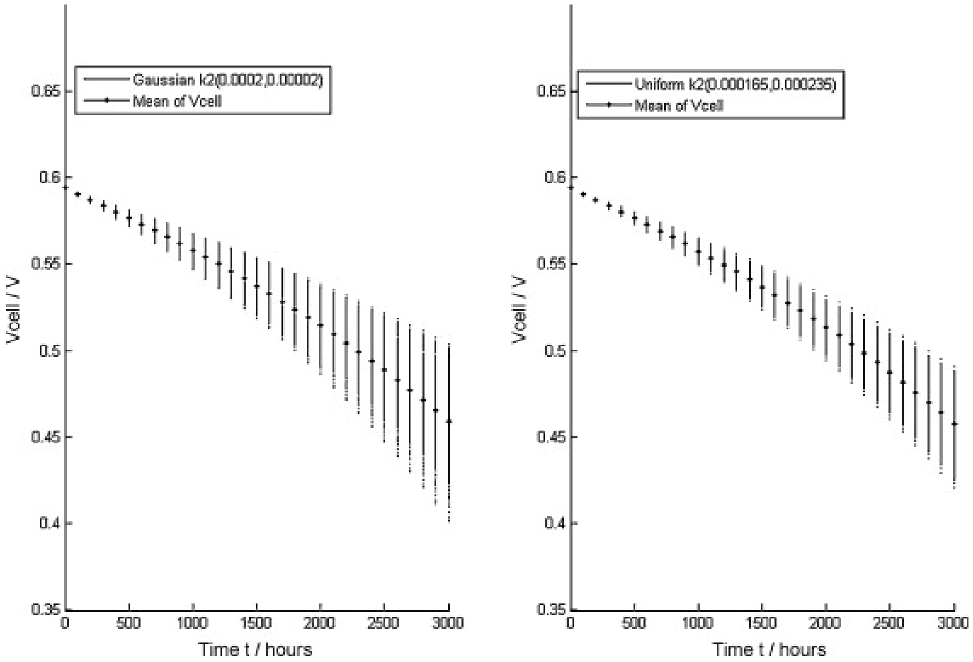

FIGURE 2.10: Cell voltage versus time at current=30 A, where temperature is constant at 80°C and degradation rate is generated randomly with mean= 0.0002 and standard deviation = 0.00002 for Gaussian distribution and for a uniform distribution with a range of 0.000165 and 0.000235

rate of water transport. Previous work has looked at the significance of temperature variation inside the cell [7, 8, 25, 26].

This section describes some of the factors causing temperature distribution such as gas flow channel width and design, existence of liquid water, and membrane thickness. The purpose of studying these causes is to estimate an appropriate temperature variation to introduce to the model in order to investigate the impact of the temperature variation on cell performance.

Misran et al. looked at the effect of temperature on water transport on cathode and anode and showing the influence of temperature at 40, 50 and 60 °C on electro-osmotic drag coefficient, water diffusion coefficient, membrane ionic conductivity and water back diffusion. A mathematical model presented by Misran et al. is a function of water activity which is itself depending on operating pressure. The experiments carried out by Misran et.al operated at 1 and 1.5 bar and 100% anode humidity and 0 to 0.5% cathode humidity [27]. The results show that the relative humidity at the inlet gas, anode, decreases with temperature along the channel length due to condensation rate, electro-osmotic drag and friction between the gas streams in the flow field.

The effect of temperature on fuel cell performance is critically dependent on cell humidity. Perez-Page and Perez-Herranz show in their paper that cell performance decreases with temperature as the membrane can be dried and results in high internal resistance [28]. To increase the performance, better hydration is required at higher temperature to increase the active area for ionic transfer and better conduction and diffusion. However, higher operating temperature can cause water evaporation in the membrane and drop the performance and on the contrary higher hydration at low operating temperature can lead to flooding in the membrane. Therefore, it is important to operate the fuel cells at the right operating and humidification temperature to avoid drying or flooding the membrane.

Pharoah et al. show that temperature distribution depends on state of water inside the cell as absorption and desorption of water causes the change in maximum temperature. Also the presence of liquid water in catalyst layer is another cause of temperature rise, as it reduces the effective diffusion coefficient of oxygen and therefore decrease the maximum achievable current due to higher resistance in active area [25]. It is shown that temperature is also significantly affected by gas flow field design and the width of the flow channels. These variables can cause the catalyst temperature to deviate between 4 to 13 $^{\circ}C$ from the end plate temperature [7]. The model used in this thesis does not capture these variables including flow channel design, two phase flow and width of flow channels in order to keep it lumped model; however, upgrading to two dimensional model can be considered as future work.

As is commonly used in fuel cell modelling, the empirical Bruggeman correlation was used in this work to estimate conductivity and diffusivity [29–31]. However, this assumes that there is no liquid water present in the cell. At low temperature and high current density there is a higher chance of liquid water formation. Under such conditions fuel cell performance may be more sensitive to temperature uncertainty and theoretical correlations such as those described by Das et al. may be considered [19].

There has been many developments in order to measure the temperature variation inside the fuel cell. One of these developments is by Inman et al. whose work is about implementing thermal sensors to obtain temperature variation inside the cell [26]. They determine that temperature is mainly affected by liquid water formation inside the cell and also heat lost due to water evaporation. Thermal sensors are also used in current research presented in Chapter 4 to measure temperature at different points across the MEA [32].

Shimpalee and Dutta looked at the temperature variation across the channel width for two different sets of input parameters [8]. One set is operating at cell temperature of 70 $^{\circ}C$ and larger molar fraction of hydrogen at the anode and oxygen at the cathode compared with set two, which is operating at temperature of 80 $^{\circ}C$ and larger membrane thickness than set one. Temperature is measured for one third, half and two thirds of the channel length. Results show that the temperature variation is between 0.1 to $4.7K$ for insulated and uninsulated boundaries.

The previous studies presented above describe the existing temperature distribution by capturing various effects on fuel cells. The purpose of this background review is to establish how much temperature is likely to vary in order to choose a sensible variation to start a statistical treatment; as a result, ±5 $^\circ C$ temperature variation is proposed to accomplish the aims of this work.

2.6 Thermal measurement

To capture the temperature distribution inside the MEA, a high resolution thermal camera is used to identify how temperature varies spatially and temporally.

There are various powerful tools to understand the performance of the fuel cells and also to validate heat transfer models including temperature mapping either with thermocouples [33–35], micro sensors measuring the temperature and humidity [36], thermistors [37] and thermal imaging [35, 38–42]. Temperature distribution inside the fuel cells is the key information to learn about water transport in order to be able to improve water management across the cell.

2.6.1 Thermal imaging and thermocouples

On of the simple tools to obtain temperature distribution is thermocouples [33]. To study temperature distribution inside fuel cells using thermocouples or micro sensors, the system needs to have an open end, where the thermocouples can reach the MEA. The down side of this approach is that the presence of the thermocouples inside the cell might affect the cell performance. Also depending on the number of thermocouples only a few points across the cell can be tested. However, on the positive side, Wilkinson et al. believe that local temperature measurements correlate well with local current densities obtained and published in literature, which means current mapping can be determined indirectly [33].

2.6.2 Open and closed cathode

The mechanical design of a fuel cell is one of the key variables which affects on the method of thermal measurements [43]. Having an open cathode is one of the options which allows air into the cell by natural convection using open flow channels to the atmosphere. There are many work in literature, which focus on using open-end cathodes to study the performance of fuel cells, temperature optimisation and imrpovement of membrane assembly [43–52].

2.7 Temperature and current mappings

Currently there is no previous work published on temperature and current mapping on PEFCs, which makes it difficult to estimate the range of uncertainty involved within the system. Therefore, in this study a high resolution thermal camera is used to record temperature for a range of 15-100°C with the images being recorded using commercial available software (ResearchIR, FLIR ATC, Croissy-Beaubourg, France)in order to measure temperature across the MEA [32].

2.8 Approach and methodology

To satisfy the objectives of this research, two models are presented, an analytical model to study the impact of temperature on intrinsic physics of the system and a statistical model to show the probabilistic effect of temperature on fuel cell performance. To establish the probabilistic behaviour, a sampling method is required to provide a normal temperature distribution into the model to show how voltage behaves with current density considering the temperature variation.

There are various types of distribution to represent the behaviour of large group of data and normal distribution (Gaussian distribution) is the most common one with symmetric shape. To avoid complexity, the input temperature distribution is assumed to be normal, which means there would be a similar probability of temperature variation above and below the operating mean temperature, in order to determine how voltage distribution would look like under temperature sensitivity at different current density.

To supply the temperature distribution, a sampling method is considered in this work to deliver the samples randomly. Monte Carlo Sampling method (MCS) is with mean operating temperature $80°C$ and standard deviation $5°C$. MCS is a computational technique to generate random numbers to consider uncertainties in physical problems and ensure a high degree of representativeness. MCS is the most commonly used techniques to generate random numbers in order to simulate some phenomena and examine the probability of the desired event occurs [53].

2.9 Summary

Previous work suggests that temperature has a significant impact on a fuel cell reaction kinetics, thermodynamics and mass and charge transfers.

This chapter reviews the previous work describing the significance of temperature on fuel cell performance; however, these studies have not analysed the sensitivity of the fuel cell performance for a given point stochastically.

The current study aims to determine the analytical and probabilistic effect of temperature uncertainty on fuel cell performance by using a simple lumped mathematical fuel cell model.

To verify the models, experiments are carried out to show the variation of temperature across the MEA.

Chapter 3

Analytical and statistical investigation into the sensitivity of PEFC performance with temperature

3.1 Model assumptions and equations

A lumped, semi-empirical, mathematical model is used to describe the electrochemical phenomena of PEFC to simulate the cell performance under temperature variation. The model considers the electrodes and the polymer membrane that form the membrane electrode assembly (MEA). The purpose of using this model is to indicate the effect of temperature on different parameters and identify their impact on overall performance. Therefore, some of the parameters, such as exchange current density and conductivity which are usually measured experimentally, are expressed by using empirical equations, which themselves can generate discrepancy due to model uncertainty. However, the focus of this work is the impact of temperature measurement uncertainty on cell performance, whereas model uncertainty is assumed negligible. In this study the following assumptions are made for the purpose of simplicity, whilst maintaining systematic fundamentals of comparison for each temperature.

The assumptions made in this work are:

- Steady state system
- Incompressible and ideal gasses
- Single phase vapour water

- Heat loss is negligible
- Pressure drop is negligible
- Current and temperature distribution is uniform
- There is no reactant consumption along the length of the flow channel (reactant distribution is homogeneous)
- No electron crossover

The equations presented in Table 3.2 are a combination of mechanistic, empirical and semi-empirical equations [10, 13, 14, 24, 54, 55]. The mechanistic models are determined based on physics of the system. These type of models are commonly known as theoretical models which are derived from physics and electrochemistry governing the subject of interest. For instance, to present the fuel cell processes in two or three dimensions, mechanistic models can be very helpful to describe the detailed and complex presentation of fuel cell performance and the flow of species in various directions.

Empirical (or analytical equations) are considered when theoretical models are not available or are difficult to obtain. In this case the data obtained from experiments should be analysed to provide a correlation between the parameters. These type of models can be constrained by the type of equipment used and might not be applicable to all relevant systems (depending on operating conditions, size and layout of the equipment). The third type of models are semi-empirical which are the combination of empirical and mechanistic models.

This work uses combination of the above models, as there are no mechanistic models available for some of the parameters (i.e. conductivity, diffusivity), in order to capture the effect of temperature on them. Conductivity and diffusivity are mainly measured experimentally rather than being calculated theoretically.

TABLE 3.1: Physical constants used in this study

Parameter	Value
Catalyst loading(L_c)	$0.125\ mg(Pt)\, cm^{-2}$
Catalyst specific area(a_{ca})	$0.4\ cm^2\, mg^{-1}$
Faradays constant(F)	$96486\, C\, mol^{-1}$
Ideal gas constant (R)	$8.314\ J\, mol^{-1}\, K^{-1}$
Membrane thickness(l)	$0.01275\ cm$
reference exchange current density(i_0^{ref})	$3 \times 10^{-9}\ A\, cm^{-2}$
Reference temperature(T_{ref})	$298\ K$
Reference pressure(P_{ref})	$1\ atm$
Reference Gibbs free energy (G_{ref})	$-228170\ J\, mol^{-1}$
Activation energy (E_c)	$76500\ J\, mol^{-1}$
Diffusion coefficient of water in membrane (D_0)	$5.5 \times 10^{-7} cm^{-2}\, s^{-1}$
Active area (A)	$25 \times 10^4\, cm^2$
Operating pressure (P)	$1.5\ atm$
Oxygen pressure (P_{O_2})	$5\ atm$
Hydrogen pressure (P_{H_2})	$3\ atm$
Water pressure (P_w)	$1\ atm$
Reference binary diffusion coefficient (D_{ij}^{ref})	$0.1\ cm^2\, s^{-1}$
GDL thickness (t_{GDL})	$0.05\ cm$
Enthalpy change (dH)	$-242367.35\ J$
Entropy change (dS)	$-84.2\ J$
Anode water activity (a_a)	0.5
Porosity (ϵ)	0.444
Number of electrons at cathode (n_c)	4
Number of electrons at anode (n_a)	2
Relative humidity of air (RH_{air})	0.5
Relative humidity of fuel (RH_{fuel})	1
Stoichiometric ratio of hydrogen(λ_{H_2})	1.25
Stoichiometric ratio of oxygen (λ_{O_2})	2
Pressure coefficient (Y)	0.5
Oxygen mole fraction (x_{O_2})	0.21

TABLE 3.2: Equations used to describe the chemical and phycical behaviour of PEFC

Names	Equations	References
Species mass flux	$M_{H_2} = \lambda_{H_2} \frac{iA}{n_a F}$	[6, 55]
	$M_{O_2} = \lambda_{O_2} \frac{iA}{n_c F}$	[6, 55]
	$M^v_{W,c} = \frac{y_{W,c,in}}{1-y_{W,c,in}} M_{O_2}$	[6, 55]
	$M^v_{W,a} = \frac{y_{W,a,in}}{1-y_{W,a,in}} M_{H_2}$	[6, 55]
	$y_{W,a,in} = RH_{Fuel} [\frac{P^{sat}_W}{P}]$	[6, 55]
	$y_{W,c,in} = RH_{air} [\frac{P^{sat}_W}{P}]$	[6, 55]
Thermodynamics	$E_0 = \frac{dH-TdS}{nF}$	[6, 10, 15]
	$E = E_0 - \frac{RT}{n_a F} \times log(\frac{p_{(w)}}{p_{(H_2)} \times p^{0.5}_{(O_2)}})$	[6, 10, 15]
Activation loss at the electrodes	$i_{0,c} = i_0^{ref} \, a_c \, L_c \, (\frac{Pr_{O_2}}{P^{ref}})^{\gamma} \, exp(\frac{-E_c}{R.T} \, (1 - \frac{T}{T^{ref}}))$	[6, 10, 15]
	$Pr_{O_2} = \frac{P_{air}}{exp(\frac{4.192 \, i}{T^{1.344}})} - P_w$	[6, 10, 15]
	$\eta_{act} = \frac{RT}{\alpha_c n_c F} \times log(\frac{i}{i_0}) + \frac{RT}{\alpha_c n_c F} \times log(\frac{i}{i_0})$	[6, 10, 15]
Ohmic loss of the membrane	$\sigma_m = (0.00514 \times c_m - 0.000326) \times exp(1268(\frac{1}{303} - \frac{1}{T}))$	[6, 10, 15]
	$c_m = 0.043 + 17.18 \times a_m - 39.85 \times a_m^2 + 36 \times a_m^3$	[6]
	$a_m = \beta \times a_a + (1 - \beta) \times a_c$	[6, 10]
	$a_a = \frac{M^v_{w,a}}{(M^v_{w,a} + M_{H_2})} \times \frac{P}{P^{sat}_w}$	[6, 10]
	$a_c = \frac{M^v_{w,c}}{(M^v_{w,c} + M_{O_2})} \times \frac{P}{P^{sat}_w}$	[6, 10]
	$\eta_{ohmic} = (\frac{l}{\sigma_m}) i$	[6, 10, 15]
Concentration loss at the electrodes	$i_{L,c} = n_c \, F \, D^{eff}$	[6, 55]
	$D_{eff} = D_{(O_2,N_2)} \, \epsilon^{1.5}$	[6, 55]
	$D_{(O_2,N_2)} = D^{ref}_{(O_2,N_2)} \, (\frac{T}{T^{ref}})^{3/2} \, (\frac{P^{ref}}{P})$	[6, 55]
	$c_{(O_2)} = x_{(O_2)} \quad \frac{P}{RT}$	[6, 55]
	$\eta_{conc} = \frac{RT}{n_c F} \, log(\frac{i_{L,c}}{i_{L,c} - i})$	[6, 55]

3.2 Analytical treatment

The analytical approach provides the understanding about the physics of the system and how temperature makes an impact on polarisation curves. The results are presented in the form of $\frac{dV}{dT}$ to propose a map that can be helpful to predict the performance for a given temperature and current density.

In the most recent studies, the operating temperature for PEFC is reported for a range of 30 to 80° C [17, 56–58] depending on hydration of the electrodes and membrane; however, Das et al. shows that the effect of temperature on polarisation curves is most significant at high current densities.[58]. To determine the sensitivity of cell voltage with the intrinsic physics of the system with respect to temperature and current density, the differential of cell voltage with respect to temperature is used at different absolute temperatures from 30 to 90° C. To estimate the gradient of voltage with temperature, numerical differentiation is used with temperature step size δT of 0.05. The smaller step size value provides more accurate approximation of the gradient. To determine a good confidence in the results 0.05 is chosen for a step size in this work to calculate the gradient for over 1000 points within the defined range of temperature. Equation 3.1 describes how voltage as a function of current density and temperature, $V(i, T)$ changes with respect to temperature:

$$\frac{dV}{dT} = \frac{V_2 - V_1}{T_2 - T_1} \tag{3.1}$$

To determine dV/dT, the mathematical model presented in Table 3.2 needs to be running at various operating temperatures from 30 to 90°C to plot the obtained voltage versus temperature at various current densities as it can be seen partially in Figure 3.1.

Figure 3.1 shows that the differential can be found by small step changes along the curve in order to find the most accurate value for the slope. This section looks at the derivatives of the voltage with respect to temperature and current density to present the three dimensional surface map of $\frac{dV}{dT}$ versus temperature and current density. As mentioned previously, this work does not consider the crossover effect on fuel cell performance due to using simple lumped model for calculations and also to eliminate the effect of losses due to hydrogen crossover; therefore, the high *OCV* is obtained from the theoretical study, which might be slightly higher than what is usually measured practically.

The key purpose of this analysis is to obtain an understanding about the range of uncertainty involved within the physics of the system. This study helps the fuel cell developers to confirm that the voltage variation obtained from the cell is within the changes in the physics of the system and if it exceeds the range of variation, there are other variables, which need to be considered as a source of producing uncertainty including the effect of degradation and membrane swelling.

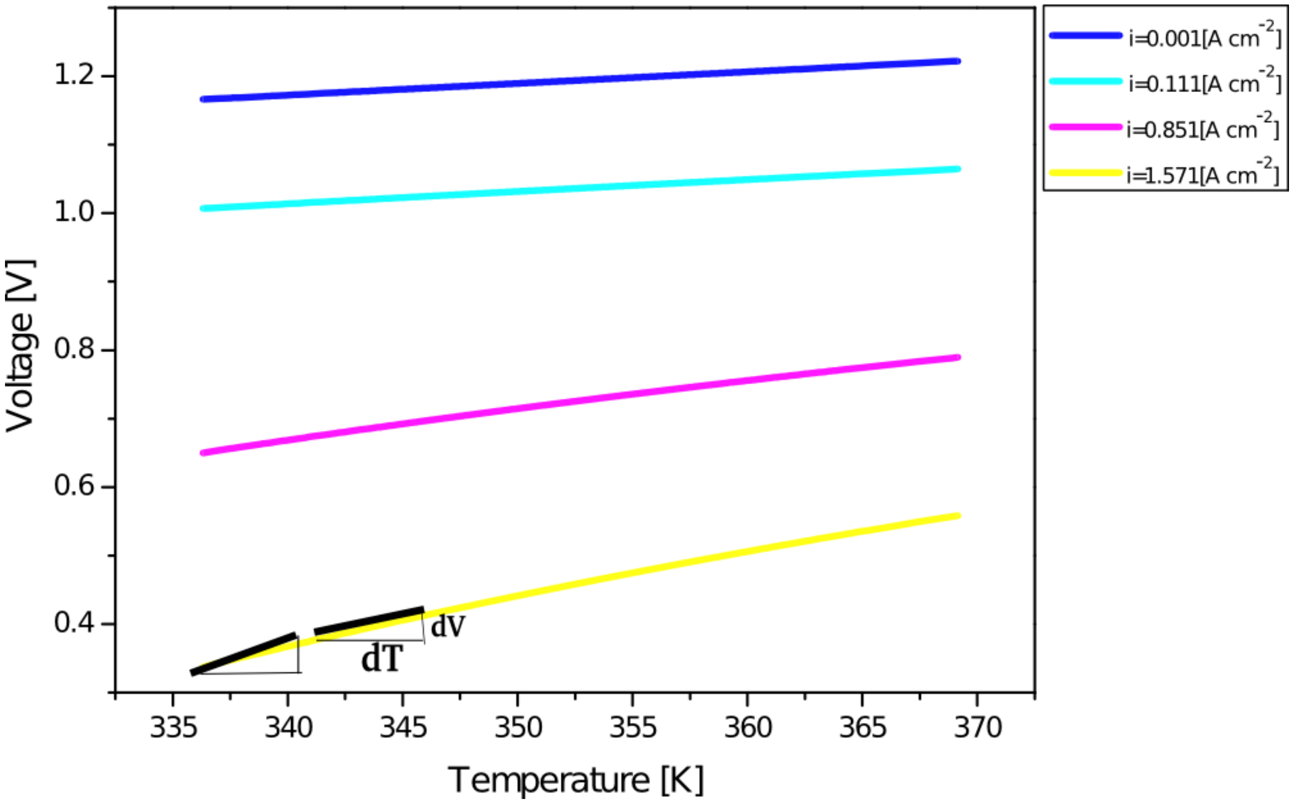

FIGURE 3.1: Shows how the gradient of a curve can be found analytically

3.3 Statistical treatment

To predict the probabilistic deviation of cell voltage due to uncertainty in temperature, a statistical analysis is used that employs a Monte Carlo Simulation (MCS) to provide a random normal distribution of temperature samples. A normal distribution (Gaussian) is employed as it is the most widely used distribution with similar standard deviation value on both sides of the mean value, which makes the distribution symmetric [59].

To establish the effect of temperature, the standard deviation of $\pm 5°C$ is selected for 10,000 samples. Previous studies have reported 3-11 $°C$ temperature variation in a fuel cell due to different uncertainties and operating conditions [7, 8, 24]. Also the tests carried out on the Intelligent Energy (IL) stack in this work, justifies the similar value of $12°C$ across the cell. Therefore, to characterise the effect of temperature on a fuel cell performance, the average of $\pm$ $5°C$ is selected preliminary to assess the performance of the system. It is important to choose a suitable sample size which is large enough to give sufficient confidence in the results but not so large as to lead to unnecessary processing time. To assess this, the model was run from 100 samples to 100,000 samples in order to develop a distribution curve.

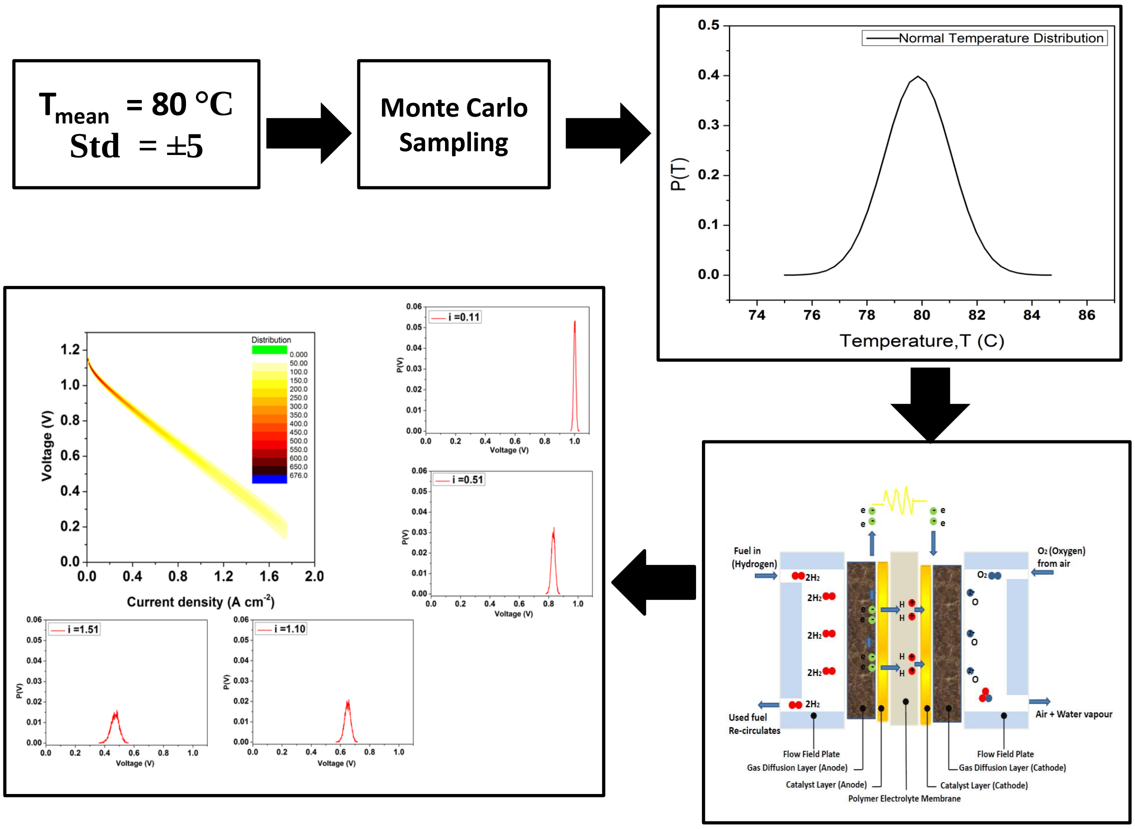

Figure 3.2: Stochastic sampling and deterministic model

Due to the nonlinearity in this model, the running time would significantly increases above the sampling size of 10,000 due to processing more data. To find the sample size, the variance of error for MCS generating input temperature samples is calculated.

Table 3.3 shows how different sample size and bin size can affect the variance of error, V_{error}. A sample size of 10,000 was chosen as a suitable trade-off between accuracy and processing time. Bin is defined as a disjoint category that mainly used for statistical analysis to represet a group of observations (i.e. histogram).

To generate the samples, Equation 3.2 is implemented in Octave [60], a high level programming language that provides access to a number of solvers for linear and nonlinear numerical computations [61], where T is temperature, T_{mean} is mean temperature, σ is standard deviation and randn(n,m) is a function that randomly generates a normal distributions of n numbers in m columns.

$$T = T_{mean} + \sigma.randn(n, m) \tag{3.2}$$

The obtained data are characterised by statistical analysis: skewness and coefficient of variation (CV), to present the degree of asymmetry of the distributions and measure

TABLE 3.3: Shows how number of samples and bin size affect the accuaracy of the results

Sample size	**Bin size**	$\mathbf{V_{error}}$
100	10	0.5
$1,000$	100	0.158
$10,000$	$1,000$	0.05
$100,000$	$10,000$	0.0158

of dispersion of voltage. As shown in Figure 3.3, positive skew shows that there is a longer tail on the right side of the mean value and negative skew indicates the opposite, when there is a longer tail on the left side of the distribution. A distribution curve is classified as symmetrical when the skewness is zero. Because of the nature of the model and logarithmic expressions used in the model, Equation 3.3 is used to calculate the skewness, where N is the total number of samples [62].

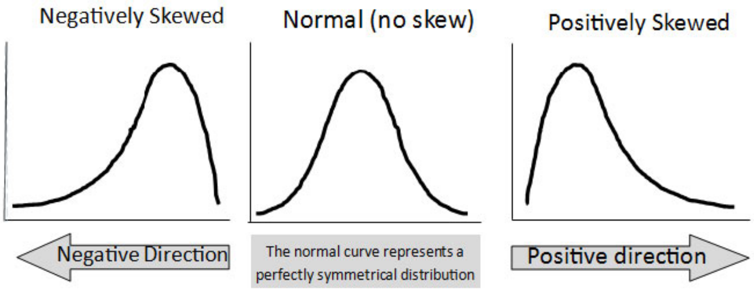

FIGURE 3.3: This figure shows the zero, positive and negative skewness

$$Skewness = \frac{(\Sigma(x - \mu(x))^2)/N}{\sigma^3} \tag{3.3}$$

To verify the skewness, Equation 3.4 is used to indicate the degree of skewness by comparing the obtained values with the standard error of skew (SES)[63].

$$SES = \sqrt{\frac{6}{N}} \tag{3.4}$$

The Coefficient of variation (CV), which is often expressed in percentage is used to compare the standard deviation of data at diverse mean values [6], where σ is standard deviation of distribution and μ is the mean value [64].

$$CV = \frac{\sigma}{\mu} \tag{3.5}$$

3.4 Summary

The two approaches presented in this work set out to determine the effect of temperature variation on cell polarisation V-I curves to establish a voltage distribution map for different current densities and temperature. This map tend to show a comparison of the sensitivity of the physics of the cell and the continuous (probabilistic) effect of temperature on cell voltage in order to propose an effective polarisation area or 'band' in contrast to the most commonly used term polarisation 'curve'.

This approach can be also used to establish whether the cell performance is affected by other criteria such as degradation of the membrane or GDL, presence of liquid water and poor diffusion due to low porosity if the variation of cell voltage exceeds the presented polarisation area under temperature uncertainty.

Chapter 4

Experimentation

This study looks at different experiments to investigate temperature variation across the MEA using thermal camera and temperature/current mapping. To validate the model presented in the previous chapter, a commercial closed-cathode fuel cell is used to validate the model at operating temperature of 80°C.

To look at temperature measurement uncertainty across the MEA, industrial fuel cell stack and a single cell provided by Intelligent Energy are used to measure how much temperature varies for given points with time using thermal camera and temperature/current mapping. Primarily, a thermal camera was used to look at the middle cell of an IE stack as well as a single cell to compare the temperature variations after 25 minutes of reaching equilibruim. However, during my writing up, IE provided us with a new temperature/current mapping plate, which allowed us to look at larger area inside the fuel cell rather than only capturing the external surface temperature with thermal camera.

As it can be seen in Figure 4.1, this chapter describes the tests run by the commercial closed-cathode fuel cell, an industrial single cell and a stack provided by IE using the temperature/current mapping approach to establish temperature distributions due to measurement uncertainty inside the MEA.

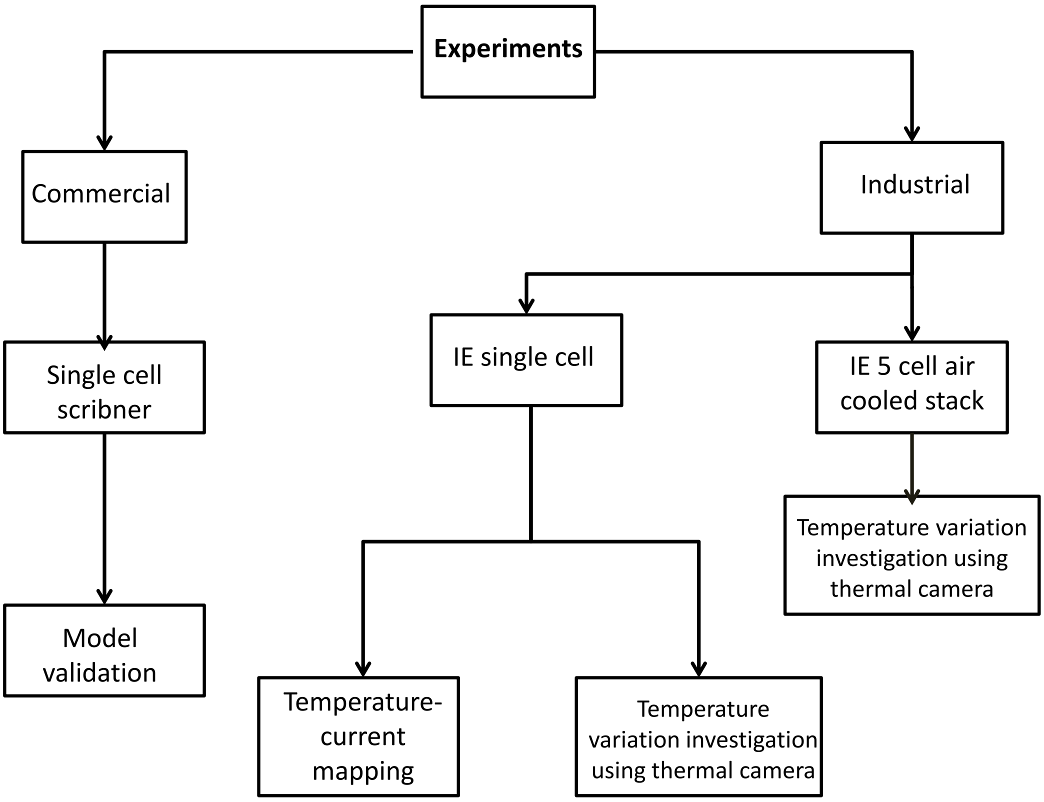

FIGURE 4.1: Summarises the experiments and the approaches taken in this study

4.1 Commercial single cell operation to validate the model

To validate the mathematical model with experiment, fuel cell testing was conducted using a commercial single fuel cell. As can be seen in Figure 4.2, two graphite monopolar plates were sandwiched by two gold-plated current collectors that are connected to load bank cables. To reduce any discrepancy in the cell voltage measured due to resistive losses in the load bank cables, voltage sense leads were attached to the PCB current collectors. To measure the temperature of the cell, thermocouples were inserted into the heating plates and connected to an external heater.

The aim is to get the polarisation V-I curves at the temperature 80° C and use the data collected to validate the model; to establish the discrepancy of the thermocouples, the temperature on external heater is noted in order to account for the level of uncertainty involved in measurement. In this case there is 0.25% fluctuation of temperature due to the external heater.

To determine the polarisation curves, the fuel cell is operated at flow rate 18 $ml\,A^{-1}\,min^{-1}$, with anode and cathode relative humidity of 100% and oxidant and fuel temperature

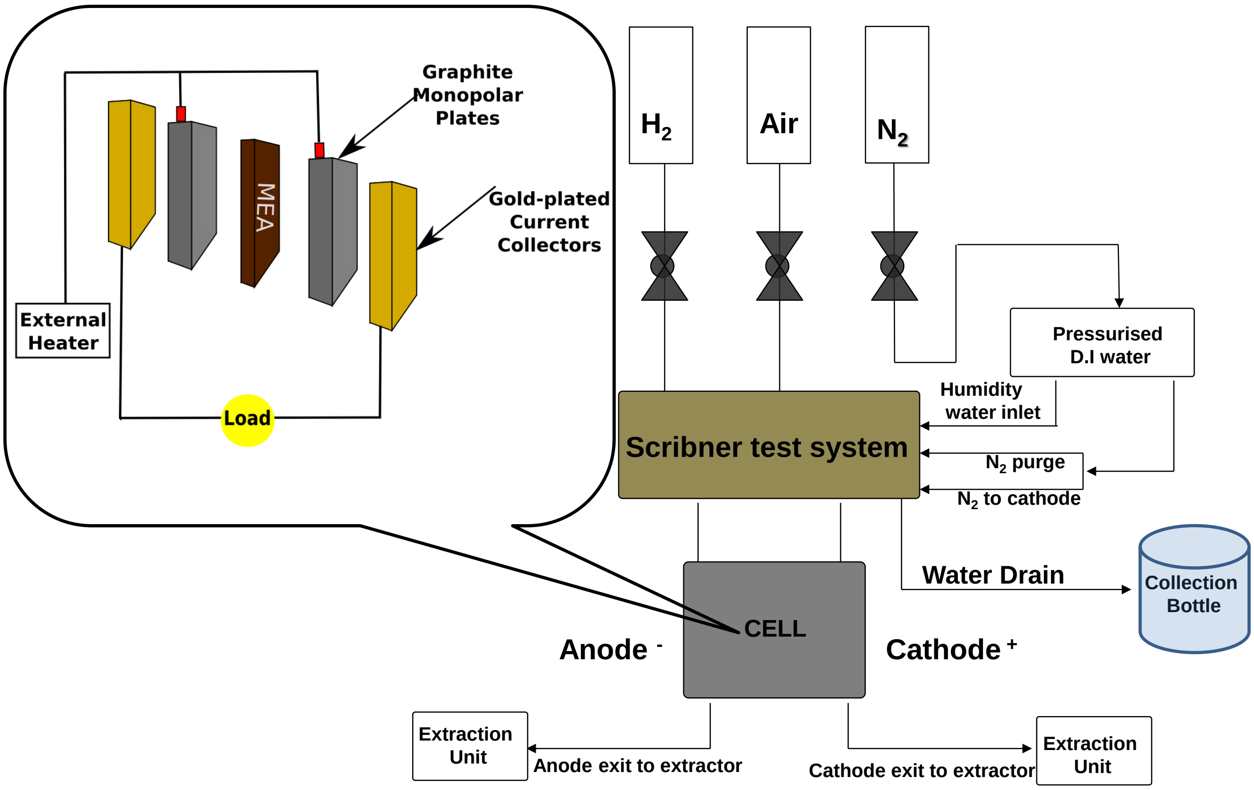

FIGURE 4.2: Schematic diagram of a single cell and the scribner

80° C. The membrane dimension is 64 cm^2 with active geometric area of (GDL) 3.3 $cm \times 1cm$.

The data are recorded by increasing the load by 50 $mA\,cm^{-2}$ steps from OCV and to allow the corresponding voltage to stabilise for 60 s before moving to the next load level.

To activate the newly fabricated polymer electrolyte membrane fuel cell, a conditioning process is needed to make the new cell ready for the performance. This break-in period can take hours or days to establish the maximum performance depending on the type of the cell and the experiments. The process is to increase the performance gradually until it reaches a plateau without any further increase.

4.1.1 Methodology

The MEA cell had to be conditioned before the experiment started in order to reach steady state and to obtain optimal performance from the fuel cell. The membrane has to be well hydrated to reduce resistivity and the temperature of the cell and gases were allowed to reach the required operating value of 80°C in order to reach optimal conductivity levels. While the desired temperatures are attained, which took about an hour, the fuel cell has kept at a constant current density of 0.1 Acm^{-2} for 15 minutes, which has then increased to 0.3 Acm^{-2} for 15 minutes and finally to 0.5 Acm^{-2} for 30 minutes. The lower current densities were used at the start of the conditioning because at this stage the membrane is still very dry, which means high resistivity and lower conductivity, making it unlikely to sustain the reaction at higher current densities. However, as the temperature of the cell and gases reaches the optimum operating values the membrane resistivity reduces and the cell is able to operate at higher current densities. During conditioning, the MEA is processed and a drastic improvement in performance has seen by a sudden increase in voltage, which is due to membrane humidification from the gases and also self-humidification as a result of the cell reactions taking place. The cell conditioning stops when the operating parameters are at the optimum level and the voltage generated at various current densities are stable over a period of time.

To validate the model with experiments, polarisation V-I curves obtained from the tests completed on a commercial single cell to fit the model. The manipulation parameters are chosen to be activation energy E_c, porosity ϵ and open circuit voltage, E_0. By data fitting, it can be seen how far the design values set in the model differ from the experiments.

4.2 Industrial (IE) fuel cell to study temperature variation

To validate the model with a fuel cell stack, an industrial fuel cell test rig provided by IE is used to operate with hydrogen as a fuel and air coming from the atmosphere that has been through the cooling channels by fans. Figure 4.3 shows the schematic diagram of the testing rig. It can be seen that pure hydrogen enters with pressure of 5 bar through two valves, which are used to ensure a safe hydrogen shutdown in a case of emergency. If there is any issue with hydrogen, the valves are designed to open and close manually or automatically to avoid any incidents. Then the hydrogen goes into the pressure regulator to get to a pressure of 0.4 bar. To measure the pressure of hydrogen to ensure it is stable and not dropping, hydrogen goes into the pressure transducer before entering the cell. Hydrogen stays in the cell unless the purge valve opens, when hydrogen flows into purge bottle and then extractor. The main purpose of having a purge bottle is to collect liquid water from the cell.

On the other side, air goes into the cooling channels from the cathode side and a PID controller is used to control the temperature to avoid the stack from overheating. To cool down the system, three fans on the cathode side are used to force the air into the cooling channels when the system gets heated up. A K-type thermocouple was used to record the internal temperature in the central area of the fuel cell and operate the PID controller.

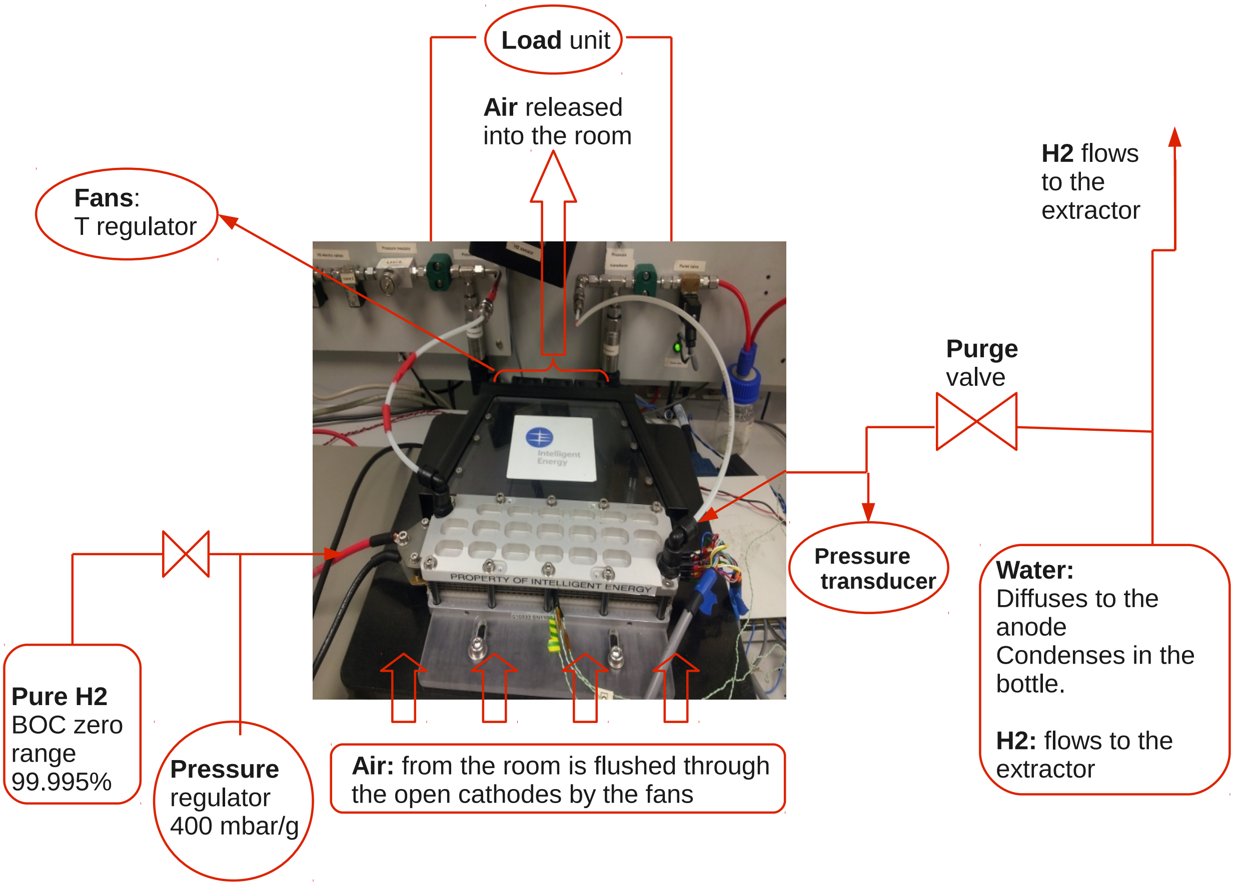

FIGURE 4.3: Schematic diagram of IE air cooled stack

A similar configuration of air cooled stack has used for a single cell to operate the system. The only difference is that the cooling fans used for the stack are more powerful due to higher generated heat.

4.2.1 Methodology

Temperature mapping, either with thermocouples [33–35, 50], micro sensors (measuring the temperature and humidity)[36], thermistors [37], thermal imaging [35, 38–42, 65] of fuel cells has shown to be a powerful tool to understand the performance and validate heat transfer models. Having an open cathode fuel cell stack has the advantage of making the temperature measurement process easier by using the thermal imaging approach. As stated in Chapter 2, open cathode operation relies on natural convection of air into the electrodes rather than pressurised feeding oxygen into the system.

Thermal imaging was performed using a 640 × 512 focal plane array InSb camera (SC5600MB FLIR, UK). The camera was calibrated for the temperature range in question $(15 - 100\,^{\circ})$ C with the images being recorded using commercially available software (ResearchIR, FLIR ATC, Croissy-Beaubourg, France). Images were recorded at a frequency of 25 Hz for a period greater than 10 minutes to ensure a statistically significant number of data points were collected.

To determine how the temperature changes at a specific current density in different locations along the cell, the tests are carried out in middle cell of IE stack only for the purpose of simplicity, which can be seen in Figure 4.4. To measure the temperature of the middle cell, the top and bottom cells of the stack were covered with card papers and also to reduce the background noise causing false reading, the back of the thermal camera was covered with cloth to allow the readings less affected by external uncertainties. These tests are carried out to compare temperature distribution in a stack and a single cell, both provided by IE, to show the effect of configuration and flow channels and sizing on generating uncertainty.

The camera starts recording for 10 minutes after the system reached the equilibrium. The reason for choosing 10 minutes is to provide sufficient number of data for statistical analysis. The system operates and recorded at constant temperature for current densities of 0.33, 0.5, 0.67 and 0.78 Acm^{-2}.(20, 30, 40 and 46 A)

To establish the effect of time on distribution of temperature at different locations along the cell, the temperature for given points are recorded for 25 minutes once the system reaches equilibrium. The purpose of these tests are to determine temperature distribution with time and how the mean of the distribution changes. The objective is to establish the probability of temperature uncertainty with time and the impact on the shape of the distribution and the degree of asymmetry.

As shown in Figure 4.4 there are four points selected on the MEA of the middle cell and it is named SP1 to SP4 from fuel entrance towards the 'dead-end'. This work looks at the distribution of temperature variation over time at these four points to compare how time and distance affect on temperature variation whilst other variables are kept constant. The similar tests are carried out on a single PEFC for comparison, which the results are presented in Figure 6.3.

4.2.2 Current and temperature mapping on an industrial (IE) single cell

This section aims to confirm the range of temperature measurement uncertainty in PEFCs using current/temperature mapping at 16 segments of the IE PEFC single cell. As shown in Figure 4.5 if a single cell is divided to 16 equal segments, air enters from the top(segment 1-4) and leaves the cell from the bottom (segment 13-16) and hydrogen goes

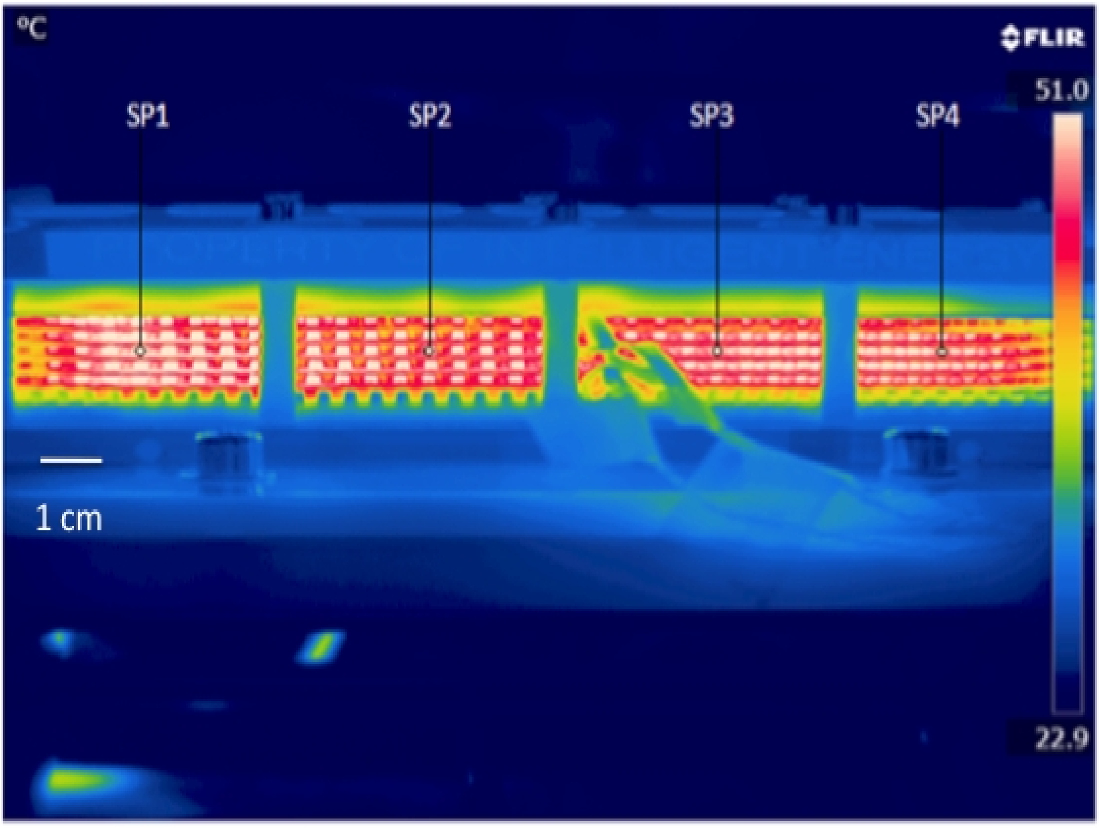

FIGURE 4.4: Thermal image of fuel cell stack after equilibrating for 25 minutes. This figure shows temperature distribution in four given points along the MEA of a middle cell of an industrial IE stack to compare how temperature distribution changes along the MEA considering air entering from back to front and the fuel enters from left to right

in from the left (segment 1-13) and leaves from the right (segment 4-16) [66]. This sensor plate uses shunt resistors and copper meanders to measure current and temperature at each segment.

The data obtained from the current/temperature mapping are used to fit the model presented in this work and also to compare the results with the modelling study described in chapter 3. The aim is to use the temperature and current mapping to determine temperature variation temporally and spatially and compare it with the work presented in Chapter 3, where temperature uncertainty is kept constant as $\pm 5°C$ along the polarisation area. The challenge is to show that in reality temperature uncertainty changes with wider variation with increasing current densities in polarisation area.

4.2.3 Methodology

To establish the empirical relationship between current density and temperature, Figure 4.7 is obtained to show the relationship between temperature and current density. It

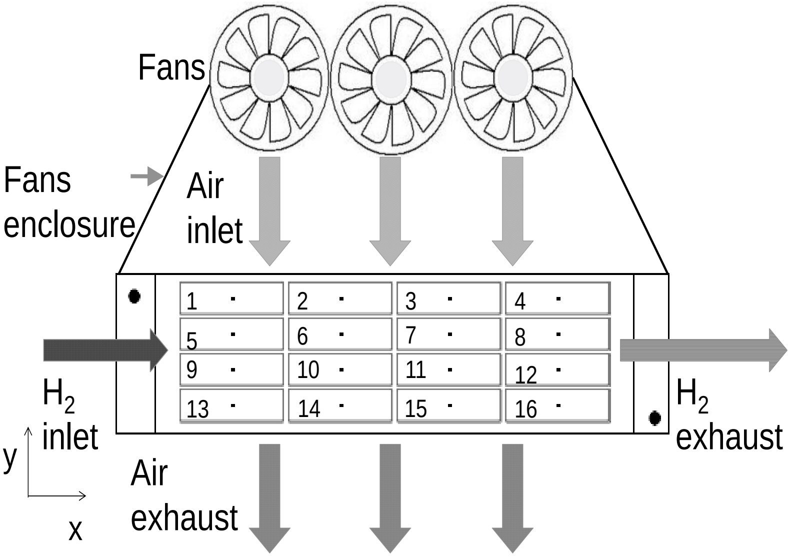

FIGURE 4.5: Shows a top view from a single cell splitting to 16 parts, where fans blow air from top (seg 1-4) to bottom (seg 13-16) and hydrogen enters from left (1-13) to right (4-16)

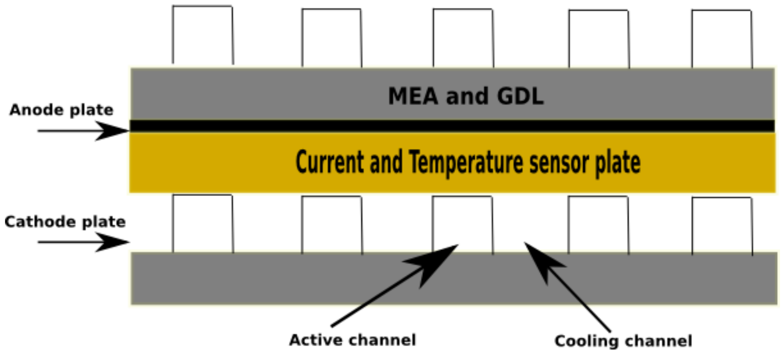

FIGURE 4.6: Shows how temperature current sensor plate lies within a fuel cell

can be seen that temperature increases exponentially with current density, which can be the results of heat accumulation due to larger current flow. Figure 4.7 is used to calculate the empirical correlation between temperature and current as it is described in Equation 4.1.

$$T = 36.60583i^3 - 19.36523i^2 + 26.69182i + 22.83177 \tag{4.1}$$

Where T is temperature and i is current density. Equation 4.1 is added to the mathematical model described in chapter 3 to simulate voltage.

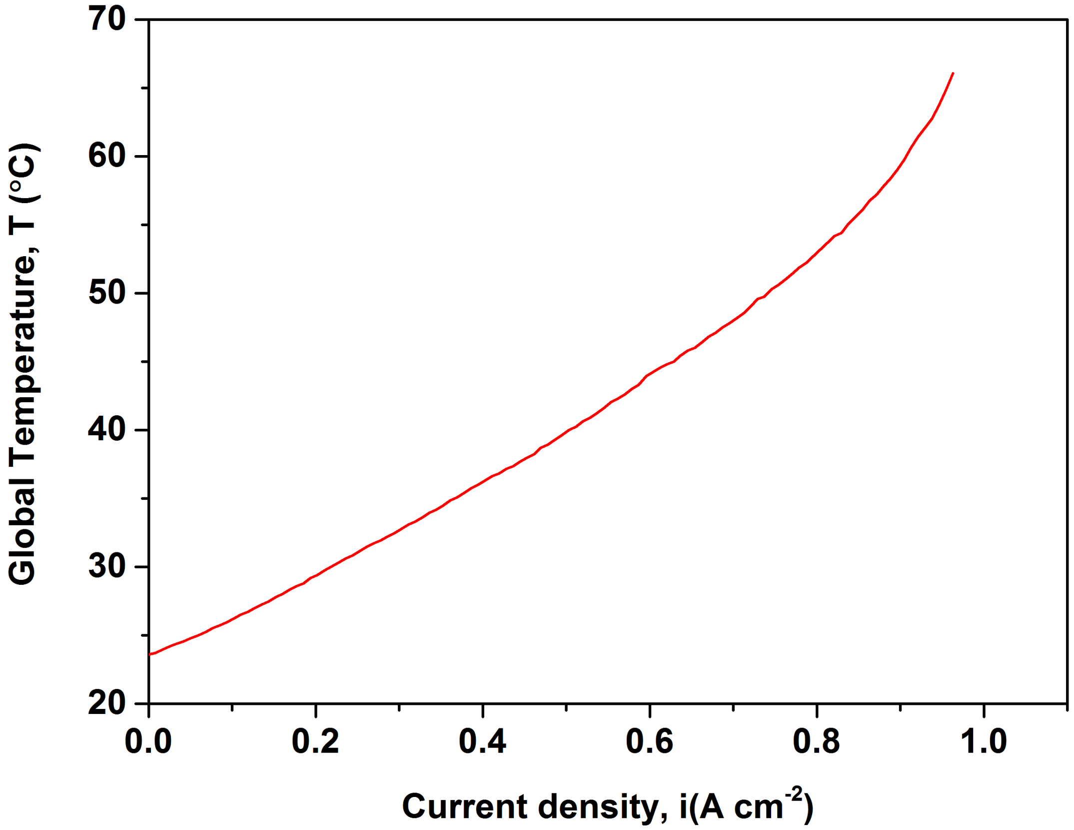

FIGURE 4.7: This graph shows how global temperature changes with current density over 16 segments of PEFC stack. The temperature values are found by taking the average of temperature over 16 segments

4.2.4 Validation of the model by using an industrial (IE) stack

This section shows a model validation study by using real data from literature [15, 57]. A parameter estimation technique is applied in this work to determine the key model parameters and also to validate the overall model behaviour by comparing the performance of a system experimentally and theoretically.

The presented empirical correlation that is used to fit the model into the experimental data is presented in Figure 4.8. This figure shows that there is a good relationship between the experiments and the model used in this paper; however, there is a slight difference when it gets to higher current density where mass limitation region dominates, which can be the result of model limitation to capture precisely what happens inside the stack.

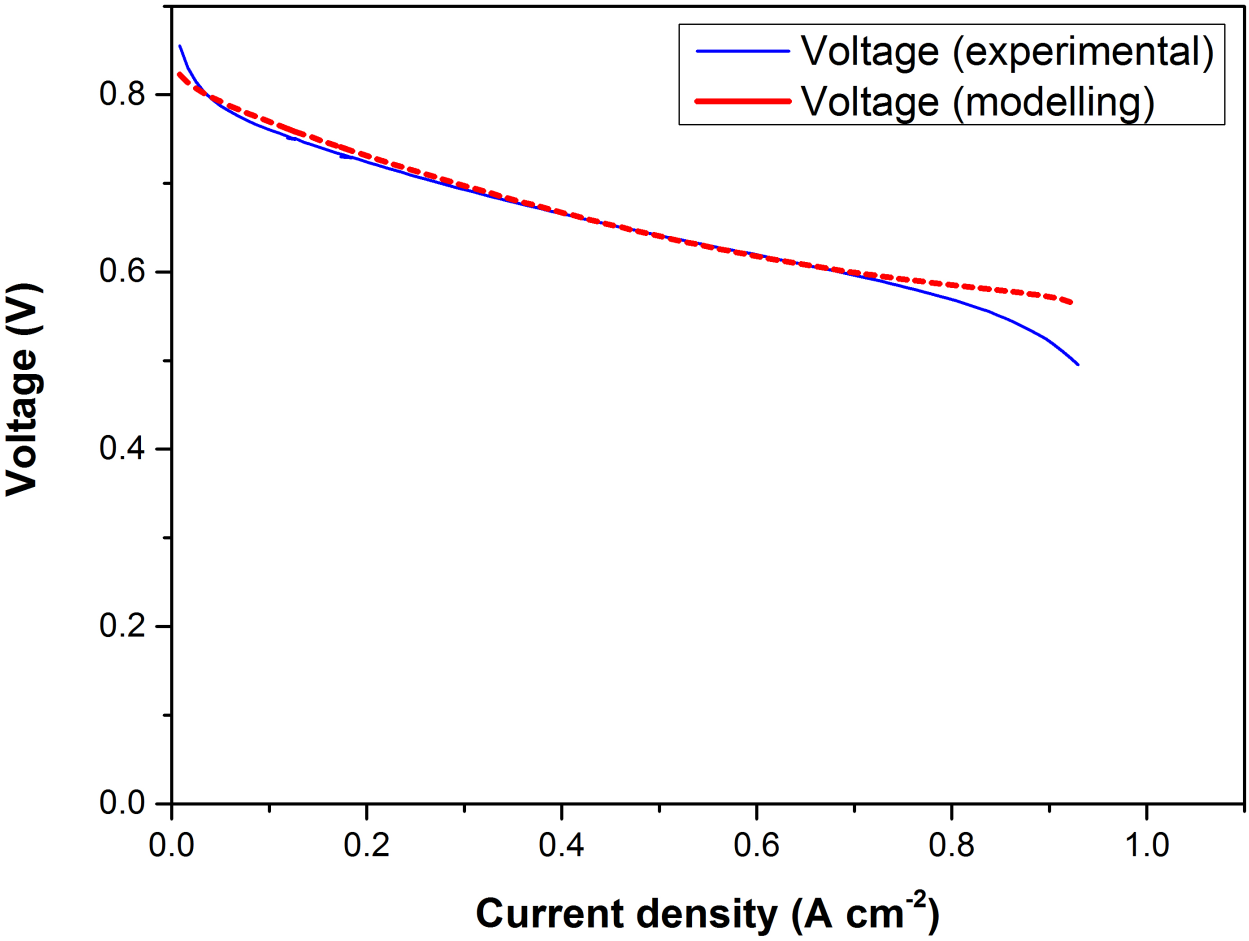

FIGURE 4.8: Compares the experimental data with modelling results

4.3 Summary

This chapter describes the experimental setup of two different fuel cell systems for two purposes. First to validate the model presented in Chapter 3 using a commercial single cell to look at temperature variation and secondly to use the IE fuel cell stack and the IE single cell to measure temperature using a thermal imaging camera. Thermal imaging is one of the most common ways of thermal measurement. The use of thermal imaging is described to measure temperature on the middle cell in a 5-cell air cooled PEFC to study the effect of time on temperature variation at four different points along the MEA of the cell.

Temperature-current mapping is a useful technique to measure the thermal sensitivity of different parts of the cell with respect to any changes in operating conditions. In this work, this technique is used to capture the sensitivity of single PEFC in order to compare the obtained results with the theoretical data presented in the previous chapter.

Chapter 5

Modelling results

This section aims to show the sensitivity of fuel cell performance with temperature by looking at voltage distribution across the polarisation curve. To characterise the voltage distribution, statistical and numerical methods are performed to establish the effect of analytical and stochastic approaches on the fundamental physics of fuel cell performance.

5.1 Analytical approach

As mentioned in previous chapters, polarisation curves are made of different voltage losses in fuel cells and temperature has a significant impact on these losses. The Figure 5.1 shows a case study on the effect of three temperature values on the thermodynamics, kinetics, ohmic and mass limitation losses in PEFC model.

It can be seen that temperature has a greater impact on internal membrane resistance in comparison with kinetics and mass transport limitations, which they are both a function of temperature with respect to exchange current density and diffusivity, respectively. Internal resistance depends on conductivity, which itself is a function of temperature and membrane hydration.

Figure 5.1(a) shows the impact of temperature on OCV which is independent of current density and changes with reactants and products concentration. The graph shows that at higher temperature; less free energy is required to do useful work, in other words, for hydrogen oxidation the Gibbs free energy decreases with temperature which results in reduced OCV as it is described earlier in Equation 2.11.

Figure 5.1(b) shows that voltage loss due to kinetics of reacion increases with temperature, which results in reduced current flow.

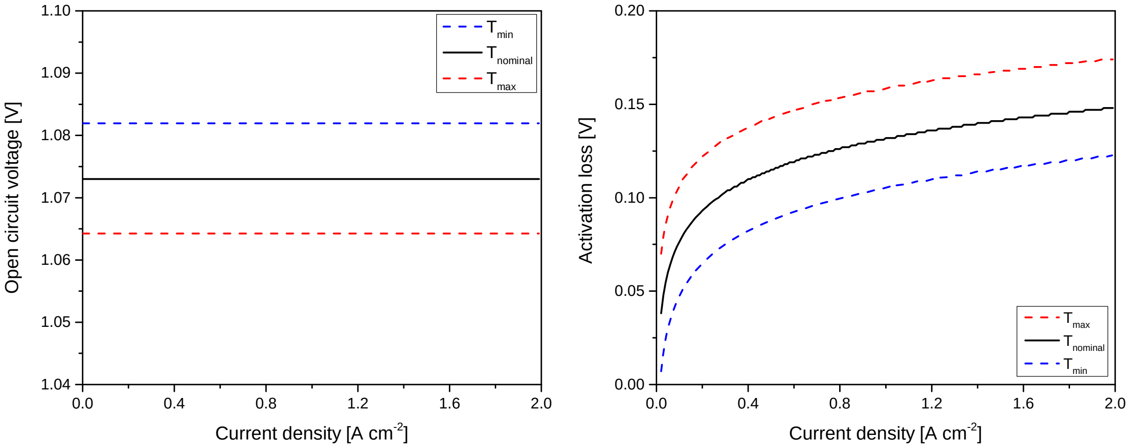

(a) Open circuit voltage decreases with temperature

(b) Activation loss vs. current density for 3 temperature values

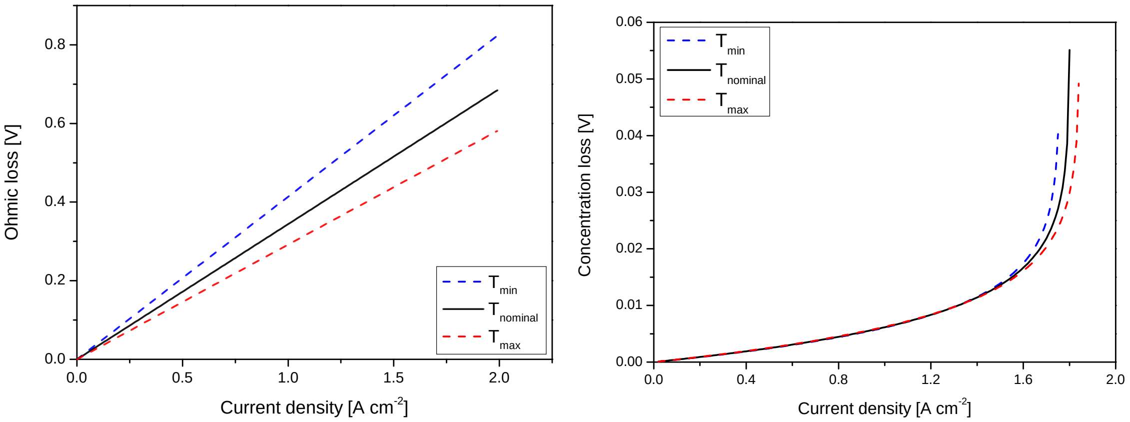

(c) Ohmic loss vs. current density for 3 temperature values

(d) Concentration loss vs. current density for 3 temperature values

FIGURE 5.1: Voltage losses are plotted separately versus current density for three temperature values where $T_{nominal}$ is 80° C and T_{min} and T_{max} are the lower and higher by 5° C than the nominal temperature. This figure shows the behaviour of losses with temperature variation versus current density

Ohmic loss is due to resistance to charge transfer and it is dominated by conduction in electrolyte membrane. Figure 5.1(c) shows that Ohmic loss is also affected by temperature due to dehydration of membrane and consequent Ohmic resistance increase.

Concentration loss (mass limitation loss) dominates at higher current density. Temperature improves the diffusion of species into the GDL/catalyst leading to better and faster supply of reactants, which can be seen in Figure 5.1(d).

The graphs described above are simple versions of surface contour plots presented in Figure 5.2, which shows the impact of a range of temperature on voltage at various current densities.

Figure 5.3 shows the variation of differential cell voltage with respect to temperature as a function of current density and absolute operating temperature. It can be seen

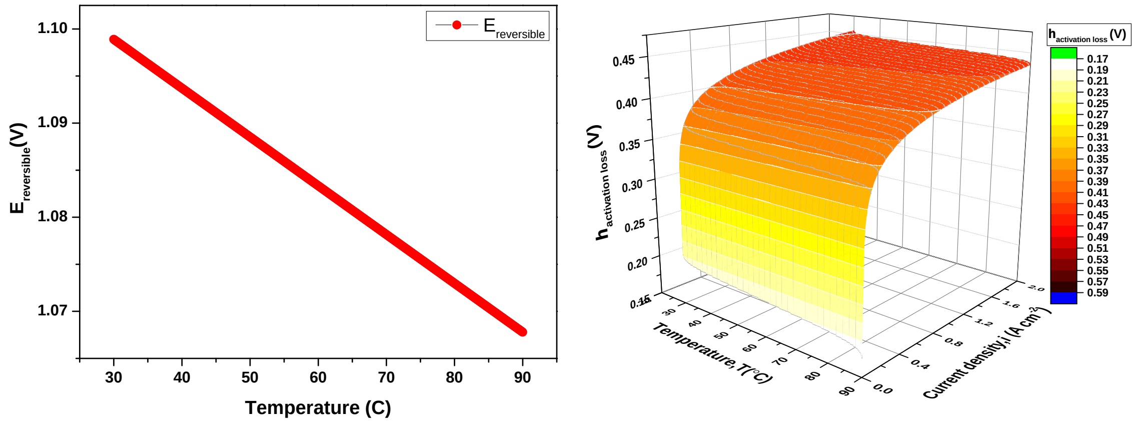

(a) Open circuit voltage decreases with temperature

(b) Activation loss vs. current density for 3 temperature values

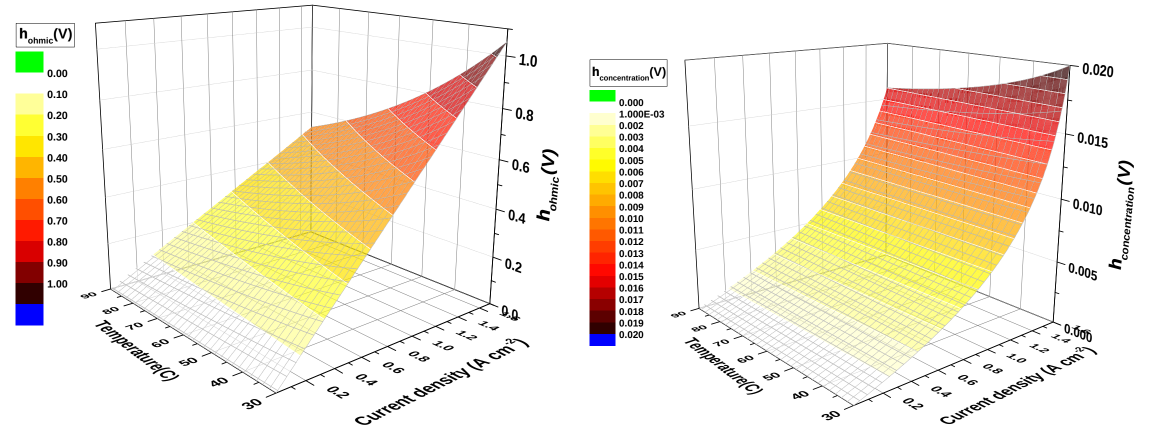

(c) Ohmic loss vs.current density for 3 temperature values

(d) Concentration loss vs.current density for 3 temperature values

FIGURE 5.2: These four figures are the contour plots of Figure 5.1 to show the continuous changes of each voltage loss with respect to current density and temperature. The trends are colourcoded to show that at darker colour there is a higher voltage loss which has a greater manifest at higher current density and lower temperature.

that the PEFC becomes more sensitive to temperature change with increasing current density and reduced temperature, increasing to over 10 $mV\,^{\circ}C^{-1}$ above 1 $A\,cm^{-2}$ from temperature 30 to $90^{\circ}C$.

The effect of temperature on the various loss mechanisms can be seen in Figure 5.2. The following observations can be made: (i) the entropy change associated with the formation of water leads to a small change in OCV over this temperature range; (ii) electrokinetics improve with temperature resulting in lower activation loss due to exponential increase in i_0 with temperature; (iii) Ohmic loss increases linearly with current, increased temperature results in a reduction of the resistance inside the cell due to increased proton conductivity; (iv) concentration loss, which is mainly dominant at higher current density, also reduces with temperature due to improved diffusion, gas mobility and

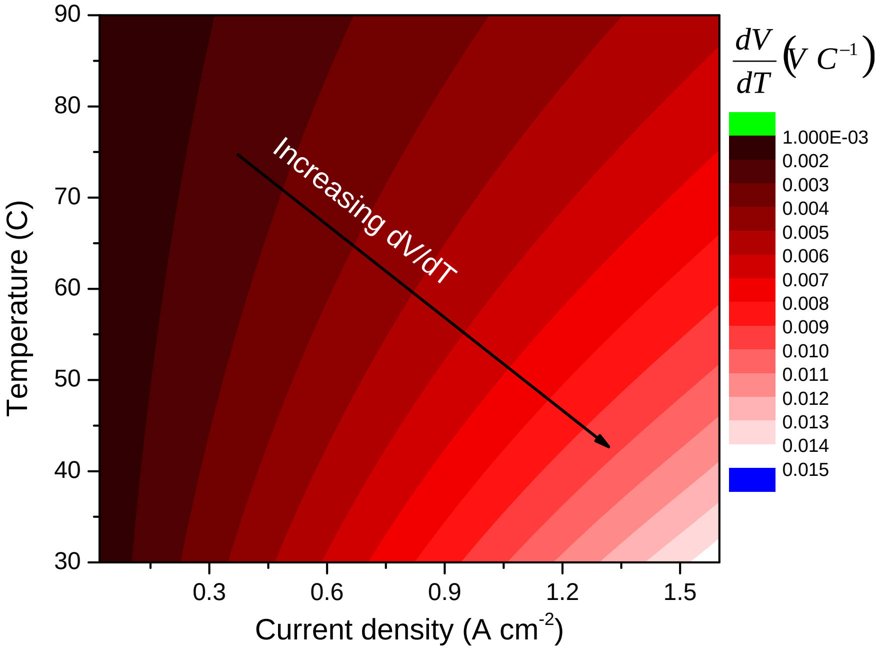

FIGURE 5.3: This figure shows voltage differentiation with respect to temperature versus temperature and current density in a contour format. The lighter colour presents the higher voltage variation with temperature

species concentration, resulting in better mass transport and larger limiting current density.

Temperature has an exponential effect on exchange current density as it is shown in Figure 5.4. Assuming to operate two identical fuel cells at 80°C and 60 ° C with ±5°C temperature variation, it is expected to see larger variation of exchange current density at 80°C due to exponential impact of temperature on i_0 used in this work. The mathematical model used to describe i_0 is an empirical correlation using the third electrode to measure the net current transferred across the MEA. The model is a function of temperature, catalysts loading and area, cathode pressure and activation energy.[14]

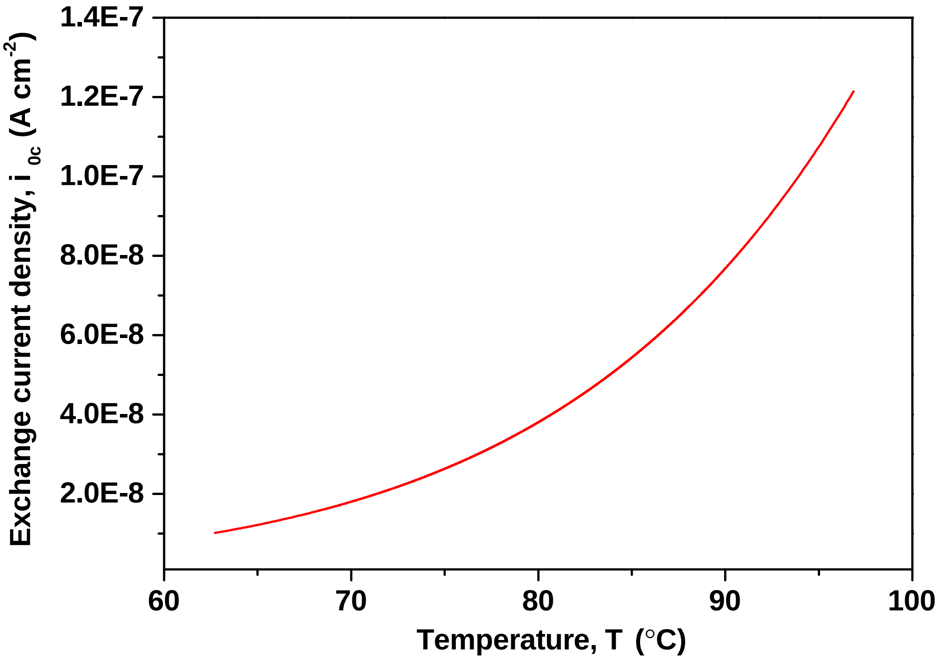

FIGURE 5.4: $i_{0,c}$ behaves exponentially with temperature considering ±5° C temperature uncertainty, this graph shows the average value of exchange current density at each operating temperature

5.2 Statistical approach

To capture the probabilistic behaviour of cell performance under temperature uncertainly, MCS sampling was used to provide temperature input samples for a mean operating temperature of $80\,°C$ and standard deviation of $\pm 5\,°C$. The samples generated by MCS are introduced into the deterministic lumped mathematical PEFC model to determine cell voltage for various current densities.

It is apparent from Figure 5.5 that voltage distribution is not uniform at different current densities. The colour map shows that as current density increases, the 'width' of the distribution increases. This figure clearly shows that the expectation of a polarisation response to conform to a single line is not reasonable when there is uncertainty associated with temperature (or other operating parameters). Rather, a polarisation area better describes the situation. It can be seen in Figure 5.5 that theoretical performance shows higher sensitivity at larger current density due to non-linearity of the model.

Figure 5.6 is also presented to confirm the above statement by showing the distribution of voltage due to temperature sensitivity at different parts of the polarisation plot, where it can be seen that the distributions widen as current density increases.

To calculate the degree of asymmetry of a distribution over various current densities, the skewness is determined to show the effect of temperature variation on cell performance.

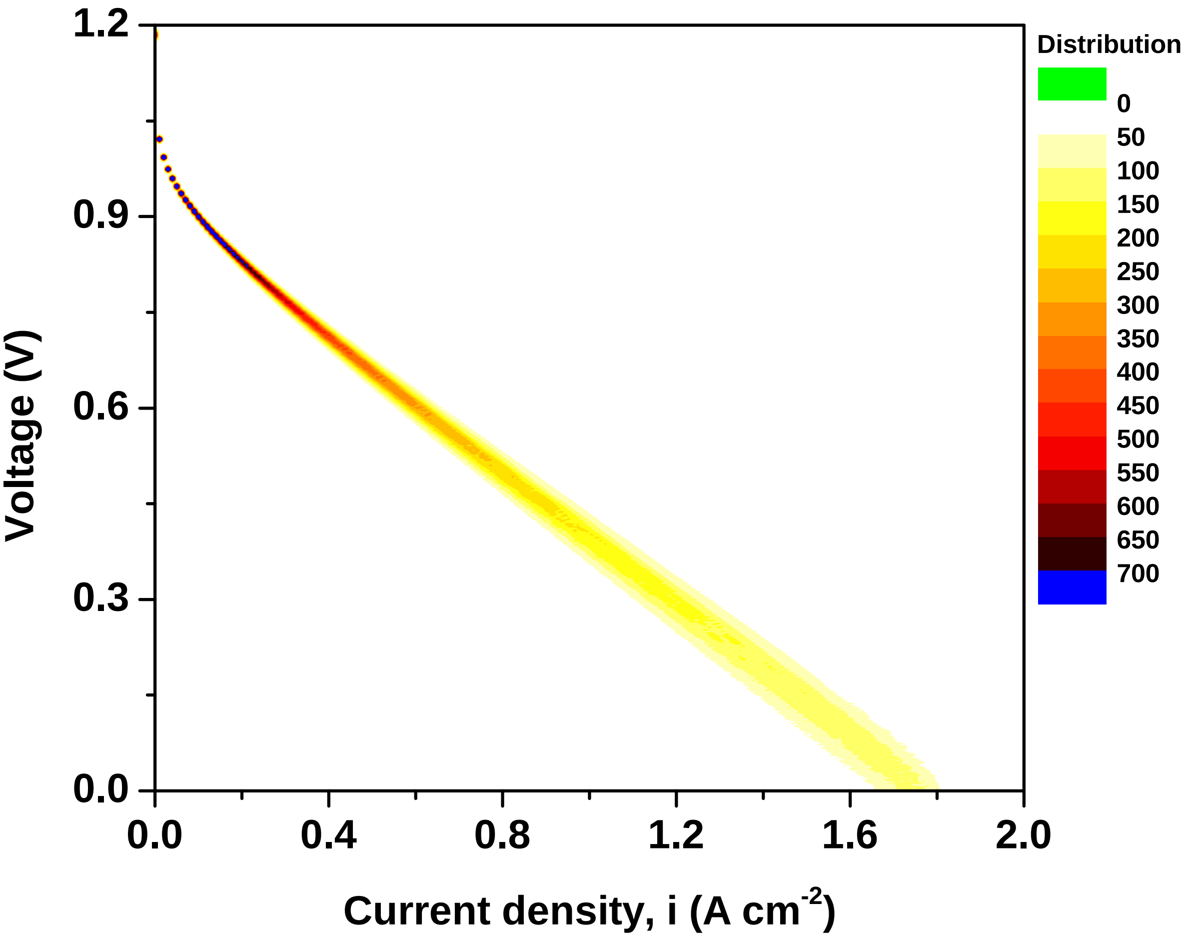

FIGURE 5.5: Contour plot of V-I area at mean operating temperature of $80°C$ with standard deviation of $\pm 5°C$ generated by MCS

It can be seen in Figure 5.7, there is a tendency towards lower voltage in the polarisation V-I area due to higher overpotential and probabilistic effect of temperature on the cell performance. The skewness of the voltage distribution becomes more negative with increased current density, i.e. fuel cell voltage will be more likely to be biased towards lower voltage. To establish the extent of skewness, Equation 3.4 is used to determine the SES. The results obtained from Equation 3.4 show that over the current density of 0.2 Acm^{-2} the magnitude of the skewness is larger than twice the SES. This indicates that the distribution can be regarded as significantly skewed towards a lower voltage with increasing current.

To determine the importance of mean operating temperature on cell performance, the CV is calculated at various current densities. Figure 5.8(a) shows how CV changes at different operating temperatures (30 - 90 °C) taking a temperature uncertainty of ±5° C. The purpose of this calculation is to study the sensitivity of the system with respect to mean operating temperature for the specific variation of uncertainty. The results show

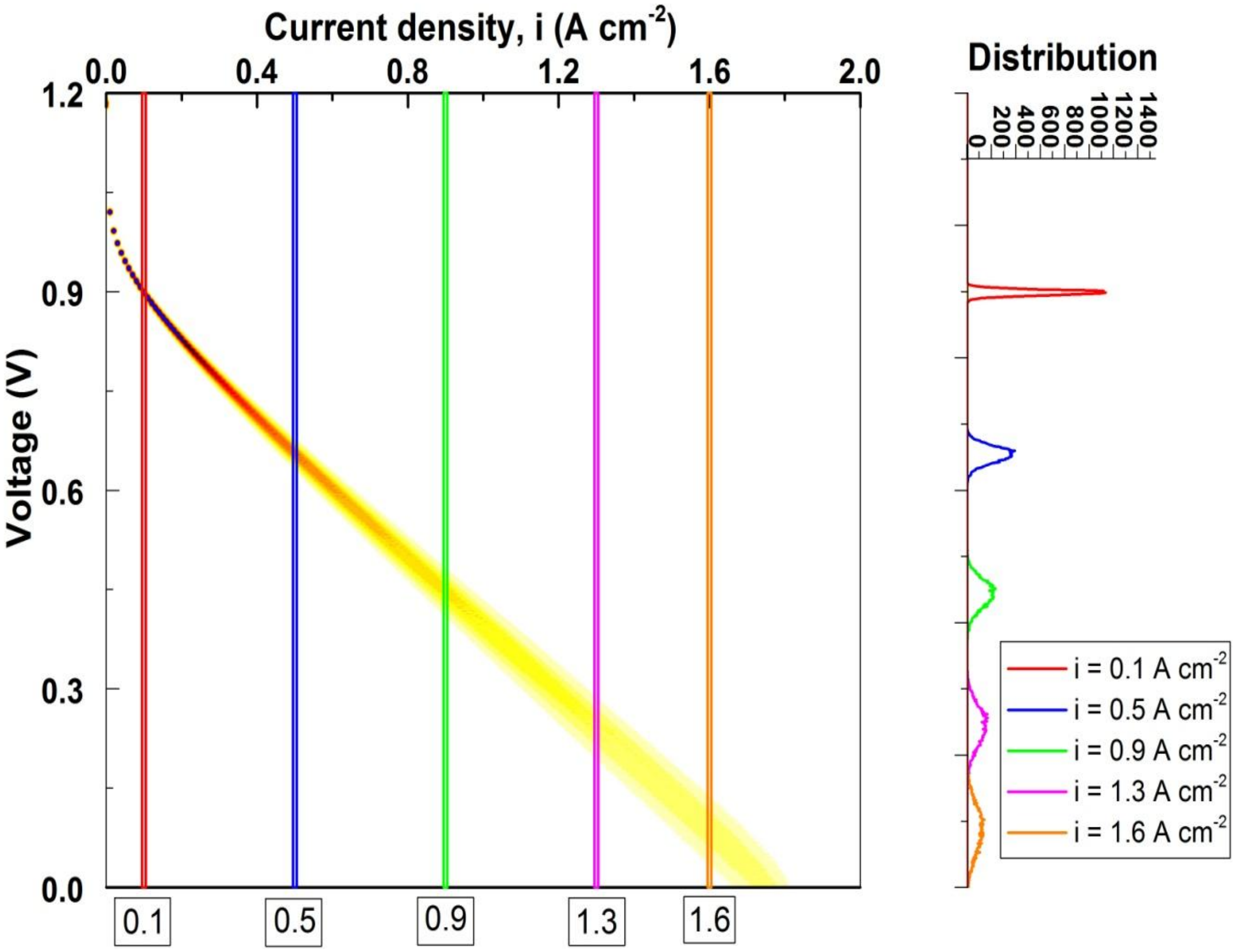

FIGURE 5.6: Contour plot of V-I area at mean operating temperature of 80°C with standard deviation of ±5°C generated by MCS and compare voltage distributions at different current density

that the system is more sensitive at lower temperature due to larger resistance and poor kinetics and mass transport resulting in higher overpotentials and larger distribution of voltage, which helps fuel cell developers to know the range of impact of uncertainties on cell performance with increasing current density. Figure 5.8(a) shows there is over 50% variation in voltage from 0 to $1.6 A\,cm^{-2}$, which confirms the same phenomena also described in analytical section.

To establish how dispersion of cell voltage relates to the given temperature uncertainty δT, the CV of cell voltage is calculated for different values and presented in Figure 5.8(b). It can be seen that regardless of mean operating temperature the δT increases monotonically at current density 0.6 $\mathrm{A}\,cm^{-2}$. However, it should be stressed that this model does not include the relationship between temperature and current density. The author believes that an upgraded model that considers the relationship between current density and temperature can estimate the effect of temperature uncertainty on overall

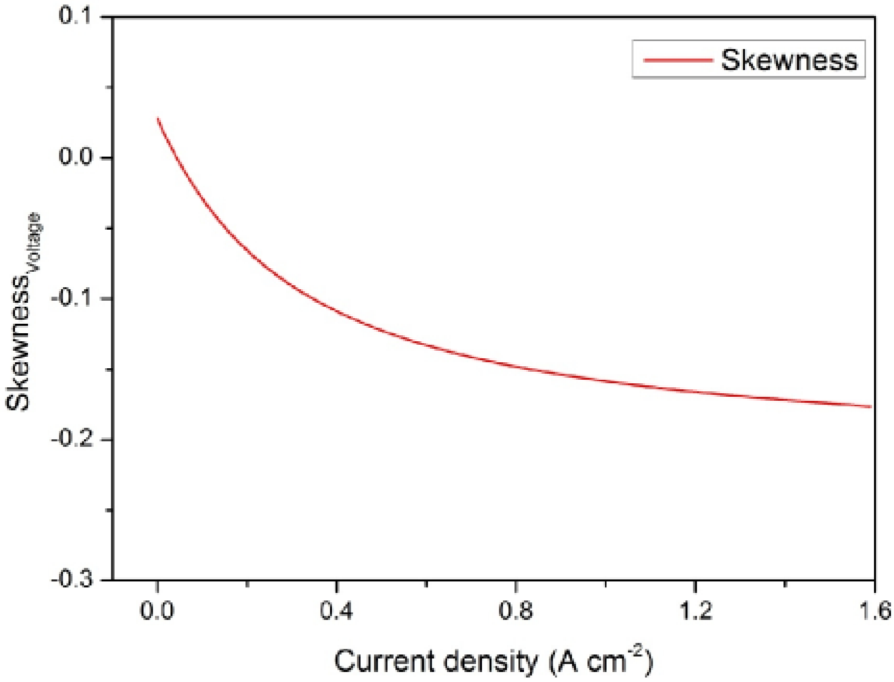

FIGURE 5.7: Skewness of *V-I* polarisation "area" at operating temperature of 80° C and standard deviation of 5° C

cell performance more accurately since with increasing current density, the system heats up and temperature increases too, which can possibly generates more uncertainty.

To assess the sensitivity of the cell performance regarding the standard deviation of temperature uncertainty, δT of $\pm 2, 5, 7, 10°C$ are examined at the mean operating temperature of $30, 40, 50, 60, 70, 80°C$. The polarisation curves obtained for each δT are analysed and CV is calculated for a current density $0.6Acm^{-2}$ to compare the variation of cell voltage with respect to various mean operating temperature and temperature uncertainty. The simulation shows that there is a linear increase in voltage variation with increased uncertainty and reducing temperature. It can be seen from Figure 5.8(b) that the CV increases for almost 10% from δT value $\pm 2°C$ to $\pm 10°C$ operating at $30°C$ and only 3% at operating temperature of $90°C$. It is clear from Figure 5.8(b) that the model shows higher sensitivity at lower temperature with larger δT.

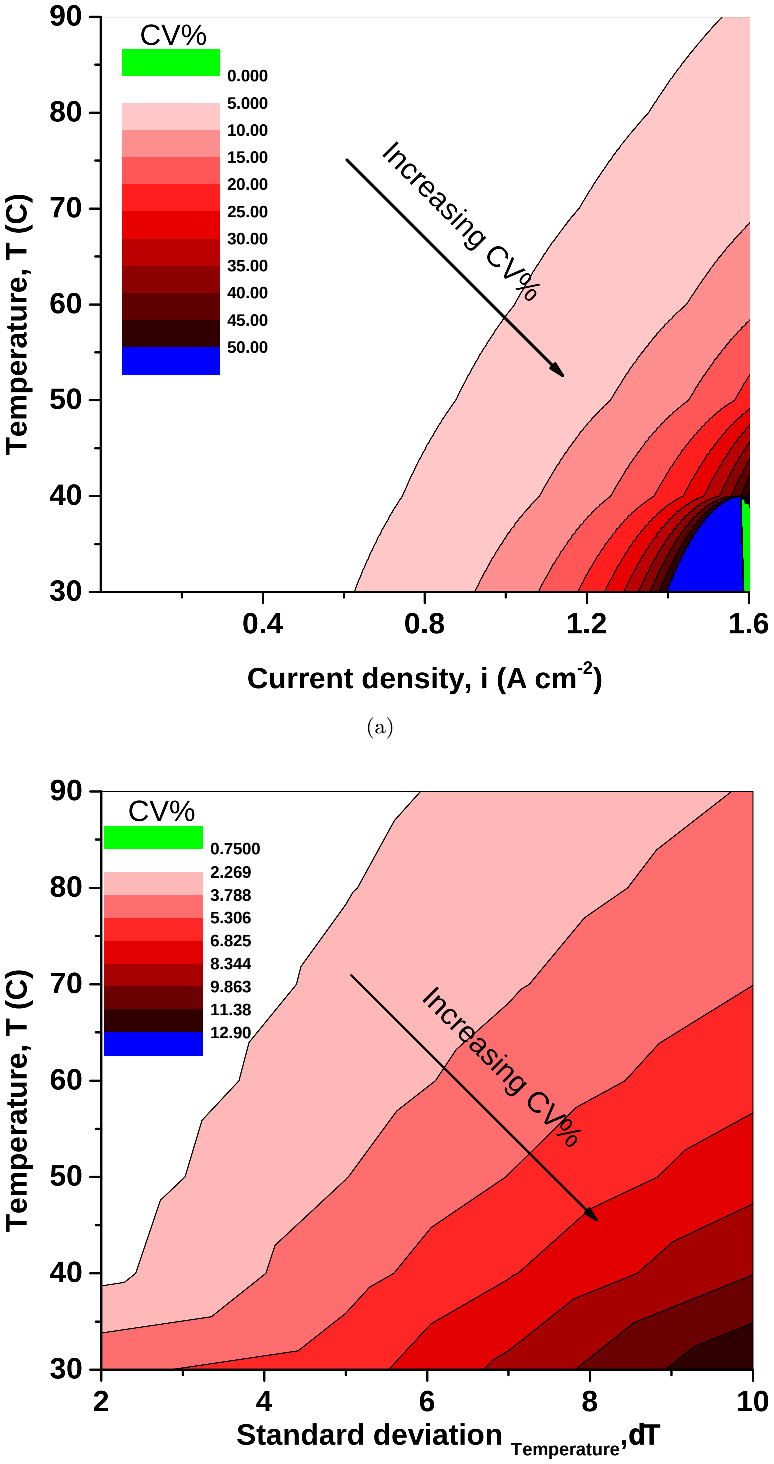

(a)

(b)

FIGURE 5.8: (a) CV changes with $\delta T = \pm 5$ at different operating temperatures. (b) CV changes at various operating temperatures for a range of $\delta T = \pm 2, 5, 7, 10°C$ at current density of $0.6 A\,cm^{-2}$.

5.3 Summary

By comparing the two treatments (analytical and statistical), it can be seen that they both confirm that voltage distribution magnifies with current density and reducing temperature due to non-linearity in the models with respect to temperature and current density.

This chapter presented the theoretical analysis on the effect of temperature uncertainty on fuel cell performance assuming ±5°C temperature variation across the MEA using literature. However, to justify this study, the experiments described in Chapter 4 were performed in order to obtain real temperature data to confirm temperature variation across the MEA. Then the experimental results obtained in Chapter 4 substituted into the model to modify the polarisation area with real data. Next chapter shows the results obtained from the experiments.

Chapter 6

Experimental results

6.1 Model validation using a commercial fuel cell

This section shows the performance of commercial fuel cell at $80°C$ to establish the range of temperature variation while running at constant temperature. The polarisation curves presented in Figure 6.1 show that there is a lower Open Circuit Voltage (OCV) compared to the one presented by theoretical data due to making the assumption of no electron cross-over in modeling chapter. These data confirm that in reality the achieved OCV does hardly get over $1\,V$ due to efficiency of the system. Also thesse tests shows that there was $\pm 0.5\,°C$ temperature variation from OCV to 1.5 $A cm^{-2}$, which is negligible in comparison with temperature uncertainty in fuel cell stack presented later on in this chapter.

6.2 Temperature distribution investigation on industrial fuel cells using a thermal camera

This section presents the results obtained from experiments using thermal imaging camera to measure temperature variation across the MEA over time. The aim is to achieve two goals, first to show how temperature variation changes over time and whether the changes are linear or nonlinear. Secondly to establish temperature variation ranges across the MEA.

In the second section of this chapter, current and temperature mapping is used to establish how temperature varies with current density over 16 sigments of a single cell. The modified polarisation area is presented later in this chapter using the real temperature

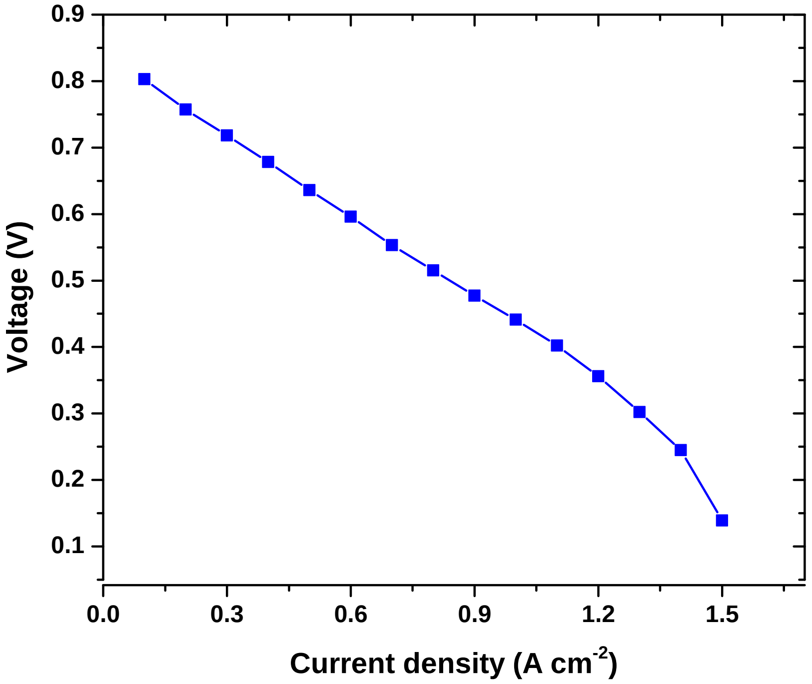

FIGURE 6.1: Polarisation curve obtained from a commercial fuel cell operating at 80°C

data in order to be compared with the polarisation area obtained by using theoretical data in Chapter 3.

6.2.1 Spatial study

To establish the temperature variation at various current densities, thermal imaging is performed on a stack. Figure 6.2 shows a thermal image of the stack from the front where air exits the system. It can be seen that at 40A (0.67 $A cm^{-2}$) temperature variation in the MEA region spans X - Y with almost 12°C difference between the active and cooling channels, where active is white and cooling channels are red regions.

To look at the thermal images with increased current density, it can be seen that temperature variation in the MEA region increases with current density due to increasing rate of reaction. (See **Appendix**)

In conducting the experiment using the thermal imaging camera a pixel resolution of approximately 0.35×10^{-3} m was achieved. The noise-equivalent temperature difference (NETD), a measure of the signal-to-noise ratio, of the camera during the experiments was recorded as 19 mK during the experiment enabling a high thermal resolution to be reported.

To ensure the system was described accurately, a calibration was conducted in order to eliminate environmental reflections. To achieve this, a diffuse reflector was used to enable the environmental emissivity to be set to 1. In investigating the temperatures of

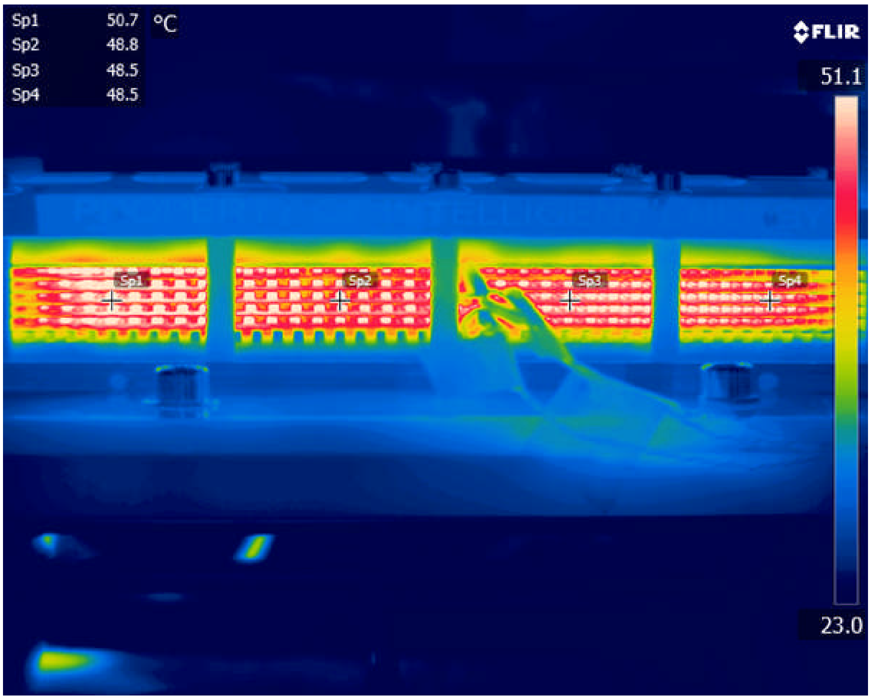

FIGURE 6.2: Thermal image of fuel cell stack at a current loading of 40A (0.67 $A\,cm^{-2}$) after equilibrating for 25 minutes. There are four points marked on the middle cell of the stack for comparison

the stack, each channel represented a cavity that could be considered to be a quasi-black body [67]. This allows an emissivity approaching 1 to be used; in this case a conservative 0.98 was chosen. By utilising this technique a direct comparison can be made between the active and cooling channels without the need to calculate the emissivity of each channel.

TABLE 6.1: Statistical variables for four points along the MEA at current density 0.67 $A\,cm^{-2}$ and 25 minutes operation

Statistical variables/location	**SP1**	**SP2**	**SP3**	**SP4**
Mean (Single cell) ° C	32.40	35.25	34.34	34.70
Mean (Stack) ° C	46.70	44.79	44.68	44.58
CV (Single cell)%	16.20	19.00	16.60	17.35
CV (Stack)%	0.32	0.33	0.38	0.53

Figure 6.3 is illustrated to compare the temperature variation spatially at four points along the MEA for the industrial IE stack and a single cell at current density 0.67 $A\,cm^{-2}$ for 25 minutes under similar operating conditions. Results are plotted in Figure 6.3 showing the stack data in red and single cell data in black. The purpose of this comparison is to identify the effect of sizing including multiple cells on temperature variation and ultimately on the cell performance at different locations along the MEA.

The CV and mean calculations are carried out to show a Gaussian distribution for each point, which are presented in Table 6.1. It can be seen that for the stack the range of temperature changes from almost 44 to 47 °C from the hydrogen gas entrance to the 'dead-end', which shows the temperature inconsistency at different points in MEA. The CV of SP1 to SP4 increases by almost 25% showing that the spatial distribution itself has ranging temporal variation. The Table 6.1 illustrates that the mean temperature of localised distributions decreases along the cell by approximately 2.3% from the gas entrance to the 'dead-end' of the cell due to gas cooling within the cell.

It can be seen that distribution widens from 0.5 to 1°C from SP1 to SP4 while the mean of distribution shifts towards lower temperature. This figure indicates that the mean temperature reduces with distance, which can be the effect of resistance and heat loss.

To look at the same behaviour on a single cell system, Figure 6.3 shows that the mean of the black distribution curves vary in wider ranges, the mean of temperature distribution increases for about 7% and the CV increases for about 3.5%. The data shows that the single cell is less affected by temperature variation spatially from SP1 to SP4 compared to the stack; however, the variation for a similar location in a single cell is approximately 20% compared to the stack, which shows the single cell is more sensitive with temperature. To design a fuel cell stack, it is essential to consider the sizing and the number of the cells, which might have an impact on sensitivity of the system with temperature.

6.2.2 Temporal study

To study the effect of time on temperature variations, both IE rigs (single cell and stack) ran under similar operating conditions at current density $0.67 A\,cm^{-2}$ for 30 minutes and the data recorded every 5 minutes to compare temperature variations at a given point. Figure 6.4 presents the results obtained for 30 minutes of operation in the stack at SP3. The system mean temperature reduces by almost 0.18% and the CV increases by 13% with time.

To study the effect of temporal variation in a single cell, SP3 is chosen and the temperature is recorded for over 30 minutes and presented in Figure 6.5. It can be seen that the CV reduces from interval one (5 minutes) to interval six (30 minutes). The results show that the temperature variation increases for about 0.2% and mean temperature shifts to higher temperature for about 0.04%. To compare the two systems it can be seen that the temporal effect is larger at the stack than the single cell.

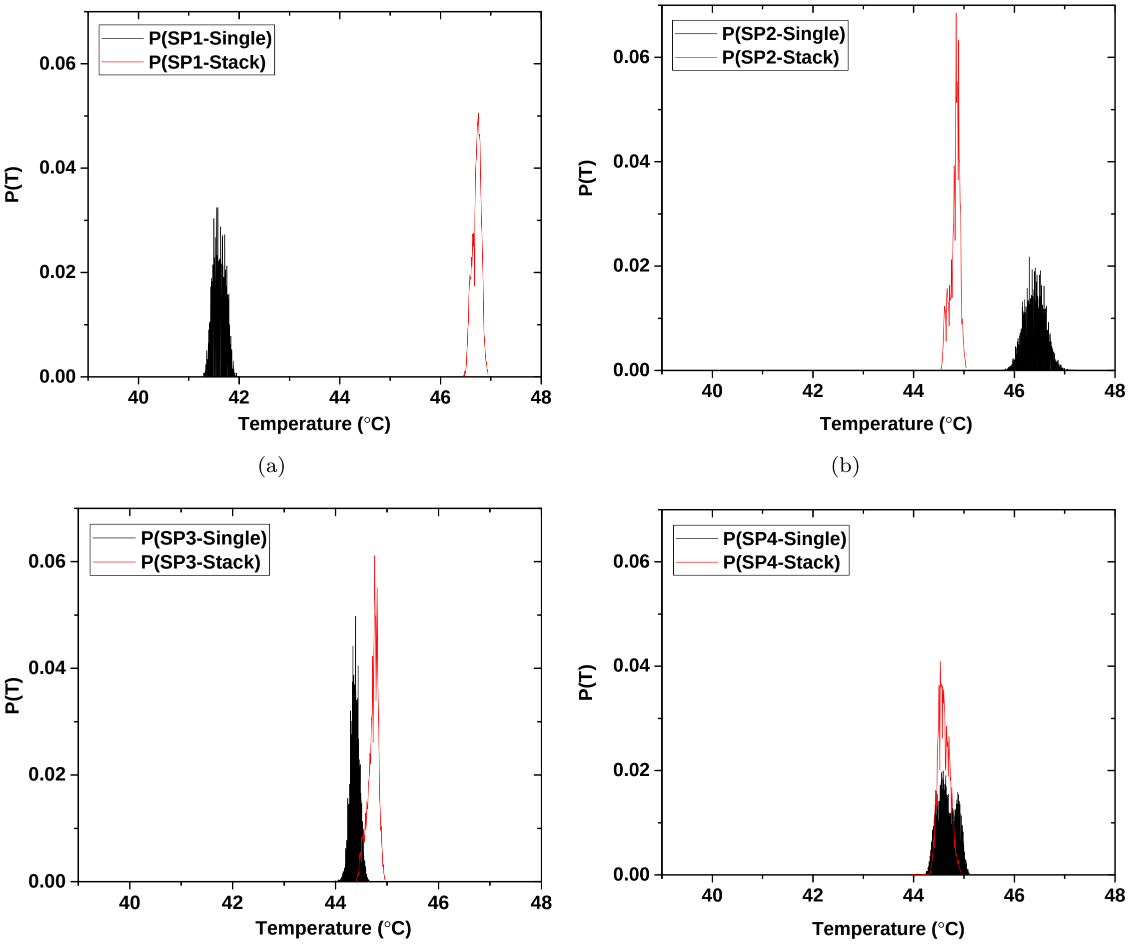

(a) (b)

(c) (d)

FIGURE 6.3: Temperature distribution at four locations along the MEA of a middle cell in air-cooled stack (red) and a single cell (black) at current 40A collecected for 25 minutes

6.3 Effect of local temperature on polarisation area using temperature/current mapping

The section uses temperature mapping data to calculate the temperature variation across 16 segments for various current densities to obtain effective polarisation areas. Figure 6.6 shows an example of temperature measurement across the 16 segments of a cell.

To look at variation at each current density individually, Figure 6.7 is presented to show how the standard deviation of temperature at 16 segments varies with current density along the polarisation area.

It is shown in Figure 6.7 that variation increases upto the point where the limiting current is reached. These data are used to identify the standard deviation of temperature variation in order to plot the polarisation area by substituting the data found

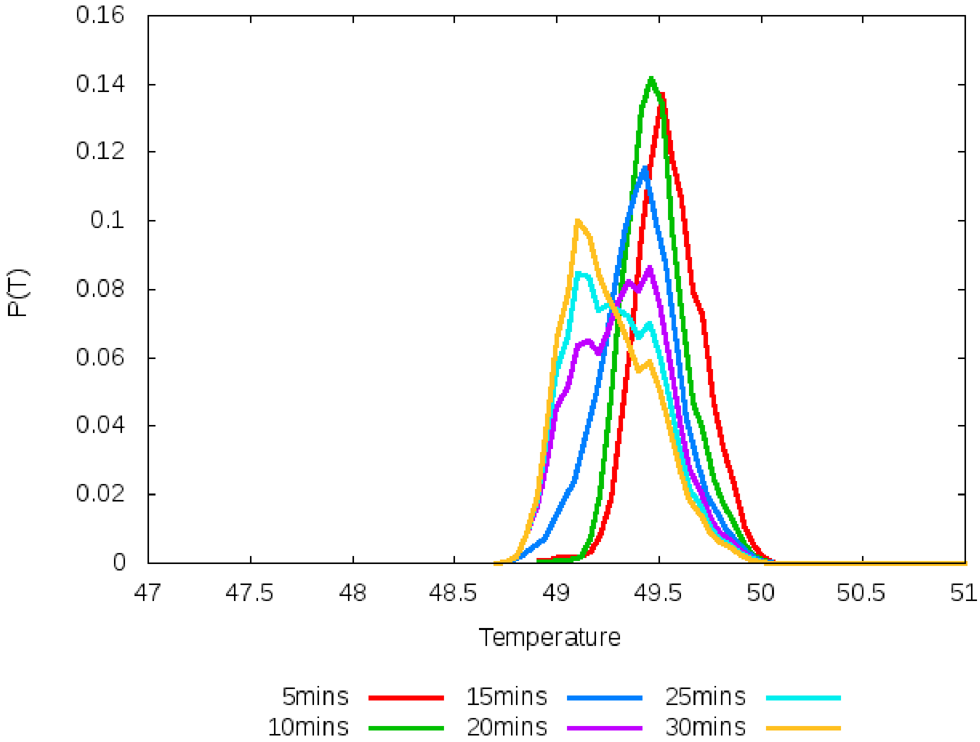

FIGURE 6.4: Temperature distribution obtained at different operating time for SP3 for stack

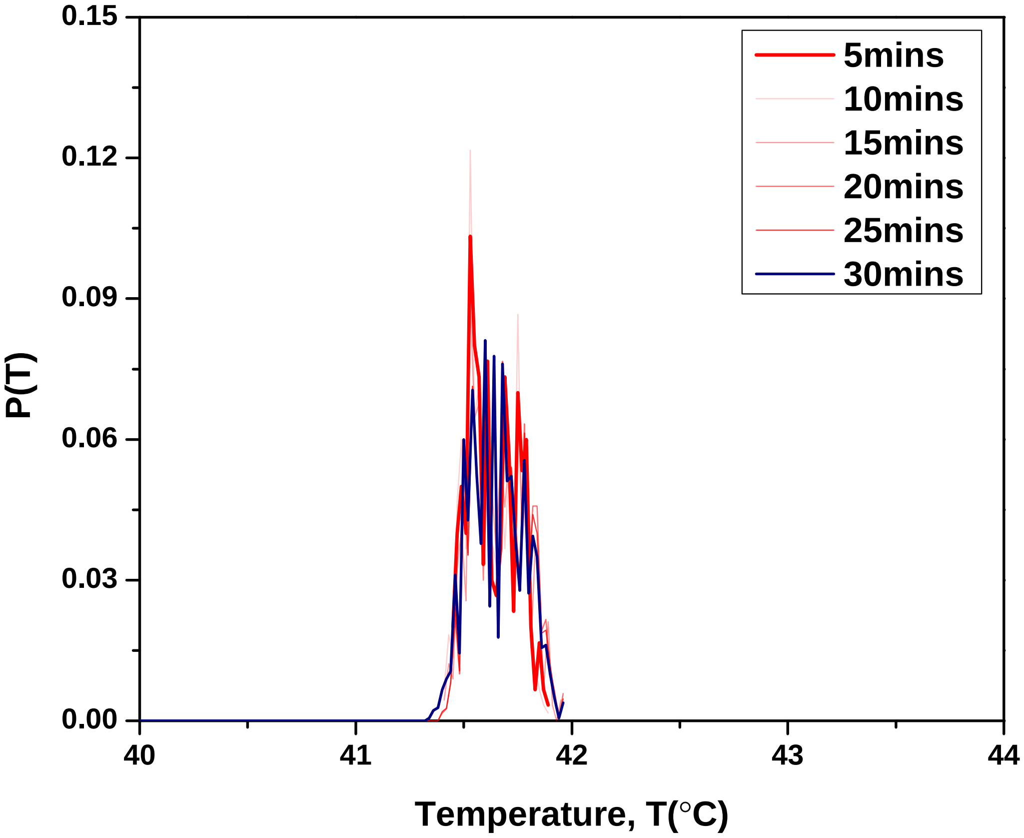

FIGURE 6.5: Single cell thermal image at SP3 at 6 time intervals to study the effect of time on temperature distribution

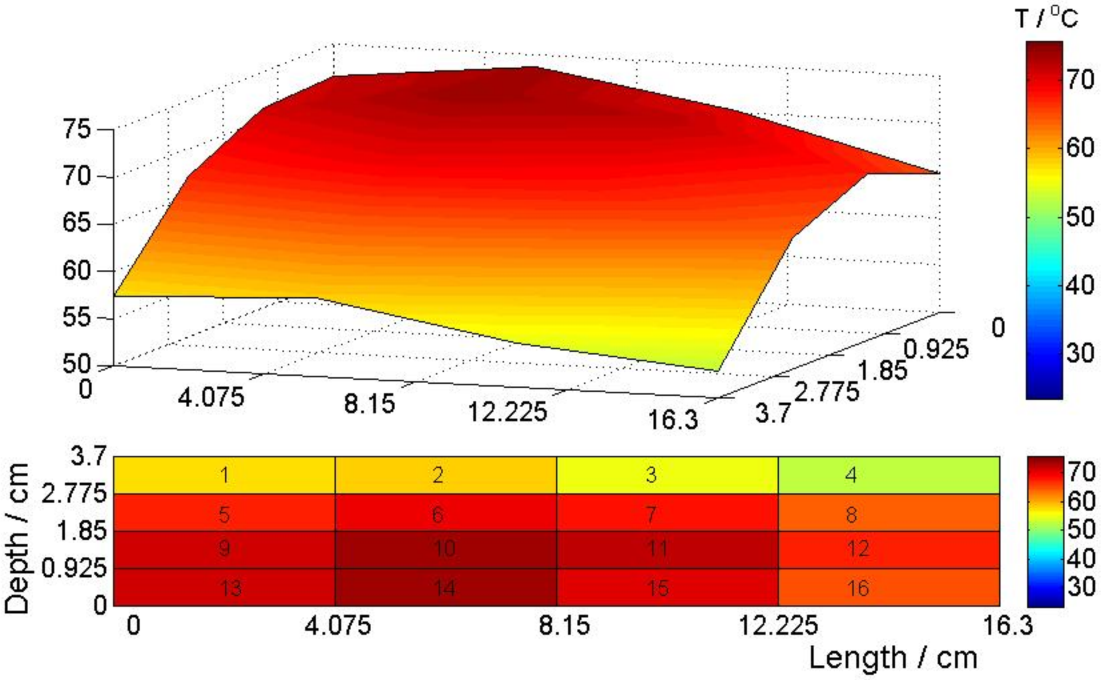

FIGURE 6.6: Temperature variation across 16 segments at current 0.97 A to show the hot spot across the cell (refer to Figure 4.5)

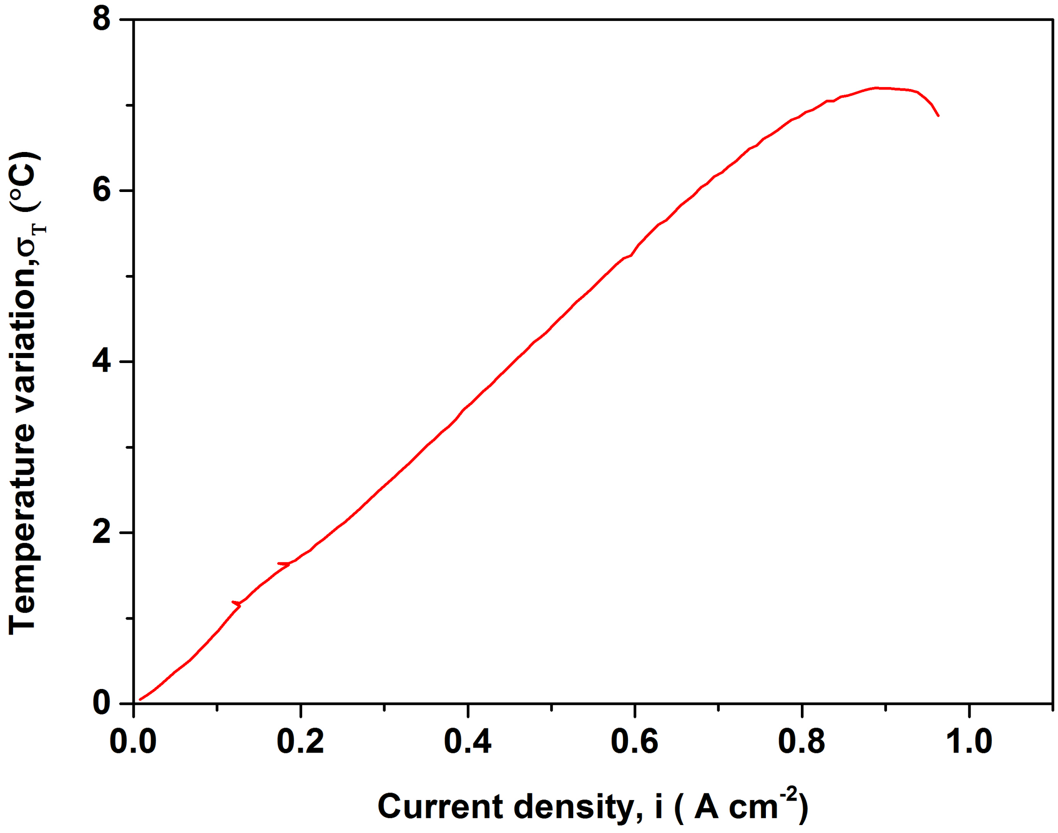

FIGURE 6.7: Shows temperature variation, σ, with current density. The temperature variation is calculated for the 16 segments at each current density

from the current /temperature mapping into the model used in Chapter 3. Previously the polarisation area was plotted in Figure 6.8 assuming there is $\pm 5°C$ temperature uncertainty consistently across polarisation area; however, these findings confirm that the uncertainty changes with current density.

To analyse the sensitivity of polarisation area with temperature distributions, the following Figures 6.8 and 6.9 are presented to compare the modelling and experimental data.

It was previously shown in Figure 5.5 in Chapter 5, how the polarisation area is affected by a constant temperature uncertainty of ±5°C across all current densities. However, this work aims to show how temperature uncertainty varies with current density and incorporate this into modelling study. The polarisation area obtained from temperature and current mapping is shown in Figure 6.9. This figure confirms that kinetics is less affected by temperature uncertainty at lower current density and as it goes towards larger current density, the effect of temperature uncertainty magnifies and gets significantly larger up to the point reaching mass limitation.

This experiment confirms that there is a nonlinear relationship between current and temperature, which explains the variation in voltage losses once there is a change in temperature. These data shows that at high current density there is a higher sensitivity of voltage with temperature variation over time. It is critical to state that there are other sources of uncertainty which have not been mentioned here including as degradation and membrane swelling that can worsen these findings [24].

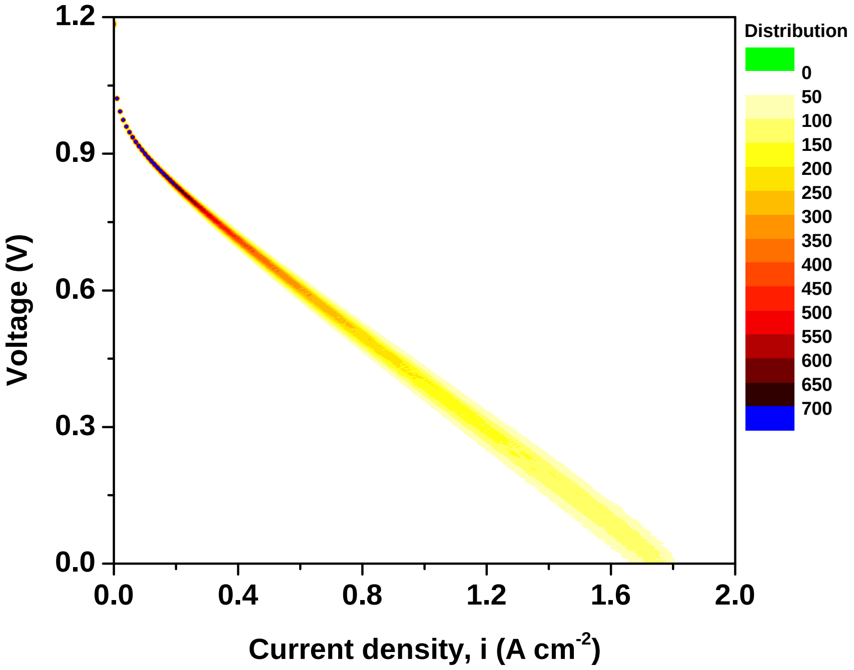

FIGURE 6.8: Polarisation *V*-*I* area with ±5°C temperature uncertainty using MCS (theoritical data). The darker colours show that the distributions have higher peaks and smaller CV than the lighter colours

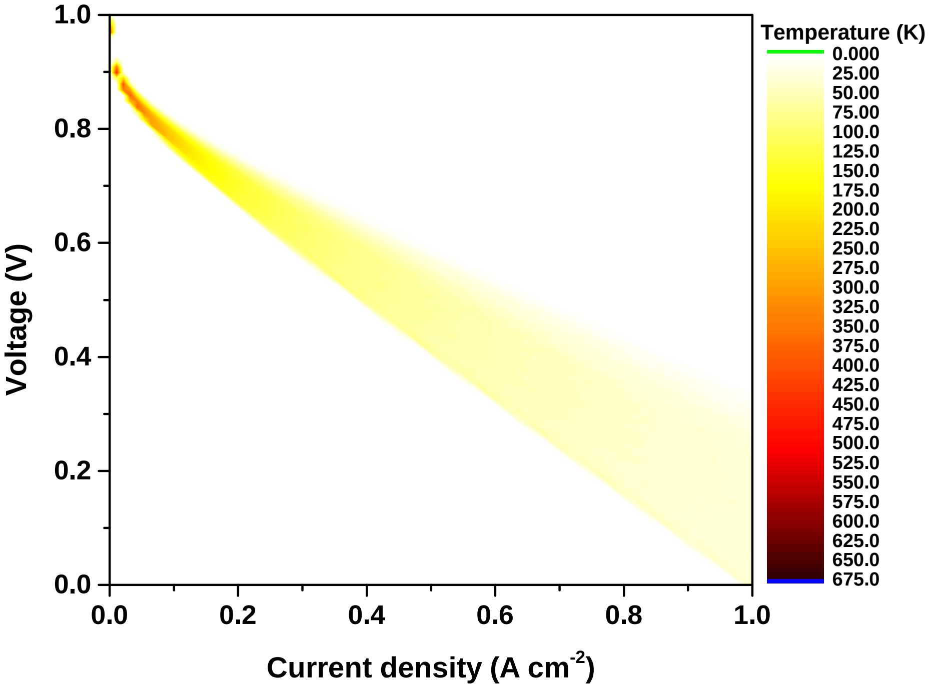

FIGURE 6.9: Polarisation *V*-*I* area with various temperature uncertainty using temperature mapping data (experimental data)

6.4 Summary

Thermal imaging on an operational PEFC stack allows the spatial and temporal variation in temperature to be assessed. The experiments show that the width of temperature distribution decreases spatially towards the 'dead-end' of the stack. As it can be seen in Figure 6.2, a temperature variation of over 12 °C was observed across the active area of the stack (air exit face), whereas the variation across the central MEA was almost 2.5°C with standard deviation of ±0.5°C temporally.

Also this chapter shows that temperature uncertainty does not stay constant with current density and has the tendency to increase. By comparing the polarisation contour maps from modelling study and experimental data, it can be seen that the shape of polarisation area changes with given temperature uncertainty across all current densities whereas the other plot does not changes massively with current density assuming the δT stays constant at ±5°C.

This case study shows that to predict the range of temperature uncertainty in the system, it is crucial to consider the operating current and temperature as well as the size of the cell in order to identify the hot spots.

Chapter 7

Conclusion and future work

7.1 Conclusion

Temperature is a key parameter for determining PEFC performance and uncertainty, as this parameter is reflected in the variability in the polarisation response. An analytical and statistical approach has been used to determine the sensitivity and probability of performance variation as a function of current density and nominal operating temperature.

Lower cell temperatures and higher current densities are predicted to lead to the greatest variation in performance for a given temperature change or statistical variation ('uncertainty'). The study has identified an effective polarization 'area' or 'band', in contrast to the widely quoted polarization 'curve', as being the most appropriate way to represent model predictions of fuel cell performance.

The cell performance variation due to temperature distribution at a given point in the *V-I* polarisation area translates into negative skewness. This means that there is a tendency for the *V-I* area to be biased towards a lower voltage. Therefore, reported polarisation data will tend to err on the side of poorer perceived performance due to the natural variation in temperature for a given system.

Thermal imaging on an operational PEFC stack allows the spatial and temporal variation in temperature to be assessed. The experiments show that the width of temperature distribution decreases spatially towards the dead-end of the stack. A temperature variation of over 12°C was observed across the active area of the stack (air exit face), whereas the variation across the central MEA was ~ 2.5°C and the temporal variation has a standard deviation of ± 0.5°C.

Temperature mapping is also used to measure the real temperature data across the 16 segments of the cell in order to show temperature variation with current density in order to modify the polarisation area. The results show that the temperature variation increases with current densities and changes the shape of the polarisation plot.

7.2 Future work

The results presented in this work can lead to further investogation into the following areas:

- Upgrade the mathematical model to describe water management and dimensions of the fuel cell and also to capture the layout of flow channels in order to establish more accurate temperature variation with respect to different designs and operating conditions.
- Modify the model to capture the relationship between current density and temperature with respect to time. The aim is to give a better interpretation of sensitivity of temperature with respect to current density over time.
- Look at different parts of fuel cells i.e. GDL and cooling channels to study the temperature variation, which will lead to improvement in design in a case of significantly larger variation.

Chapter 8

Appendix

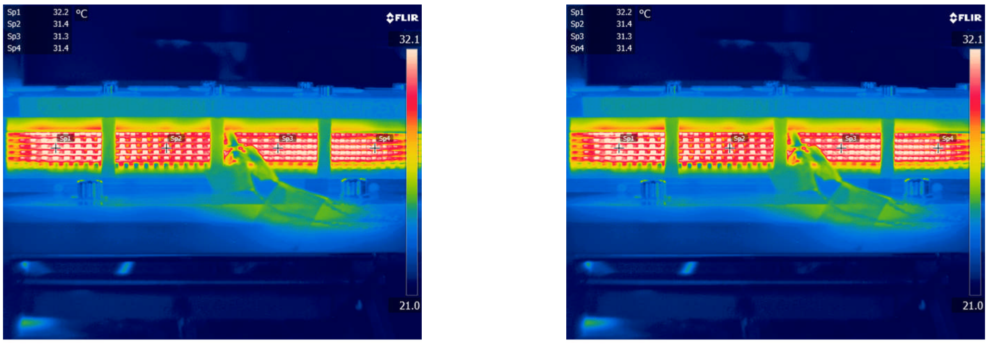

(a) At current 20A (0.33 Acm^2) after equilibrating for 5 minutes

(b) At current 20A (0.33 Acm^2) after equilibrating for 25 minutes

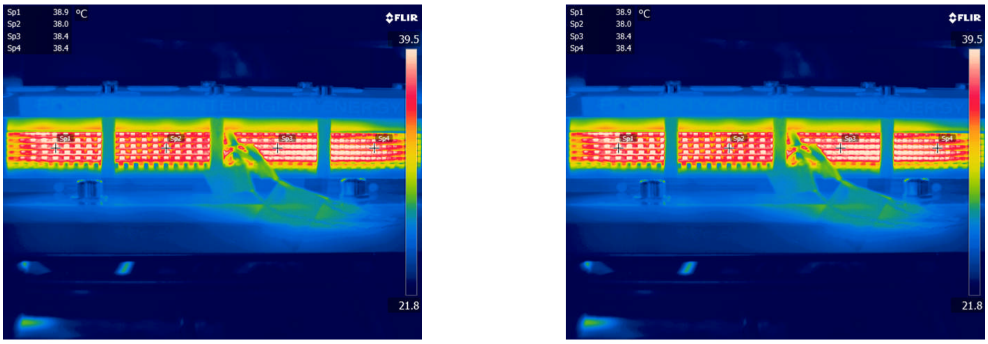

(c) At current 30A (0.5 Acm^2) after equilibrating for 5 minutes

(d) At current 30A (0.5 Acm^2) after equilibrating for 25 minutes

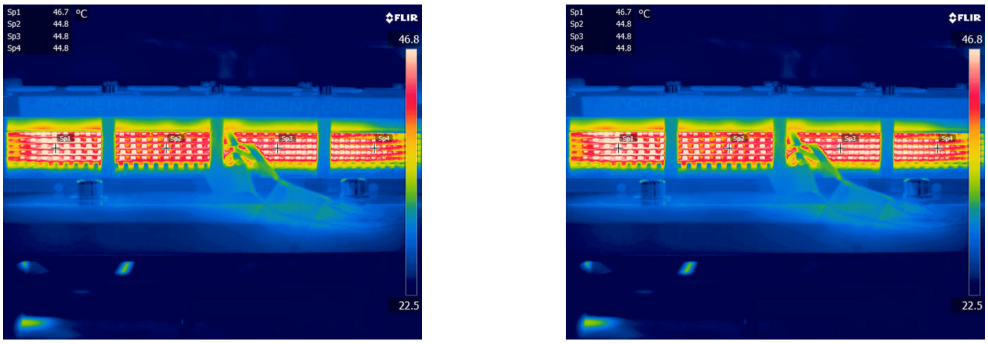

(e) At current 40A (0.67 Acm^2) after equilibrating for 5 minutes

(f) At current 40A (0.67 Acm^2) after equilibrating for 25 minutes

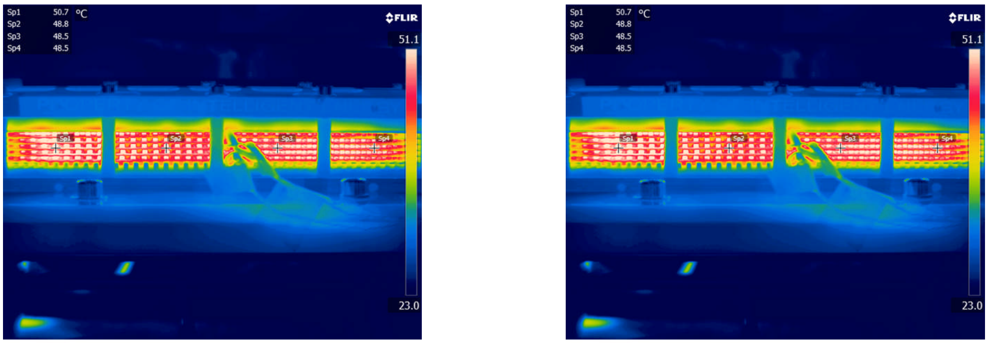

(g) At current 46A (0.78 Acm^2) after equilibrating for 5 minutes

(h) At current 46A (0.78 Acm^2) after equilibrating for 25 minutes

FIGURE 8.1: Thermal image of IE stack at a polarisation after equilibrating for 25 minues

Chapter 9

Publication 1

Available online at www.sciencedirect.com

ScienceDirect

journal homepage: www.elsevier.com/locate/he

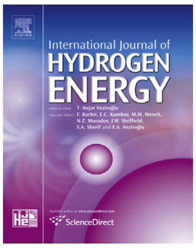

Effect of temperature uncertainty on polymer electrolyte fuel cell performance☆

Mozhdeh Noorkami[a], James B. Robinson[a], Quentin Meyer[a],
Oluwamayowa A. Obeisun[a], Eric S. Fraga[a], Tobias Reisch[b],
Paul R. Shearing[a], Daniel J.L. Brett[a,*]

[a] *Electrochemical Innovation Lab, Department of Chemical Engineering, UCL, Torrington Place, London WC1E 7JE, United Kingdom*
[b] *Intelligent Energy, Charnwood Building, Holywell Park, Ashby Road, Loughborough, Leicestershire LE11 3GB, United Kingdom*

ARTICLE INFO

Article history:
Received 31 July 2013
Received in revised form
23 October 2013
Accepted 26 October 2013
Available online 5 December 2013

Keywords:
Polymer electrolyte fuel cell
Polarisation area
Temperature uncertainty
Monte Carlo sampling
Thermal imaging

ABSTRACT

The temperature of operation is a key parameter in determining the performance and durability of a polymer electrolyte fuel cell (PEFC). Controlling temperature and understanding its distribution and dynamic response is vital for effective operation and design of better systems. The sensitivity to temperature means that uncertainty in this parameter leads to variable response and can mask other factors affecting performance. It is important to be able to determine the impact of temperature uncertainly and quantify how much PEFC operation is influenced under different operating conditions. Here, a simple lumped mathematical model is used to describe PEFC performance under temperature uncertainty. An analytical approach gives a measure of the sensitivity of performance to temperature at different nominal operating temperatures and electrical loadings. Whereas a statistical approach, using Monte Carlo stochastic sampling, provides a 'probability map' of PEFC polarisation behaviour. As such, a polarisation 'area' or 'band' is considered as opposed to a polarisation 'curve'. Results show that temperature variation has the greatest effect at higher currents and lower nominal operating temperatures. Thermal imaging of a commercial air-cooled stack is included to illustrate the temporal and spatial temperature variation experienced in real systems.

1. Introduction

A polymer electrolyte fuel cell (PEFC) is a device that converts chemical energy in fuels directly into electricity with high efficiency, no combustion or moving parts [1]. The advantages of this type of fuel cell includes low operating temperature, quick start-up, planar configuration and easier sealing due to the use of a solid electrolyte [2–9]. However, water management issues require careful consideration to ensure good protonic conductivity in the electrolyte while avoiding electrode flooding that limits reactant access and results in mass

---

☆ This is an open-access article distributed under the terms of the Creative Commons Attribution-NonCommercial-No Derivative Works License, which permits non-commercial use, distribution, and reproduction in any medium, provided the original author and source are credited.

* *Corresponding author*. Tel.: +44 (0) 20 7679 3310.
E-mail address: d.brett@ucl.ac.uk (D.J.L. Brett).
URL: http://www.ucl.ac.uk/electrochemical-innovation-lab

0360-3199/$ – see front matter Copyright © 2013, The Authors. Published by Elsevier Ltd. All rights reserved.
http://dx.doi.org/10.1016/j.ijhydene.2013.10.156

transport limitations [10]. To achieve this, it is important to run the system at the optimum operating conditions by applying efficient control methodologies. There are many factors which affect performance, ranging from fundamental thermodynamic properties; ionic, electronic and mass transport mechanisms; heat transfer and electro-kinetics [11–13]. For all these processes, temperature is a major determining factor and control is essential for understanding how fuel cells operate, optimising performance, and developing better and longer lasting devices.

When operating fuel cells, there is always a level of 'uncertainty' in the operating parameters and physical state of the system that leads to variable and unpredictable performance. This uncertainty can be due to fluctuations and distribution of operating parameters, measurement accuracy, random errors, unoptimised/unstable control, etc. [14]. Temperature is one of the parameters with the highest uncertainty as it is a function of operating point, reactant flow rate and ambient conditions; it is also temporally variant under dynamic conditions and spatially heterogeneous.

The sensitivity of fuel cell operation with respect to temperature has been reported in the literature [15–17]. Studies have focussed on the impact of operating temperature on fuel cell performance, and also uncertainty as a part of the control system [18,19].

Temperature is an important component in fuel cell operation, and plays a key role in cell performance [20,21]. Water transport is directly influenced by temperature, affecting the mobility of species in the electrolyte and access and removal of water at the electrodes and propensity to flooding [10]. Thermal imaging has increasingly become a popular tool for the investigation of fuel cells. It provides high spatial resolution imaging and allowing non-contact measurements, so avoiding potential interference with fuel cell operation. Thermal imaging can be used to identify defects and/or areas of unusually low or high activity on the surface of fuel cells. Aieta et al. have shown how catalyst loading defects can be investigated using thermal imaging [22]. Hakenjos et al. measured the current and temperature distribution using IR thermography in order to obtain the temperature distribution along the GDL of a PEMFC [23]. They also observed flow-field flooding through images taken from temperature distribution. Daino et al. have performed similar work aimed at identifying temperature gradients along GDL layers within PEMFCs [24].

In this paper, a simple mathematical lumped model is used to examine the effect of temperature on the parameters and fundamental physical and chemical properties that determine PEFC performance. First, an analytical approach is adopted that examines the sensitivity of the equations to small changes in temperature by using the differential dV/dT to map the operating range of polarisation and nominal operating temperature. However, this does not capture the stochastic nature of the uncertainty associated with practical operation, so a second analysis is performed that applies a statistical treatment to develop a 'probability map' of fuel cell polarisation performance.

In order to support the statistical study, an experimental characterisation of a commercial air-cooled stack is performed that uses high-resolution thermal imaging to characterise the kind of spatial and temporal temperature uncertainty that can be expected in a practical operating system.

The intention of this study is to provide fuel cell developers with a basis for estimating the expected level of uncertainty in polarisation performance based on a given uncertainty in the temperature of the system (spatial and temporal). A key outcome is that conventional polarisation curves should be considered as 'polarisation areas' or 'bands' with variable uncertainty across their operating range.

1.1. *Temperature uncertainty in fuel cell operation*

Temperature distribution within fuel cells has been modelled using a range of techniques and length scales; for example, Shimpalee and Dutta describe the temperature variation across the flow channel width [21] and Pharoah and Burheim at the cell level [20]. However, models rarely consider the effect of measurement and physical uncertainty on cell performance.

Mawardi and Pitchumani investigated the impacts of uncertainty in materials and operating parameters on fuel cell performance by using a one dimensional, non-isothermal mathematical model [14]. Parametric analysis was used to determine how cell voltage and power density change with uncertainty, where the input samples were generated stochastically using the Latin Hypercube Sampling (LHS) method.

To show the significance of temperature on other variables like degradation rate, Placca et al. demonstrated the effect of the interaction between temperature and degradation rate on overall performance of fuel cells [25]. The Response Surface Method (RSM) was applied in this study to analyse the effect of uncertainty in these variables on polarisation ($V–I$) curves. However, no attempt was made to quantify the association between the measurement uncertainty and temporal and spatial temperature distribution.

2. Model development

For the purpose of analytical and statistical analysis, a mathematical model is required to describe the thermodynamics of the system, kinetics, mass and charge transfer as a function of temperature.

2.1. *Model assumptions and equations*

A lumped, semi-empirical, mathematical model is used to simulate PEFC operation [10,11]. The purpose of using this model is to indicate the effect of temperature on different parameters and identify their impact on overall performance. Therefore, some of the parameters, such as exchange current density and conductivity, which are usually measured experimentally, are expressed using empirical equations, which themselves can generate discrepancy due to model uncertainty. However, the focus of this work is the impact of temperature uncertainty on cell performance, whereas model uncertainty is assumed negligible. The following assumptions are applied: (i) steady state system; (ii) incompressible and ideal gases; (iii) single phase vapour water; (iv) heat loss is negligible; (v) pressure drop is negligible; (vi) current distribution is uniform; and (vii) there is no reactant consumption along the length of the flow channel (reactant distribution is homogeneous).

Simple lumped models of PEFC operation are well documented and have been used for a wide variety of applications [11]. The model used here follows a well-established protocol with the key equations summarised in Table 1 [10,26–29], and the physical constants and parameters defined in Table 2 [10,11,17,25–28]. The important role of temperature in determining PEFC performance is evident by the common appearance of T in the governing equations, which include logarithmic, exponential, power and linear functions.

As is commonly used in fuel cell modelling, the empirical Bruggeman correlation was used to estimate conductivity and diffusivity [30–32]. However, this assumes that there is no liquid water present in the cell. At low temperature and high current density there is a higher chance of liquid water formation. Under such conditions fuel cell performance may be more sensitive to temperature uncertainty and theoretical correlations such as those described by Das et al. may be considered [33].

Table 1 – List of equations used to describe the physical mode of the PEFC.

Name	Equations
Species mass flux	$M_{H_2} = \lambda_{H_2}\frac{iA}{n_a F}$ $M_{O_2} = \lambda_{O_2}\frac{iA}{n_c F}$ $M^{v}_{H_2O,c} = \left\lvert\frac{y_{H_2O_{in}}}{1-y_{H_2O_{in}}}\right\rvert_c M_{O_2}$ $M^{v}_{H_2O,a} = \left\lvert\frac{y_{H_2O_{in}}}{1-y_{H_2O_{in}}}\right\rvert_a M_{H_2}$ $y_{H_2O,a} = RH_{fuel}\frac{P^{sat}_{H_2O}}{P}$ $y_{H_2O,c} = RH_{air}\frac{P^{sat}_{H_2O}}{P}$
Thermodynamic	$E_0 = \frac{dH-TdS}{nF}$ $E_{rev} = E_0 - \frac{RT}{nF}\ln\left(\frac{P_{H_2O}}{P_{H_2}P^{0.5}_{O_2}}\right)$ $P^{sat}_{H_2O} = \exp((2.95\times10^{-2})T - (9.18\times10^{-5})T^2 + (1.44\times10^{-7})T^3 - 2.18)$
Activation loss at the electrodes	$i_0 = i_0^{ref} a_c L_c \left(\frac{Pr_{O_2}}{P^{ref}}\right)^{\gamma}\exp\left(\frac{-E_c}{RT}\left(1-\frac{T}{T^{ref}}\right)\right)$ $Pr_{O_2} = \frac{P_{air}}{\exp\left(\frac{4.192i}{T^{1.344}}\right)} - P_{H_2O}$ $\eta_{act} = \left[\frac{RT}{\alpha nF}\ln\frac{i}{i_0}\right]_a + \left[\frac{RT}{\alpha nF}\ln\frac{i}{i_0}\right]_c$
Ohmic loss at the membrane	$\kappa_{mem} = (0.00514c_m - 0.000326)\exp\left(1268\left(\frac{1}{303}-\frac{1}{T}\right)\right)$ $c_m = 0.043 + 17.18a_m - 39.85a_m^2 + 36a_m^3$ $a_m = \beta a_a + (1-\beta)a_c$ $a_a = \frac{M^{v}_{H_2O,a}}{M^{v}_{H_2O,a}+M_{H_2}}\cdot\frac{P}{P^{sat}_{H_2O}}$ $a_c = \frac{M^{v}_{H_2O,c}}{M^{v}_{H_2O,c}+M_{O_2}}\cdot\frac{P}{P^{sat}_{H_2O}}$ $\eta_{ohmic} = R\cdot i = \frac{l_{mem}}{\kappa_{mem}}\cdot i$
Concentration loss at the electrodes	$i_{L,c} = n_c F D^{eff}\frac{c_{O_2}}{\delta_{GDL}}$ $D^{eff} = D_{O_2/N_2}\varepsilon^{1.5}$ $D_{O_2/N_2} = D^{ref}_{O_2/N_2}\left(\frac{T}{T^{ref}}\right)^{3/2}\left(\frac{P^{ref}}{P}\right)$ $C_{O_2} = x_{O_2}\frac{P}{RT}$ $\eta_{con} = \left[\frac{RT}{\alpha nF}\ln\frac{i_L}{i_L-i}\right]_a + \left[\frac{RT}{\alpha nF}\ln\frac{i_L}{i_L-i}\right]_c$

Table 2 – Physical constants used in the model.

Parameter	Value
Catalyst loading (L_c)	0.125 mg(Pt) cm^{-2}
Catalyst-specific area (a_{ca})	0.4 cm^2 mg^{-1}
Faraday's constant (F)	96,486 C mol^{-1}
Ideal gas constant (R)	8.314 J mol^{-1} K^{-1}
Membrane thickness (l)	0.01275 cm
Reference exchange current density (i_0^{ref})	3×10^{-9} A cm^{-2}
Reference temperature (T_{ref})	298 K
Reference pressure (P_{ref})	1 atm
Reference Gibbs free energy (G_{ref})	−228,170 J mol^{-1}
Activation energy (E_c)	76,500 J mol^{-1}
Diffusion coefficient of water in membrane (D_0)	5.5×10^{-7} cm^2 s^{-1}
Active area (A)	25×10^4 cm^2
Operating pressure (P)	1.5 atm
Oxygen pressure (P_{O_2})	5 atm
Hydrogen pressure (P_{H_2})	3 atm
Water pressure (P_w)	1 atm
Reference binary diffusion coefficient (D^{ref}_{ij})	0.1 cm^2 s^{-1}
GDL thickness (t_{GDL})	0.05 cm
Enthalpy change (dH)	−242,367.25 J
Entropy change (dS)	−84.2 J
Cathode water activity (α_c)	0.3
Anode water activity (α_a)	0.5
Porosity (ε)	0.444
Number of electrons at cathode (n_c)	4
Number of electrons at anode (n_a)	2
Relative humidity of air (RH_{air})	0.5
Relative humidity of fuel (RH_{fuel})	1
Stoichiometric ratio of hydrogen (λ_{H_2})	1.25
Stoichiometric ratio of oxygen (λ_{O_2})	2
Pressure coefficient (γ)	0.5
Oxygen mole fraction (x_{O_2})	0.21

The overall polarisation curve is generated by subtracting the relevant over-potentials from the open circuit potential:

$$V = E_{rev} - \eta_{act} - \eta_{ohmic} - \eta_{con} \tag{1}$$

where, E_{rev} is open circuit voltage at zero current density. The Nernst equation is used to describe the thermodynamics. η_{act} is the activation loss due to kinetics of reaction, which depends on the rate of the reactions at the surface of the electrodes. η_{ohm} is the ohmic loss taken to be exclusively due to the ionic resistance of the electrolyte membrane, which is a function of water content and temperature. η_{con} is concentration loss and is a function of the activity of reactants and products and also rate of diffusion of species through the GDL.

2.2. Analytical treatment

The effect of operating temperature on PEFC performance is commonly reported in the range of 30–80 °C [15–17,34], with Das et al. showing that the effect is most significant at high current densities [34].

To determine the sensitivity of cell voltage, based on the intrinsic physics of the system, with respect to temperature and current density, the differential of cell voltage with

Table 3 – Variance of error as a function of sample and bin size.

Sample size	Bin size	V_{error}
100	10	0.5
1000	100	0.158
10,000	1000	0.05
100,000	10,000	0.0158

respect to temperature is determined by applying a small change in temperature (0.05 °C) to the model equations, such that:

$$\frac{dV}{dT} \approx \frac{V_2 - V_1}{T_2 - T_1} \tag{2}$$

2.3. *Statistical treatment*

To predict the probabilistic deviation of cell voltage due to uncertainty in temperature, a statistical analysis is used that employs a Monte Carlo Simulation (MCS) to provide a random normal distribution of temperature samples. A normal distribution (Gaussian) is employed to describe the statistical spread (uncertainty) of temperatures [35].

To establish the effect of temperature, the standard deviation of ±5 °C is selected for 10,000 samples. Previous studies have reported 3–11 °C temperature variation in a fuel cell due to different uncertainties and operating conditions [20,21,25]. Also, the tests carried out on the commercial stack suggests that this is an appropriate base-case for examining temperature uncertainty.

It is important to choose a suitable sample size which is large enough to give sufficient confidence in the results, but not so large as to lead to unnecessary processing time. To assess this, the model was run from 100 to 100,000 samples in order to develop a distribution curve.

Table 3 shows how different sample size and bin size can affect the variance of error (V_{error}). A sample size of 10,000 was chosen as a suitable trade-off between accuracy and processing time.

To generate the samples, Equation (3) [36] is implemented in Octave (GNU Octave), a high level programming language that provides access to a number of solvers for linear and nonlinear numerical computations [37].

$$T = T_{mean} + \sigma \cdot \mathrm{randn}(n, m) \tag{3}$$

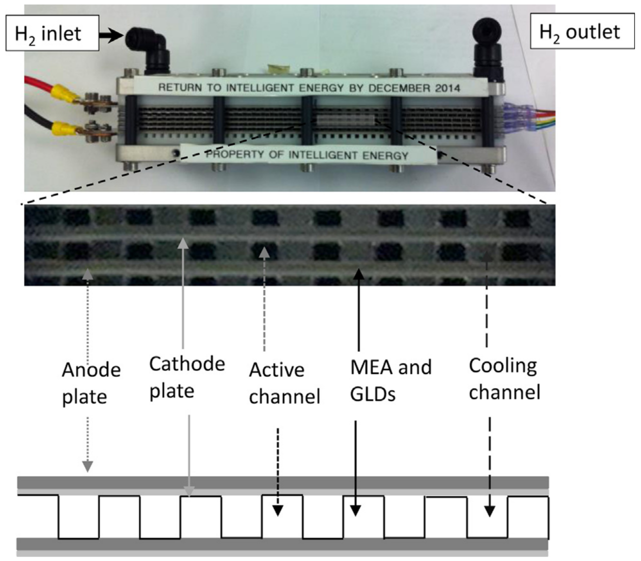

Fig. 2 – Picture and sketch of the fuel cell stack showing the active and cooling channels.

where T_{mean} is the mean operating temperature and σ is the standard deviation of distribution.

The obtained data are characterised by statistical analysis: skewness and coefficient of variance (CV), to present the degree of asymmetry of the distributions and measure of dispersion of voltage. Positive skew has a longer tail on the right hand side (higher values) of the mean value and negative skew is bias towards lower values. A distribution curve is classified as symmetrical when the skewness is zero. Because of the nature of the model and logarithmic expressions used in the model, Equation (4) is used to calculate the skewness, where N is the total number of samples [38]:

$$\text{skewness} = \frac{\left(\sum (x - \mu(x))^3\right) / N}{\sigma^3} \tag{4}$$

To verify the skewness, Equation (5) is used to indicate the degree of skewness by comparing the obtained values with the standard error of skew (SES) [39].

$$\text{SES} = \sqrt{\frac{6}{N}} \tag{5}$$

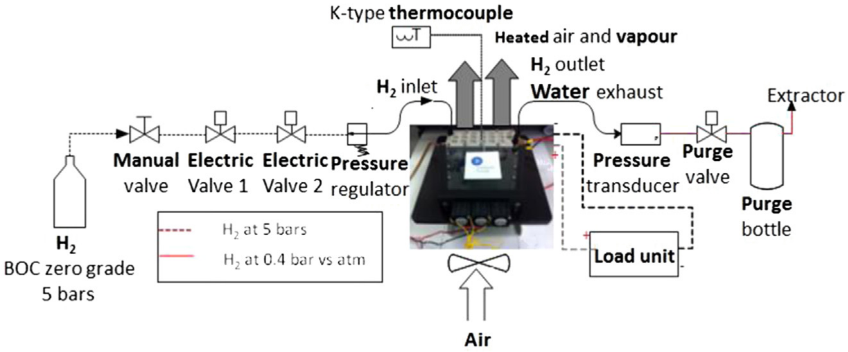

Fig. 1 – Experimental test station for the 5 cell stack.

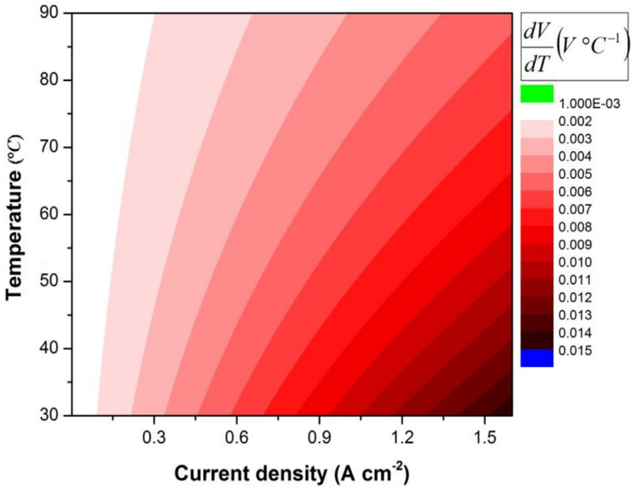

Fig. 3 – **Sensitivity map based on analytical analysis showing differential change in voltage with temperature (d*V*/d*T*) as a function of nominal operating temperature and current density.**

The coefficient of variance (CV), which is often expressed as a percentage, is used to compare the standard deviation of data at diverse mean values [14], where σ is standard deviation of distribution and μ is the mean value [40].

$$\mathrm{CV} = \frac{\sigma}{\mu} \tag{6}$$

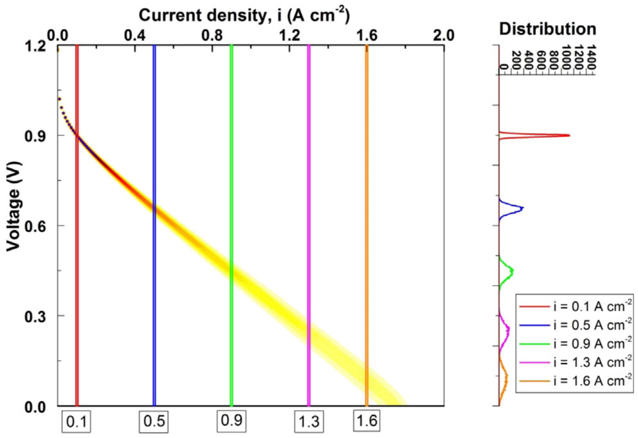

Fig. 5 – **Contour plot of *V*–*I* polarisation 'area' at mean operating temperature of 80 °C with standard deviation of ±5 °C generated by MCS. Plot to the right hand side shows the voltage distribution at current density of 0.1, 0.5, 0.9, 1.3, and 1.7 A cm^{-2}.**

3. Experimental

3.1. *Stack operation*

Fuel cell stack operation was carried out using a 5-cell air cooled (AC) open-cathode stack (Intelligent Energy Ltd., UK) [41,42].

This test station, displayed Fig. 1, is used to supply dry, non-heated, pressurized hydrogen in dead-ended mode to the anodes, and oxygen is supplied to the cathode using three fans blowing ambient air through the open cathodes (stack and channel

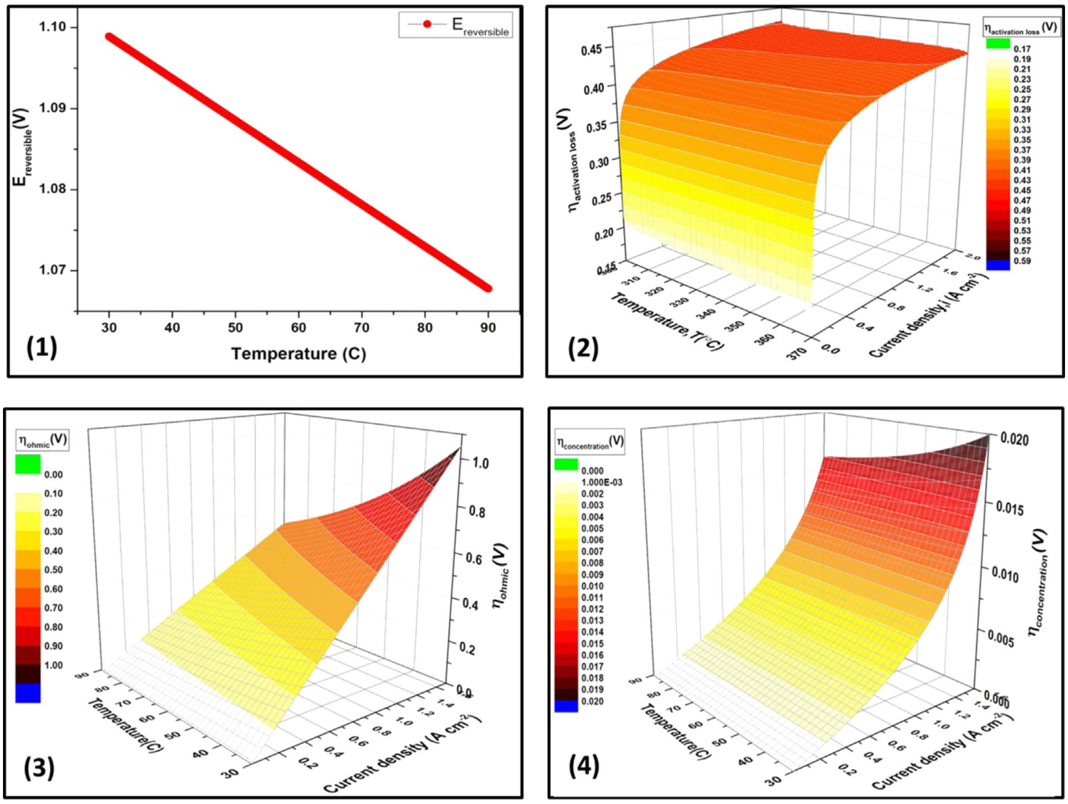

Fig. 4 – **Effect of temperature on (1) OCV, (2) activation loss, (3) Ohmic loss and (4) concentration loss.**

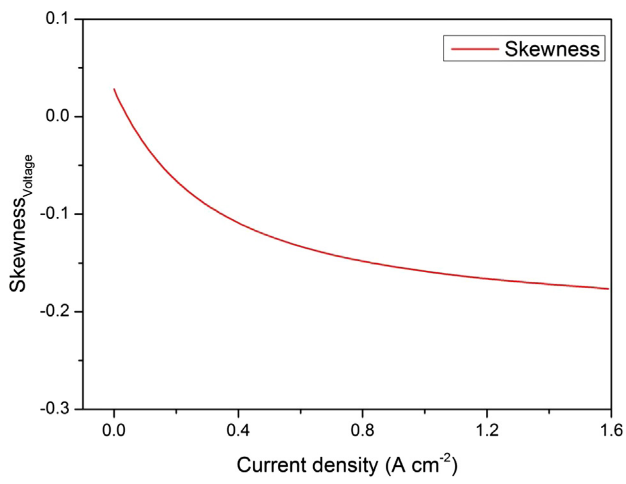

Fig. 6 – Skewness of V–I polarisation 'area' at operating temperature of 80 °C and standard deviation of ±5 °C.

configuration shown in Fig. 2). The fans are powered by a programmable power supply (3649A Agilent), and the fuel cell was loaded using an Agilent 6060B load unit; each controlled using bespoke software (LabVIEW, National Instruments) using a GPIB interface. Each of the 5 cells has a membrane surface area of 60 cm^2.

Due to its unique design, it does not require any external heating and operates from room temperature. Heat is generated by the electrochemical reactions and Joule heating.

A K-type thermocouple was used to record the internal temperature in the central area of the fuel cell and operate the PID controller. The PID controller treats the temperature as an input, and changes the speed of the fans in order to regulate the temperature to its predefined setpoint.

3.2. *Heat management and thermal imaging*

Temperature mapping, either with thermocouples [43–46], micro sensors measuring the temperature and humidity [47], thermistors [48], thermal imaging [23] [49–54], of fuel cells has shown to be a powerful tool to understand the performance and validate heat transfer models. The open-cathode configuration of the AC stack makes it an ideal system for thermal imaging because it is possible to directly point the camera at the active and cooling channels.

Thermal imaging was performed using a 640 × 512 focal plane array InSb camera (SC5600MB FLIR, UK). The camera was calibrated for the temperature range in question (15–100 °C) with the images being recorded using commercially available software (ResearchIR, FLIR ATC, Croissy-Beaubourg, France). Images were recorded at a frequency of 25 Hz for a period greater than 10 min to ensure a statistically significant number of data points were collected.

4. Results and discussion

4.1. *Analytical interpretation*

The analytical approach provides insight into the physics of the system and how temperature makes an impact on performance. Fig. 3 shows the variation in differential cell voltage with respect to temperature as a function of current density and absolute operating temperature. It can be seen that the PEFC becomes more sensitive to temperature change with increasing current density and reduced temperature; increasing to over 10 mV °C^{-1} above 1 A cm^{-2} from 30 to 90 °C.

The effect of temperature on the various loss mechanisms can be seen in Fig. 4. The following observations can be made: (i) the entropy change associated with the formation of water leads to a small change in OCV over this temperature range; (ii) electro-kinetics improve with temperature resulting in lower activation loss due to exponential increase in ORR i_0 with temperature; (iii) Ohmic loss increases linearly with current, increased temperature results in a reduction of the resistance inside the cell due to increased proton conductivity; (iv) concentration loss, which is mainly dominant at higher

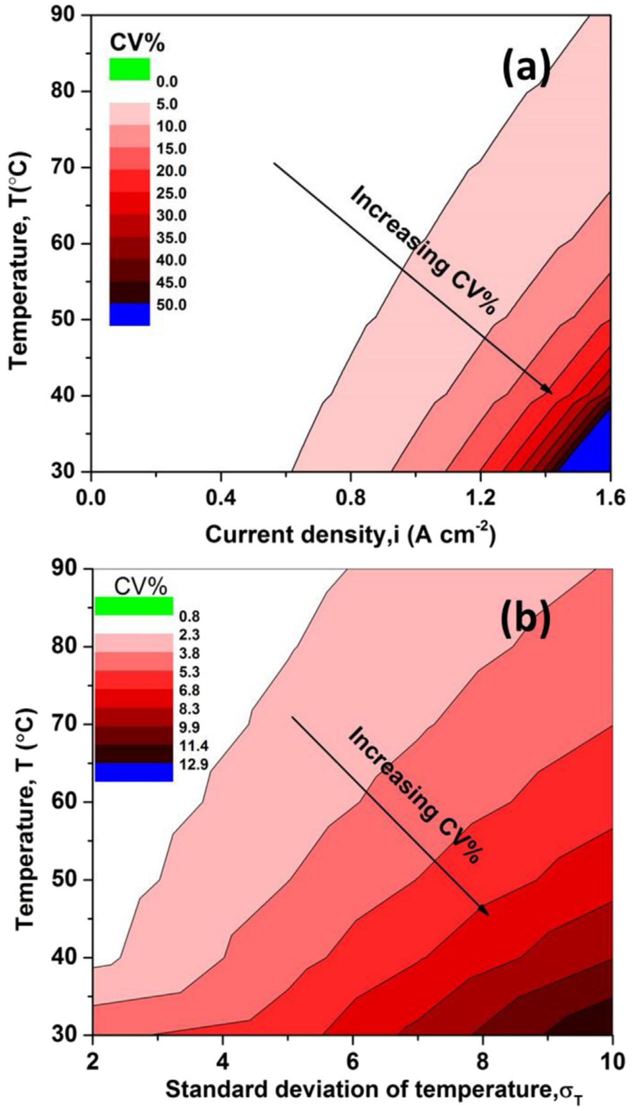

Fig. 7 – Contour plots showing: (a) how CV changes at different mean operating temperatures for ±5 °C; (b) how CV changes at an operating temperature of 80 °C with various standard deviation of temperature uncertainty at $i = 0.6$ A cm^{-2}.

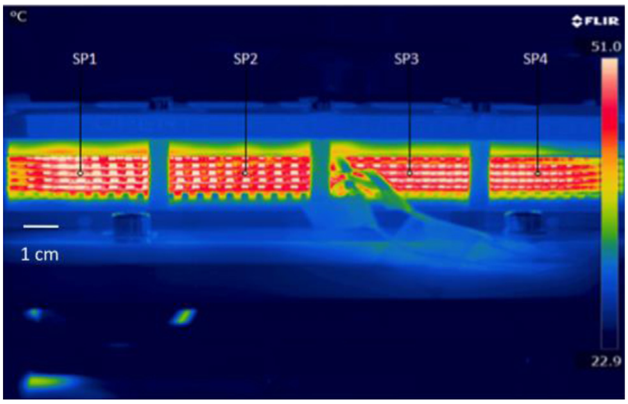

Fig. 8 – Thermal image of fuel cell stack at a current loading of 46 A (0.78 A cm^{-2}) after equilibrating for 25 min.

current density, also reduces with temperature due to improved diffusion, gas mobility and species concentration resulting in better mass transport and larger limiting current density.

4.2. *Statistical interpretation*

To capture the probabilistic behaviour of cell performance under temperature uncertainly, MCS sampling was used to provide temperature input samples for a mean operating temperature of 80 °C and standard deviation of ±5 °C. The samples generated by MCS are introduced into the deterministic lumped mathematical PEFC model to obtain cell voltage for various current densities.

It is apparent from Fig. 5 that voltage distribution is not uniform at different current densities. The colour map shows that as current density increases, the width of the distribution increases. This figure clearly shows that the expectation of a polarisation response to conform to a single 'line' is not reasonable when there is uncertainty associated with temperature (or other operating parameters). Rather, a polarisation 'area' or 'band' better describes the situation.

It can be seen in Fig. 5 that performance shows higher sensitivity at larger current density due to non-linearity of the model which is more dominant at higher current density.

To calculate the degree of asymmetry of a distribution over various current densities, the skewness is determined to show the effect of temperature variation on cell performance. It can be seen in Fig. 6, there is a tendency towards lower voltage in the *V*–*I* polarisation area due to higher overpotential and probabilistic effect of temperature on the cell performance. It can be seen that skewness of the voltage distribution becomes more negative with increased current density, i.e. fuel cell voltage will be more likely to be biased towards lower voltage. To establish the extent of skewness, Equation (5) is used to determine the SES. The results show that over a current density of 0.2 A cm^{-2} the magnitude of the skewness is larger than twice the SES. This indicates that the distribution can be regarded as significantly skewed towards a lower voltage with increasing current.

Fig. 7(a) shows how CV changes at different operating temperatures (30–90 °C), taking a temperature uncertainty of ±5 °C. The trend across current and temperature is qualitatively the same as that observed in the analytical analysis; however, this interpretation allows the probability at each condition to be quantified.

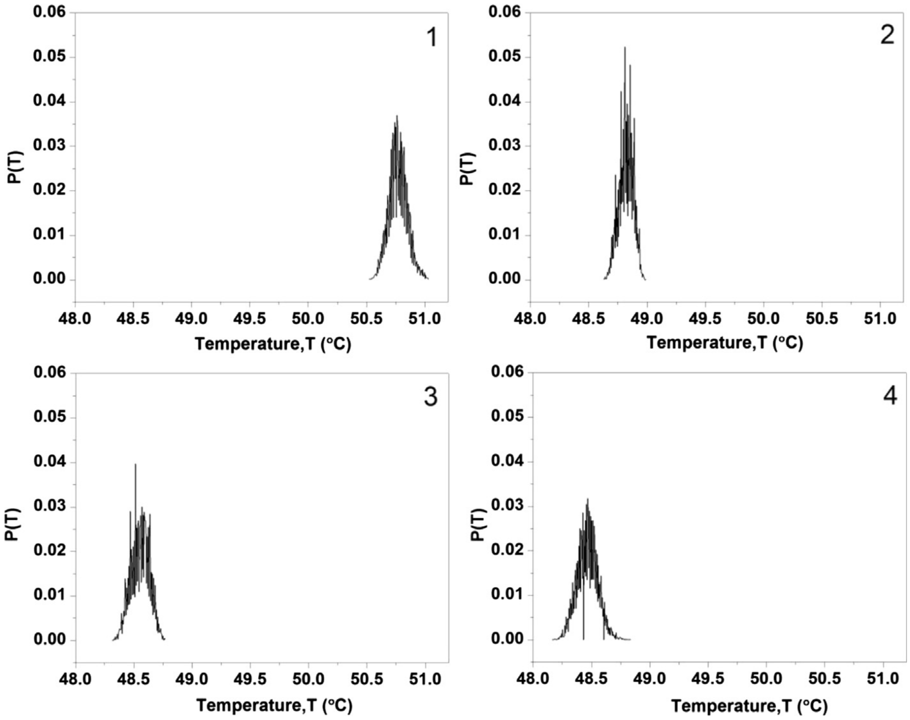

Fig. 9 – Temperature distribution after 25 min fuel cell operation at current density 0.78 A cm^{-2}. Figs. 1–4 show the four points (SP1–SP4) along the middle cell. SP1 is the closest point to H_2 entrance and SP4 is the furthest.

Table 4 – -Statistical variables for four points along the MEA at current density 0.78 A cm^{-2} after 25 min of data collection.

Statistical variables	SP1	SP2	SP3	SP4
Mean	50.8	48.8	48.5	48.5
CV%	0.044	0.041	0.037	0.08
Skewness	1.4×10^{-13}	1.3×10^{-13}	8.6×10^{-14}	5.2×10^{-14}

To establish how dispersion of cell voltage relates to the given temperature uncertainty, the CV of cell voltage is calculated for different σ_T values at a current density of 0.6 A cm^{-2} (Fig. 7(b)). It can be seen that regardless of temperature uncertainty the σ_T increases monotonically.

4.3. *Stack testing*

4.3.1. *Thermal imaging*

Thermal imaging measurements achieved a pixel resolution of ~0.35 mm. The noise-equivalent temperature difference (NETD), a measure of the signal-to-noise ratio, of the camera during the experiments was recorded as 19 mK, demonstrating a high thermal resolution.

A calibration was conducted in order to eliminate environmental reflections. To achieve this, a diffuse reflector was used to enable the environmental emissivity to be set to unity. In investigating the temperature distribution of the stack, each channel represented a cavity that could be considered to be a quasi-black body [55]. This allows an emissivity approaching unity to be used; in this case, 0.98 was chosen. By utilising this technique a direct comparison can be made between the active and cooling channels without the need to calculate the emissivity of each channel.

Fig. 8 shows a thermal image of the stack seen from the side with air exiting the system. It can be seen that there is substantial temperature variation across the stack with ~12 °C difference between the active and cooling channels (active –white and cooling – red). The figure also shows the position of four different point measurements (SP1–SP4) made along the central cell in the stack, used to assess lateral temperature variation in space and time.

4.3.2. *Statistical interpretation of experimental temperature distribution*

The temporal temperature distribution for each of the four points displays a Gaussian distribution (Fig. 9), the statistical characterisation for each point is shown in Table 4. It can be seen that the CV of location 1 to location 4 increases by almost 50% showing that the spatial distribution itself has ranging temporal variation. Also in the same table it can be seen that the skewness is effectively zero.

5. Conclusion

Temperature is a key parameter for determining PEFC performance and uncertainty in this parameter is reflected in the variability in the polarisation response. An analytical and statistical approach has been used to determine the sensitivity and probability of performance variation as a function of current density and nominal operating temperature.

Lower cell temperatures and higher current densities are predicted to lead to the greatest variation in performance for a given temperature change or statistical variation ('uncertainty'). The study has identified an effective polarization 'area' or 'band', in contrast to the widely quoted polarization 'curve', as being the most appropriate way to represent model predictions of fuel cell performance.

The cell performance variation due to temperature distribution at a given point in the V–I polarisation area translates into the negative skewness. This means that there is a tendency for the V–I area to be biased towards a lower voltage. Therefore, reported polarisation data will tend to err on the side of poorer perceived performance due to the natural variation in temperature for a given system.

Thermal imaging on an operational PEFC stack allows the spatial and temporal variation in temperature to be assessed. The experiments show that the width of temperature distribution decreases spatially towards the "dead-end" of the stack. A temperature variation of over 12 °C was observed across the active area of the stack (air exit face), whereas the variation across the central MEA was ~2.5 °C and the temporal variation has a standard deviation of ±0.5 °C.

Acknowledgements

The authors would like to acknowledge EPSRC Supergen Fuel Cells for supporting the work of Noorkami and Brett (EP/G030995/1), the EPSRC 'Mind the Gap' UK/India project (EP/I037024/1) for supporting Brett and EPSRC Multiscale in-situ characterisation of degradation and reactivity in solid oxide fuel cells (EP/J001007/1) for supporting Robinson. We also acknowledge the STFC for supporting Shearing and Brett (ST/K00171X/1); and The Royal Academy of Engineering for supporting Shearing.

REFERENCES

[1] Springer TE, Zawodzinski TA, Gottesfeld S. Polymer electrolyte fuel cell model. J Electrochem Soc 1993;138(8):2334–42.

[2] Sammes N, Boersma R. Small-scale fuel cells for residential applications. J Power Sources Mar. 2000;86(1–2):98–110.

[3] Zhang Z, Huang X, Jiang J, Wu B. An improved dynamic model considering effects of temperature and equivalent internal resistance for PEM fuel cell power modules. J Power Sources Oct. 2006;161(2):1062–8.

[4] Yalcinoz T, Alam M. Improved dynamic performance of hybrid PEM fuel cells and ultracapacitors for portable applications. Int J Hydrogen Energy Apr. 2008;33(7):1932–40.

[5] El-Sharkh MY, Rahman A, Alam MS, Byrne PC, Sakla AA, Thomas T. A dynamic model for a stand-alone PEM fuel cell power plant for residential applications. J Power Sources Nov. 2004;138(1–2):199–204.

[6] El-Sharkh MY, Rahman A, Alam MS. Neural networks-based control of active and reactive power of a stand-alone PEM

fuel cell power plant. J Power Sources Sep. 2004;135(1–2):88–94.
[7] Mert SO, Dincer I, Ozcelik Z. Exergoeconomic analysis of a vehicular PEM fuel cell system. J Power Sources Feb. 2007;165(1):244–52.
[8] Gencoglu MT, Ural Z. Design of a PEM fuel cell system for residential application. Int J Hydrogen Energy Jun. 2009;34(12):5242–8.
[9] Yilanci A, Dincer I, Ozturk H. Performance analysis of a PEM fuel cell unit in a solar–hydrogen system. Int J Hydrogen Energy Dec. 2008;33(24):7538–52.
[10] Nguyen TV, White RE. A water and heat management model for proton-exchange-membrane fuel cells. J Electrochem Soc 1993;140(8).
[11] Ang SMC, Brett DJL, Fraga ES. A multi-objective optimisation model for a general polymer electrolyte membrane fuel cell system. J Power Sources 2010;195:2754–63.
[12] Das PK, Li X, Liu Z-S. Analysis of liquid water transport in cathode catalyst layer of PEM fuel cells. Int J Hydrogen Energy Mar. 2010;35(6):2403–16.
[13] Das PK, Li X, Xie Z, Liu ZS. Effects of catalyst layer structure and wettability on liquid water transport in polymer electrolyte membrane fuel cell 2011;(June):1325–39.
[14] Mawardi A, Pitchumani R. Effects of parameter uncertainty on the performance variability of proton exchange membrane (PEM) fuel cells. J Power Sources 2006;160:232–45.
[15] Srinivasulu GN, Subrahmanyam T, Rao VD. Parametric sensitivity analysis of PEM fuel cell electrochemical Model. Int J Hydrogen Energy 2011;36(22):14838–44.
[16] Tao WQ, Min CH, Liu XL, He YL, Yin BH, Jiang W. Parameter sensitivity examination and discussion of PEM fuel cell simulation model validation part I. Current status of modeling research and model development. J Power Sources 2006;160:359–73.
[17] Min CH, He YL, Liu XL, Yin BH, Jiang W, Tao WQ. Parameter sensitivity examination and discussion of PEM fuel cell simulation model validation part II: results of sensitivity analysis and validation of the model. J Power Sources 2006;160:374–85.
[18] Yan W-M, Chen C-Y, Mei S-C, Soong C-Y, Chen F. Effects of operating conditions on cell performance of PEM fuel cells with conventional or interdigitated flow field. J Power Sources Nov. 2006;162(2):1157–64.
[19] Correa G, Borello F, Santarelli M. Sensitivity analysis of temperature uncertainty in an aircraft PEM fuel cell. Int J Hydrogen Energy Nov. 2011;36(22):14745–58.
[20] Pharoah JG, Burheim OS. On the temperature distribution in polymer electrolyte fuel cells. J Power Sources 2010;195(16):5235–45.
[21] Shimpalee S, Dutta S. Distribution in PEM fuel cells. Numer Heat Trans 2000;38:111–28.
[22] Aieta NV, Das PK, Perdue A, Bender G, Herring AM, Weber AZ, et al. Applying infrared thermography as a quality-control tool for the rapid detection of polymer-electrolyte-membrane-fuel-cell catalyst-layer-thickness variations. J Power Sources Aug. 2012;211:4–11.
[23] Hakenjos A, Muenter H, Wittstadt U, Hebling C. A PEM fuel cell for combined measurement of current and temperature distribution, and flow field flooding. J Power Sources 2004;131:213–6.
[24] Daino MM, Lu Z, LaManna JM, Owejan JP, Trabold TA, Kandlikar SG. Through-plane water transport visualization in a PEMFC by visible and infrared imaging. Electrochem Solid State Lett 2011;14(6):B51.
[25] Placca L, Kouta R. Effects of temperature uncertainty on the performance of a degrading PEM fuel cell model. J Power Sources 2009;194:313–27.
[26] Nguyen TV. An along-the-channel model for proton exchange membrane fuel cells. J Electrochem Soc 1998;145(4):1149–59.
[27] O'Hayre R, Cha S-W, Colella W, Prinz FB. Fuel cell fundamentals. 2nd ed. Wiley; 2009. pp. 25–194.
[28] Spiegel C. PEM fuel cell modeling and simulation using matlab. Academic Press; 2011. p. 456.
[29] Cussler EL. Diffusion mass transfer in fluid systems. Cambridge University Press; 2009. pp. 117–60.
[30] Bernardi DM, Verbrugge MW. A mathematical model of the solid-polymer-electrolyte fuel cell 1992;139(9).
[31] Nam JH, Kaviany M. Effective diffusivity and water-saturation distribution in single- and two-layer PEMFC diffusion medium. Int J Heat Mass Trans Nov. 2003;46(24):4595–611.
[32] Meng H, Wang C-Y. Electron transport in PEFCs. J Electrochem Soc 2004;151(3):A358.
[33] Das PK, Li X, Liu Z-S. Effective transport coefficients in PEM fuel cell catalyst and gas diffusion layers: beyond Bruggeman approximation. Appl Energy Sep. 2010;87(9):2785–96.
[34] Das PK, Li X, Liu Z-S. Analytical approach to polymer electrolyte membrane fuel cell performance and optimization. J Electroanal Chem Jun. 2007;604(2):72–90.
[35] Montgomery GC, Runger Douglas C. Continuous random variables and probability distributions. In: Applied statistics and probability for engineers, 3rd ed.: John Wiley & Sons, Inc. p. 97–140.
[36] Randn, MathWorks [Online]. Available: http://www.mathworks.co.uk/help/matlab/ref/randn.html.
[37] Eaton W. GNU octave manuals [Online]. Available: http://www.gnu.org/software/octave/doc/interpreter/; 1997.
[38] Weisstein EW, Skewness, MathWorld-A Wolfram web Resource [Online]. Available: http://mathworld.wolfram.com/Skewness.html.
[39] Bell M. Skew and how skewness is calculated in statistical software, Math/Chaos Theory Suite101 [Online]. Available: http://suite101.com/article/skew-and-how-skewness-is-calculated-in-statistical-software-a231005; 2009.
[40] Fleming Michael C, Nellis Joseph G. Describing data-variability. In: Nellis Joseph G, editor. Principles of applied statistics. 1st ed. New York: Routledge; 1994. pp. 54–7.
[41] Wu J, Galli S, Lagana I, Pozio A, Monteleone G, Yuan XZ, et al. An air-cooled proton exchange membrane fuel cell with combined oxidant and coolant flow. J Power Sources Mar. 2009;188(1):199–204.
[42] Santa Rosa DT, Pinto DG, Silva VS, Silva RA, Rangel CM. High performance PEMFC stack with open-cathode at ambient pressure and temperature conditions. Int J Hydrogen Energy Dec. 2007;32(17):4350–7.
[43] Wilkinson M, Blanco M, Gu E, Martin JJ, Wilkinson DP, Zhang JJ, et al. In situ experimental technique for measurement of temperature and current distribution in proton exchange membrane fuel cells. Fuel Cell 2006:507–11.
[44] Matian M, Marquis A, Brett D, Brandon N. An experimentally validated heat transfer model for thermal management design in polymer electrolyte membrane fuel cells. Proc Inst Mech Eng Part A J Power Energy Dec. 2010;224(8):1069–81.
[45] Zhang G, Guo L, Ma L, Liu H. Simultaneous measurement of current and temperature distributions in a proton exchange membrane fuel cell. J Power Sources 2010;195(11):3597–604.
[46] Lottin O, Colinart T, Chupin S, Didierjean S. A multi-instrumented polymer exchange membrane fuel cell: observation of the in-plane non-homogeneities. J Power Sources 2008;180:748–54.
[47] Lee C, Hsieh W, Wu G. Embedded flexible micro-sensors in MEA for measuring temperature and humidity in a micro-fuel cell. Fuel Cell 2008;181:237–43.

[48] He S, Mench MM, Tadigadapa S. Thin film temperature sensor for real-time measurement of electrolyte temperature in a polymer electrolyte fuel cell. Sensors Actuat 2006;125:170–7.
[49] Wang M, Guo H, Ma C. Temperature distribution on the MEA surface of a PEMFC with serpentine channel flow bed. J Power Sources 2006;157:181–7.
[50] Guo H, Hai M, Ye F, Fang C. Experimental study of temperature distribution on anodic surface of MEA inside a PEMFC with parallel channels flow bed. Int J Hydrogen Energy 2012;37(17):13155–60.
[51] Martins LS, Gardolinski JEFC, Vargas JVC, Ordonez JC, Amico SC, Forte MMC. The experimental validation of a simplified PEMFC simulation model for design and optimization purposes. Appl Thermal Eng 2009;29(14–15):3036–48.
[52] Shimoi R, Masuda M, Fushinobu K, Kozawa Y, Okazaki K. Visualization of the membrane temperature field of a polymer electrolyte fuel cell. J Energy Resour Technol 2004;126(December):258–61.
[53] Matian M, Marquis AJ, Brandon NP. Application of thermal imaging to validate a heat transfer model for polymer electrolyte fuel cells. Int J Hydrogen Energy Nov. 2010;35(22):12308–16.
[54] Brett DJL, Aguiar P, Clague R, Marquis AJ, Schöttl S, Simpson R, et al. Application of infrared thermal imaging to the study of pellet solid oxide fuel cells. J Power Sources Mar. 2007;166(1):112–9.
[55] Vollmer M, Mollmann K-P. Infrared thermal imaging-fundamentals, research and applications; 2010. Weinheim.

Chapter 10

Publication 2

References

[1] *Carbon dioxide emissions.* United States Environmental Protection Agency, http://www.epa.gov/climatechange/ghgemissions/gases/co2.html#Trends, 2012. (last updated on: 14/06/2012).

[2] O. Edenhofer, R.P. Madruga, Y. Sokona, K. Seyboth, P. Eickemeier, P. Matscoss, G. Hansen, S. Kadner, S. Schlomer, T. Zwickel, and V. Stechow, Ch. Special Report on Renewable Energy SOurces and Climate Change MItigation. Technical report, Intergovernmental Panel on Climate Change (IPCC), 32 Avenue of the Americas, New York, NY 10013-2473, USA, 2012.

[3] Hyundai. Hyundai's leading Fuel Cell technology. http://www.hyundai.co.uk/about-us/environment/hydrogen-fuel-cell, 2013.

[4] *First hydrogen fuel cell powered ferry in UK showcases green technology.* Renewable energy focus, http://www.renewableenergyfocus.com/view/33545/first-hydrogen-fuel-cell-powered-ferry-in-uk-showcases-green-technology/, 2013.

[5] BBC. Wind Power. Technical report, Climate Change from the BBC Weather Centre, 2013. http://www.bbc.co.uk/climate/adaptation/wind_power.shtml.

[6] A. Mawardi and R. Pitchumani. Effects of parameter uncertainty on the performance variability of proton exchange membrane (pem) fuel cells. *Journal of Power Sources*, 160(1):232 – 245, 2006. ISSN 0378-7753. doi: DOI:10.1016/j.jpowsour.2006.01.017. URL http://www.sciencedirect.com/science/article/pii/S0378775306000905.

[7] J.G. Pharoah and O.S. Burheim. On the temperature distribution in polymer electrolyte fuel cells. *Journal of Power Sources*, 195(16):5235 – 5245, 2010. ISSN 0378-7753. doi: 10.1016/j.jpowsour.2010.03.024. URL http://www.sciencedirect.com/science/article/pii/S0378775310004143.

[8] S. Shimpalee and S. Dutta. Numerical prediction of temperature distribution in pem fuel cells. *Numerical Heat Transfer: Applications*, 38(2):111–128, 2010.

[9] M.G. Santarelli, M.F. Torchio, and P. Cochis. Parameters estimation of a pem fuel cell polarization curve and analysis of their behavior with temperature. *Journal of Power Sources*, 159(2):824 – 835, 2006. ISSN 0378-7753. doi:

10.1016/j.jpowsour.2005.11.099. URL http://www.sciencedirect.com/science/article/pii/S0378775305016642.

[10] T.V Nguyen and R.E. White. A water and heat management model for proton exchange membrane fuel cells. *Journal of the Electrochemical Society*, 140:2178–2186, 1993.

[11] K. Kim, M.R.V Spakovsky, M. Wang, and D.J. Nelson. A hybrid multi-level optimization approach for the dynamic synthesis/design and operation/control under uncertainty of a fuel cell system. *Energy*, 36(6):3933 – 3943, 2011. ISSN 0360-5442. doi: 10.1016/j.energy.2010.08.024. URL http://www.sciencedirect.com/science/article/pii/S0360544210004603.

[12] Toshihiko Saito, Yasuhikio Itoh, Masato Nishioka, and Yasuo Miyake. Effect of operating temperature on the performance of molten-carbonate fuel cells. *Journal of Power Sources*, 36(1):69 – 77, 1991. ISSN 0378-7753. doi: http://dx.doi.org/10.1016/0378-7753(91)80045-Y. URL http://www.sciencedirect.com/science/article/pii/037877539180045Y.

[13] R. O'Hayre, S.W Cha, W. Colella, and F. B.Prinz. *Fuel cell fundamentals*, chapter 2-5, pages 23–168. John Wiley and Sons, Inc., 2009.

[14] S. Colleen. *PEM fuel cell modelling and simulation using MATLAB*. Number 1-125. Elsevier, 2008.

[15] T. E. Springer, T. A. Zawodzinski, and S. Gottesfeld. Polymer electrolyte fuel cell model. *Journal of The Electrochemical Society*, 138(8):2334–2342, 1991. doi: 10.1149/1.2085971. URL http://link.aip.org/link/?JES/138/2334/1.

[16] J.S. Yi and T.V. Nguyen. An along-the-channel model for proton exchange membrane fuel cells. *Journal of The Electrochemical Society*, 145(4):1149–1159, 1998. doi: 10.1149/1.1838431. URL http://link.aip.org/link/?JES/145/1149/1.

[17] C.H. Min, Y.L. He, X.L. Liu, B.H. Yin, W. Jiang, and W.Q. Tao. Parameter sensitivity examination and discussion of pem fuel cell simulation model validation: Part ii: Results of sensitivity analysis and validation of the model. *Journal of Power Sources*, 160(1):374 – 385, 2006. ISSN 0378-7753. doi: DOI:10.1016/j.jpowsour.2006.01.080. URL http://www.sciencedirect.com/science/article/pii/S0378775306001479.

[18] J.C. Amphlett, R.M. Baumert, R.F. Mann, B.A. Peppley, P.R. Roberge, and A. Rodrigues. Parametric modelling of the performance of a 5-kw proton-exchange membrane fuel cell stack. *Journal of Power Sources*, 49(13):349 – 356, 1994.

[19] P. K. Das, X. Li, and Z-S. Liu. Effective transport coefficients in PEM fuel cell catalyst and gas diffusion layers: beyond bruggeman approximation. *Applied Energy*, 87(9):2785 – 2796, 2010. ISSN 0306-2619. doi: http://dx.doi.org/10.1016/j.

apenergy.2009.05.006. URL `http://www.sciencedirect.com/science/article/pii/S0306261909001974`.

[20] G. Giannakoudis, A. I. Papadopoulos, P. Seferlis, and S. Voutetakis. Optimum design and operation under uncertainty of power systems using renewable energy sources and hydrogen storage. *International Journal of Hydrogen Energy*, 35(3): 872 – 891, 2010. ISSN 0360-3199. doi: 10.1016/j.ijhydene.2009.11.044. URL `http://www.sciencedirect.com/science/article/pii/S0360319909018138`.

[21] J. Kim, S.M. Lee, S. Srinivasan, and C.E. Chamberlin. Modeling of proton exchange membrane fuel cell performance with an empirical equation. *Journal of The Electrochemical Society*, 142(8):2670–2674, 1995. doi: 10.1149/1.2050072. URL `http://link.aip.org/link/?JES/142/2670/1`.

[22] G. Squadrito, G. Maggio, E. Passalacqua, F. Lufrano, and A. Patti. Empirical equation for polymer electrolyte fuel cell PEFC behaviour. *Journal of Applied Electrochemistry*, 29(12):1449–1455, 1999. URL `www.scopus.com`.

[23] A. Rowe and X. Li. Mathematical modeling of proton exchange membrane fuel cells. *Journal of Power Sources*, 102(1-2):82 – 96, 2001. ISSN 0378-7753. doi: DOI:10.1016/S0378-7753(01)00798-4. URL `http://www.sciencedirect.com/science/article/pii/S0378775301007984`.

[24] L. Placca, R. Kouta, J.F. Blachot, and W. Charon. Effects of temperature uncertainty on the performance of a degrading PEM fuel cell model. *Journal of Power Sources*, 194(1):313 – 327, 2009. ISSN 0378-7753. doi: 10.1016/j.jpowsour.2009.05.013. URL `http://www.sciencedirect.com/science/article/pii/S037877530900888X`.

[25] J. T. Gostick, M. A. Loannidis, M. D. Pritzker, and M. W. Fowler. Impact of liquid water on reactant mass transfer in PEM fuel cell electrodes. *The Society of Solid-State and Electrochemical Science and Technology*, 157(4):563–571, 2010.

[26] K. Inman, X. Wang, and B. Sangeorzan. Design of an optical thermal sensor for proton exchange membrane fuel cell temperature measurement using phosphor thermometry. *Journal of Power Sources*, 195(15):4753 – 4757, 2010.

[27] E. Misran, N. S. M. Hassan, W. R. W. Daud, E. H. Majlan, and Masli Irwan Rosli. Water transport characteristics of a PEM fuel cell at various operating pressures and temperatures. *International Journal of Hydrogen Energy*, 38(22):9401 – 9408, 2013. ISSN 0360-3199. doi: http://dx.doi.org/10.1016/j.ijhydene.2012.12.076. URL `http://www.sciencedirect.com/science/article/pii/S0360319912027462`.

[28] M. Perez-Page and V. Perez-Herranz. Effect of the Operation and Humidification Temperatures on the Performance of a Pem Fuel Cell Stack on Dead-End Mode. *International Journal of Electrochemical Science*, 6:492–505, 2011.

[29] D.M. Bernardi and M.W. Verbrugge. A mathematical model of a gas diffusion electrode bonded to a polymer electrolyte. *AlChE*, 37(8):1151–1163, 1991.

[30] J. H. Nam and M. Kaviany. Effective diffusivity and water-saturation distribution in single- and two-layer PEMFC diffusion medium. *International Journal of Heat Mass Tranport*, 46:4595, 2003. doi: 10.1016/S0017-9310(03)00305-3. URL `http://dx.doi.org/10.1016/S0017-9310(03)00305-3`.

[31] H. Meng and CY. Wang. Electron transport in PEFCs. *Journal Of The Electrochemical Society*, 151(3):A358–A367, March 2004.

[32] M. Noorkami, J.B. Robinson, Q. Meyer, I.A. Obeisun, E.S. Fraga, T. Reisch, P.R. Shearing, and D.J.L Brett. Effect of Temperature Uncertainty on Polymer Electrolyte Fuel Cell Performance. *International Journal of Hydrogen Energy*, 39:1439–1448, 2013.

[33] M. Wilkinson, M. Blanco, E. Gu, J. J. Martin, D. P. Wilkinson, J. J. Zhang, and H. Wang. In situ experimental technique for measurement of temperature and current distribution in proton exchange membrane fuel cells. *Electrochemical and Solid-State Letters*, 9(11):A507–A511, 2006. doi: 10.1149/1.2338769. URL `http://esl.ecsdl.org/content/9/11/A507.abstract`.

[34] G. Zhang, L. Guo, L. Ma, and H. Liu. Simultaneous measurement of current and temperature distributions in a proton exchange membrane fuel cell. *Journal of Power Sources*, 195(11):3597 – 3604, 2010. ISSN 0378-7753. doi: http://dx.doi.org/10.1016/j.jpowsour.2009.12.016. URL `http://www.sciencedirect.com/science/article/pii/S037877530902223X`.

[35] M. Matian, A.J. Marquis, and N.P. Brandon. Application of thermal imaging to validate a heat transfer model for polymer electrolyte fuel cells. *International Journal of Hydrogen Energy*, 35(22):12308 – 12316, 2010. ISSN 0360-3199. doi: http://dx.doi.org/10.1016/j.ijhydene.2010.08.041. URL `http://www.sciencedirect.com/science/article/pii/S0360319910016800`.

[36] Ch-Y. Lee, W-J. Hsieh, and G-W. Wu. Embedded flexible micro-sensors in MEA for measuring temperature and humidity in a micro-fuel cell. *Journal of Power Sources*, 181(2):237 – 243, 2008. ISSN 0378-7753. doi: http://dx.doi.org/10.1016/j.jpowsour.2008.01.020. URL `http://www.sciencedirect.com/science/article/pii/S0378775308000906`.

[37] S. He, M. M. Mench, and S. Tadigadapa. Thin film temperature sensor for real-time measurement of electrolyte temperature in a polymer electrolyte fuel cell. *Sensors and Actuators A: Physical*, 125(2):170 – 177, 2006. ISSN 0924-4247. doi: http://dx.doi.org/10.1016/j.sna.2005.05.021. URL `http://www.sciencedirect.com/science/article/pii/S0924424705003821`.

[38] M. Wang, H. Guo, and Ch. Ma. Temperature distribution on the MEA surface of a PEMFC with serpentine channel flow bed. *Journal of Power Sources*, 157(1):181 – 187, 2006. ISSN 0378-7753. doi: http://dx.doi.org/10.1016/j.jpowsour.2005.08.012. URL `http://www.sciencedirect.com/science/article/pii/S0378775305011560`.

[39] H. Guo, M. H. Wang, F. Ye, and C.F. Ma. Experimental study of temperature distribution on anodic surface of MEA inside a PEMFC with parallel channels flow bed. *International Journal of Hydrogen Energy*, 37(17):13155 – 13160, 2012. ISSN 0360-3199. doi: http://dx.doi.org/10.1016/j.ijhydene.2012.03.138. URL `http://www.sciencedirect.com/science/article/pii/S0360319912007860`.

[40] L.S. Martins, J.E.F.C. Gardolinski, J.V.C. Vargas, J.C. Ordonez, S.C. Amico, and M.M.C. Forte. The experimental validation of a simplified PEMFC simulation model for design and optimization purposes. *Applied Thermal Engineering*, 29:3036 – 3048, 2009. ISSN 1359-4311. doi: http://dx.doi.org/10.1016/j.applthermaleng.2009.04.002. URL `http://www.sciencedirect.com/science/article/pii/S1359431109001112`.

[41] R. Shimoi, M. Masuda, and K. Fushinobu. Visualization of the Membrane Temperature Field of a Polymer Electrolyte Fuel Cell,. *Journal of Energy Resources Technology*, 126:258–261, 2004.

[42] D.J.L. Brett, P. Aguiar, R. Clague, A.J. Marquis, S. Schottl, R. Simpson, and N.P. Brandon. Application of infrared thermal imaging to the study of pellet solid oxide fuel cells. *Journal of Power Sources*, 166(1):112 – 119, 2007. ISSN 0378-7753. doi: http://dx.doi.org/10.1016/j.jpowsour.2006.12.098. URL `http://www.sciencedirect.com/science/article/pii/S0378775307000791`.

[43] O. A. Obeisun, Q. Meyer, J. Robinson, Ch. W. Gibbs, A. R. Kucernak, P. R. Shearing, and D. J.L. Brett. Development of open-cathode polymer electrolyte fuel cells using printed circuit board flow-field plates: flow geometry characterisation. *International Journal of Hydrogen Energy*, 39(32):18326 – 18336, 2014. ISSN 0360-3199. doi: http://dx.doi.org/10.1016/j.ijhydene.2014.08.106. URL `http://www.sciencedirect.com/science/article/pii/S0360319914024124`.

[44] M. Andisheh-Tadbir, A. Desouza, M. Bahrami, and E. Kjeang. Cell level modeling of the hygrothermal characteristics of open cathode polymer electrolyte membrane fuel cells. *International Journal of Hydrogen Energy*, 39(27):14993 – 15004, 2014. ISSN 0360-3199. doi: http://dx.doi.org/10.1016/j.ijhydene.2014.07.049. URL `http://www.sciencedirect.com/science/article/pii/S0360319914020084`.

[45] J. Wu, S. Galli, I. Lagana, A. Pozio, G. Monteleone, X. Z. Yuan, J. Martin, and H. Wang. An air-cooled proton exchange membrane fuel cell with combined oxidant

and coolant flow. *Journal of Power Sources*, 188(1):199 – 204, 2009. ISSN 0378-7753. doi: http://dx.doi.org/10.1016/j.jpowsour.2008.11.078. URL `http://www.sciencedirect.com/science/article/pii/S0378775308021964`.

[46] Q. Li, W. Chen, Sh. Liu, Z. Gao, and Sh. Yang. Temperature optimization and control of optimal performance for a 300w open cathode proton exchange membrane fuel cell. *Procedia Engineering*, 29(0):179 – 183, 2012. ISSN 1877-7058. doi: http://dx.doi.org/10.1016/j.proeng.2011.12.691. URL `http://www.sciencedirect.com/science/article/pii/S1877705811065283`.

[47] B. Wu, B. Li, W. Liu, J. Liu, M. Zhao, Y. Yao, J. Gu, and Z. Zou. The performance improvement of membrane and electrode assembly in open-cathode proton exchange membrane fuel cell. *International Journal of Hydrogen Energy*, 38 (25):10978 – 10984, 2013. ISSN 0360-3199. doi: http://dx.doi.org/10.1016/j.ijhydene.2013.01.149. URL `http://www.sciencedirect.com/science/article/pii/S0360319913002589`.

[48] S. Strahl, N. Gasamans, J. Llorca, and A. Husar. Experimental analysis of a degraded open-cathode PEM fuel cell stack. *International Journal of Hydrogen Energy*, 39(10):5378 – 5387, 2013. ISSN 0360-3199. doi: http://dx.doi.org/10.1016/j.ijhydene.2013.12.115. URL `http://www.sciencedirect.com/science/article/pii/S0360319913030796`.

[49] D.T. Santa Rosa, D.G. Pinto, V.S. Silva, R.A. Silva, and C.M. Rangel. High performance PEMFC stack with open-cathode at ambient pressure and temperature conditions. *International Journal of Hydrogen Energy*, 32(17):4350 – 4357, 2007. ISSN 0360-3199. doi: http://dx.doi.org/10.1016/j.ijhydene.2007.05.042. URL `http://www.sciencedirect.com/science/article/pii/S0360319907003321`.

[50] G. Maranzana, O. Lottin, Th. Colinart, S. Chupin, and S. Didierjean. A multi-instrumented polymer exchange membrane fuel cell: observation of the in-plane non-homogeneities. *Journal of Power Sources*, 180(2):748 – 754, 2008. ISSN 0378-7753. doi: http://dx.doi.org/10.1016/j.jpowsour.2008.03.002. URL `http://www.sciencedirect.com/science/article/pii/S0378775308004837`.

[51] A.P. Sasmito, E. Birgersson, K.W. Lum, and A.S. Mujumdar. Fan selection and stack design for open-cathode polymer electrolyte fuel cell stacks. *Renewable Energy*, 37(1):325 – 332, 2012. ISSN 0960-1481. doi: http://dx.doi.org/10.1016/j.renene.2011.06.037. URL `http://www.sciencedirect.com/science/article/pii/S0960148111003740`.

[52] R.A. Silva, T. Hashimoto, G.E. Thompson, and C.M. Rangel. Characterization of MEA degradation for an open air cathode PEM fuel cell. *International Journal of Hydrogen Energy*, 37(8):7299 – 7308, 2011. ISSN 0360-3199. doi: http://dx.doi.org/

10.1016/j.ijhydene.2011.12.110. URL http://www.sciencedirect.com/science/article/pii/S0360319911028333.

[53] B. Qu, X. Guo, H. Chi, and M. Pollino. Probabilistic evaluation of effect of column stiffness on seismic performance of steel plate shear walls. *Engineering Structures*, 43(0):169 – 179, 2012. ISSN 0141-0296. doi: 10.1016/j.engstruct.2012.05.020. URL http://www.sciencedirect.com/science/article/pii/S0141029612002623.

[54] W.Q. Tao, C.H. Min, X.L. Liu, Y.L. He, B.H. Yin, and W. Jiang. Parameter sensitivity examination and discussion of {PEM} fuel cell simulation model validation: Part i. current status of modeling research and model development. *Journal of Power Sources*, 160(1):359 – 373. ISSN 0378-7753. doi: http://dx.doi.org/10.1016/j.jpowsour.2006.01.078. URL http://www.sciencedirect.com/science/article/pii/S0378775306001492.

[55] Sh.M.C. Ang, D. J.L. Brett, and E.S. Fraga. A multi-objective optimisation model for a general polymer electrolyte membrane fuel cell system. *Journal of Power Sources*, 195(9):2754 – 2763, 2010. ISSN 0378-7753. doi: 10.1016/j.jpowsour.2009.10.095. URL http://www.sciencedirect.com/science/article/pii/S0378775309019727.

[56] G. N. Srinivasulu, T. Subrahmanyam, and V. D. Rao. Parametric sensitivity analysis of PEM fuel cell electrochemical model. *International Journal of Hydrogen Energy*, 36(22):14838 – 14844, 2011. ISSN 0360-3199. doi: 10.1016/j.ijhydene.2011.03.040. URL http://www.sciencedirect.com/science/article/pii/S036031991100629X.

[57] W.Q. Tao, C.H. Min, X.L. Liu, Y.L. He, B.H. Yin, and W. Jiang. Parameter sensitivity examination and discussion of pem fuel cell simulation model validation: Part i. current status of modeling research and model development. *Journal of Power Sources*, 160(1):359 – 373, 2006. ISSN 0378-7753. doi: DOI:10.1016/j.jpowsour.2006.01.078. URL http://www.sciencedirect.com/science/article/pii/S0378775306001492.

[58] P. K. Das, X. Li, and Z-S. Liu. Analytical approach to polymer electrolyte membrane fuel cell performance and optimization. *Journal of Electroanalytical Chemistry*, 604(2):72 – 90, 2007. ISSN 1572-6657. doi: http://dx.doi.org/10.1016/j.jelechem.2007.02.028. URL http://www.sciencedirect.com/science/article/pii/S0022072807001131.

[59] D.C. Montgomery and G.C. Runger. *Applied statistics and probability for engineers*. Number 173-186. John Wiley and sons, 1994.

[60] Randn. Technical report, MathWorks, http://www.mathworks.co.uk/help/matlab/ref/randn.html, 2011.

[61] J. W. Eaton. *GNU Octave manuals.* Free Software foundation, http://www.gnu.org/software/octave/doc/interpreter/, 3 edition, 1997.

[62] E.W. Weisstein. Skewness. Technical report, Wolframe Research Inc, http://mathworld.wolfram.com/Skewness.html, 2012.

[63] M Bell. Skew and How Skewness Is Calculated In Statistical Software. Technical report, Math/Chaos Theory Suite101, 2010. http://suite101.com/article/skew-and-how-skewness-is-calculated-in-statistical-software-a231005.

[64] M. C. Fleming and J. G. Nellis. *Describing Data-Variability, in Principles of Applied Statistics.* Number 54-57. Ed. New York: Routledge, 1 edition, 1994.

[65] A. Hakenjos, H. Muenter, U. Wittstadt, and Ch. Hebling. A PEM fuel cell for combined measurement of current and temperature distribution, and flow field flooding. *Journal of Power Sources*, 131:213 – 216, 2004. ISSN 0378-7753. doi: http://dx.doi.org/10.1016/j.jpowsour.2003.11.081. URL `http://www.sciencedirect.com/science/article/pii/S0378775304000448`.

[66] Q. Meyer, K. Ronaszegi, J.B. Robinson, M. Noorkami, O. Curnick, S. Ashton, A. Danelyan, T. Reisch, P. Adcock, R. Kraume, P.R. Shearing, and D.J.L. Brett. Combined current and temperature mapping in an air-cooled, open-cathode polymer electrolyte fuel cell under steady-state and dynamic conditions. *Journal of Power Sources*, 297:315 – 322, 2015. ISSN 0378-7753. doi: http://dx.doi.org/10.1016/j.jpowsour.2015.07.069. URL `http://www.sciencedirect.com/science/article/pii/S0378775315301166`.

[67] M. Vollmer and H-P Mollmann. *Infrared Thermal Imaging-Fundamentals, Research and Applications.* Wiley-VCH, 2010.